Magnetite as a Game-Changer: Exploring its potential for enhancing anaerobic degradation of phenolic wastewater in AnMBR while tackling membrane fouling challenges

by

Mostafa Elshourbagy

Student number: 5463831

in partial fulfilment of the requirements for the degree of

MASTER OF SCIENCE

in **Civil Engineering**

Environmental Engineering Track

Faculty of Civil Engineering and Geosciences

Delft University of Technology

To be defended in public on July 26th 2023

Graduation committee

Chairperson	: Prof. dr.ir. Jules van Lier, Section Sanitary Engineering, TU Delft
First Supervisor	: Dr.ir. Henri Spanjers, Section Sanitary Engineering, TU Delft
Second Supervisor	: Dr.ir. Bas Heijman, Section Sanitary Engineering, TU Delft
Daily Supervisor	: Rifki Wahyu (PhD candidate), TU Delft

Acknowledgement

This master's thesis represents the culmination of an incredible and challenging two-year journey that has tested my limits, pushed me to new heights, and shaped me into the person I am today. Reflecting upon this endeavour fills my heart with both gratitude and admiration for the countless individuals who have been instrumental in making this achievement possible. This accomplishment would not have been possible without their support, guidance, and encouragement. First and foremost, I am indebted to my thesis supervisor, Rifki Wahyu, for his unwavering guidance and constant motivation throughout this research journey. Furthermore, I am grateful to the members of my thesis committee, Jules van Lier, Henri Spanjers and Bas Heijman, for their constructive feedback, insightful suggestions, and scholarly guidance. Their expertise and willingness to share their knowledge have immensely enriched my research. I would also like to extend my heartfelt thanks to the Water Lab-TU Delft technicians for their intellectual contributions and continuous support during my academic pursuit.

I extend my sincere appreciation to all my colleagues, who generously devoted their time and shared their insights, without whom this study would not have been possible. Their contribution has been invaluable in enhancing the quality and depth of the research. My heartfelt thanks go to my family and friends for their unwavering support, understanding, and encouragement throughout this challenging endeavour. Their belief in my abilities and their unconditional love have been the pillars of strength that have sustained me during the ups and downs of this journey. Lastly, I would like to express my gratitude to the entire TU Delft community for providing a conducive academic atmosphere and resources that have facilitated my research process. I am sincerely grateful to all who have played a role, big or small, in shaping this thesis. Your contributions have been significant, and I am honoured to have had the opportunity to work with such exceptional individuals.

Thank you all for your guidance, support, and encouragement.

Mostafa Elshourbagy

June 2023

Abstract

Aromatic compounds have always been of concern regarding their toxicity to living organisms, including microorganisms. With more anthropogenic activities (e.g. coal gasification), the need for feasible treatment of industrial effluents is highly prioritised. With the anaerobic degradation process being a competitive solution, these compounds' toxic impact on the biomass is still of concern. These implications influence the stability of the degradation process; thus, there was a search for mechanisms to make the anaerobic degradation process more resilient. One potential mechanism is enhancing syntrophic collaboration between different species and its corresponding electron transfer. Syntrophic collaboration in an anaerobic environment can be conducted using intermediates (e.g. hydrogen) or direct electron transfer. Direct interspecies electron transfer (DIET) is reported to be more energy efficient and more thermodynamically favoured over other mechanisms that include mediators (hydrogen/ formic acid). Conductive and semi-conductive materials have been investigated to simulate this direct interspecies electron transfer mechanism (DIET), with various materials being researched, such as iron oxides, zero-valent metals, and even carbon-based materials.

This study investigated the impact of magnetite addition (as a DIET-stimulator) on p-cresol degradation, methane production and sludge characteristics, with a further interest in membrane fouling mitigation. This investigation was conducted with continuous flow reactors and batch reactors. The continuous configuration was based on an anaerobic membrane bioreactor (AnMBR) fed with a synthetic-coal gasification-like solution of phenol and p-cresol to investigate mainly the conversion rate of p-cresol and monitor the influence on the methane production, sludge characteristics, and membrane fouling. At the same time, batch experiments were conducted to investigate the acetoclastic methanogenic pathway and p-cresol degradation as a sole carbon source. The continuous experiment lasted for 143 days but was divided into two separate phases with two different magnetite dosages, starting with 40 mmol/L in phase (I), then replacing the sludge with acclimatised one (from the control) with the addition of the second dosage (20 mmol/L) in phase (II).

A Magnetite dosage of 40 mmol/L showed signs of biomass-suppressed conversion capacity compared to the control, by which the reactor conversion rate deteriorated by reaching 212 mgCOD/ gVSS/d (under a feed of 900 mgPh/L & 900 mgPcr/L). Phase (I) showed no significant differences in the methane production rate between control and magnetite reactors. On the other hand, the batch experiments fed with 1 gCOD/L acetate showed that the magnetite reactor had a lower acetoclastic methane production rate than the control. It was suggested that the 40 mmol/L magnetite dosage was suppressing the acetoclastic methanogens, which was further contributing to the lower conversion capacity observed in the AnMBR by the end of the phase. With the same methane being produced in control and magnetite reactors, it was also possible that either hydrogenotrophic methanogenesis or the DIET pathways were enhanced; however the absence of intermediates (e.g. VFAs) and the similarity of the COD balance supported the possibility of the latter one. During phase (II), the conversion rate of both reactors (control and magnetite) reached 74 mgPcr/ gVSS/d, approaching the highest conversion rates reported in the literature. While the acetoclastic methanogens showed no significant difference in the batch experiment, the magnetite-AnMBR's methane production rate was 10%-28% higher. Furthermore, the methane yield with magnetite supplementation showed an average enhancement of 15%. In addition, the batch experiment also showed that this magnetite dosage reduced the p-cresol conversion rate by 87% compared to the control.

Both magnetite dosages (20 mmol/L & 40 mmol/L) showed a reduction in the protein and carbohydrate content of the soluble microbial products (SMP) and the extracellular polymeric substances (EPS). Magnetite had adversely impacted the loosely-bounded EPS (regarding protein and carbohydrates), whereas it was shown to be significant compared to the control. The EPS-LB showed an inverse relation with the particle size distribution (PSD), verifying that the higher increase in the particle size could be correlated with the EPS-LB reduction by the magnetite. On the other hand, the fouling rate of the membranes showed an insignificant difference between both reactors. This was suggested to be related to the incomplete formation of a mature cake layer under the influence of low operational flux. However, with the reduction of the SMP/EPS, it was suggested that the formed cake layer would be more porous and permeable. This would mean that the cake-fouling and its corresponding resistance would be expected to be lower. As the cake layer acts as a protective barrier for the membrane, its reduction would lead to a higher risk of irreversible pore-blocking by fine particles from the magnetite and the sludge.

Graphical abstract

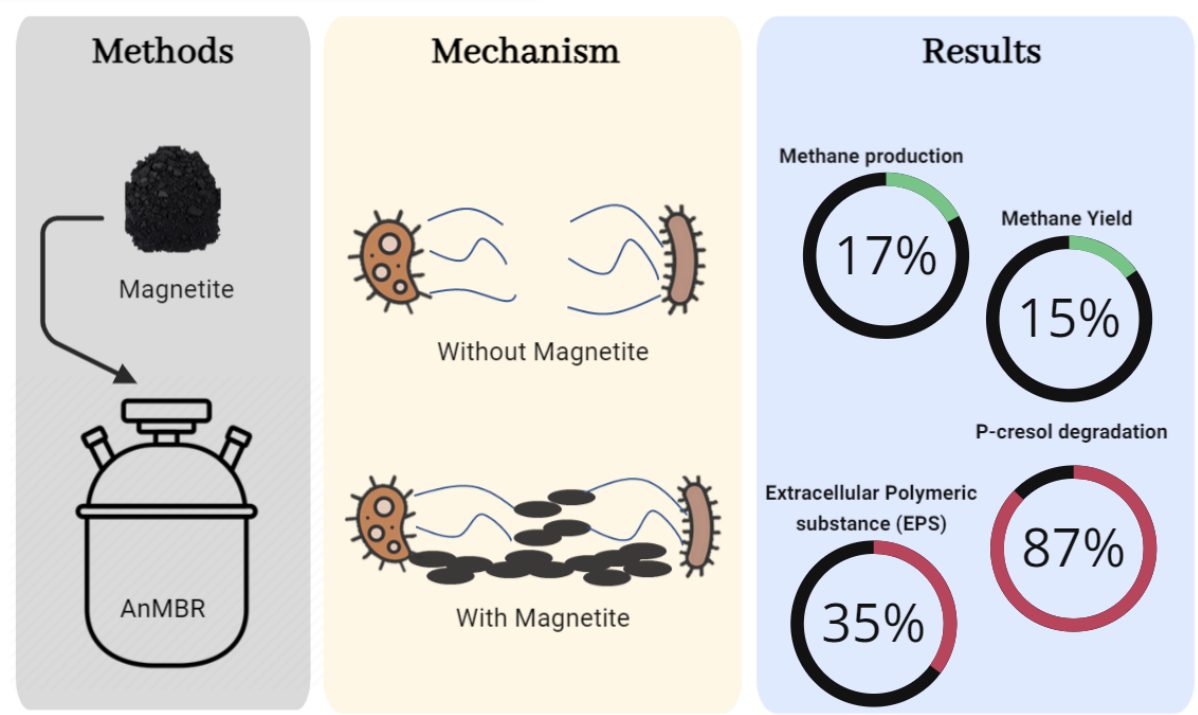

Table of Contents

Table of Figures

Table of Tables

1 Introduction

1.1 Background

As an aromatic compound, phenol exists in nature in many forms, and its resources can be natural or anthropogenic. The main anthropogenic sources are related to petrochemicals and petroleum refining activities. While various industries use phenolic compounds in their processes (either in the primary forms or derivatives), such as pharmaceuticals and chemical production, the residue is a matter of concern. According to S&P Global (2022), the current phenol demand is evaluated at 12 M metric tons/ year, with an estimated annual increase of 2.5%. This means that solving a rising trend problem should be prioritised. Phenol and its derivatives (e.g., cresols) are considered critical environmental pollutants. For example, phenols accumulation has proven to impact the growth of aquatic creatures (Said et al., 2021). With toxicity levels as low as 9-25 mg/L, an extended exposure period for humans/animals would have severe complications such as breathing difficulties, arrests, and even comas (Gupta et al., 2008; Sunil & Jayant, 2013). The criticality of the situation comes from how phenol is converted in nature. Microorganisms degrade phenol, and derivatives are produced, by which some of them are even more toxic. Other degradation pathways include interaction with UV radiation, inorganics, and nitrate ions, which are common components in open environments (Said et al., 2021). With coal gasification activities, the combination of phenol and cresol (p-cresol) is observed (Ji et al., 2016). One of the mentioned cresols is the para-form that was highlighted for its highest toxicity compared to the other isomers (Supandi et al., 2020).

Currently, wastewater is referred to as a renewable source that can be addressed for reuse, nutrient recovery and energy production. It was argued that these recovered resources (e.g. biogas as an energy source) could reduce the operational cost of the treatment plants and sustain a more circular economy (Burn, 2014; Aslam et al., 2022). For phenolic wastewater streams, several technologies have been investigated for phenol removal, such as distillation, adsorption, chemical oxidation, enzymatic treatment, pervaporation, and biodegradation (Busca et al., 2008). Additionally, biological degradation was considered one of the most cost-effective ways to deal with phenolic compounds; however, some halogenated forms are inhibitory to aerobic biomass but not anaerobic ones and specifically in higher concentration medium (Vogel et al., 1987; Said et al., 2021). Anaerobic degradation also offers low sludge production and energy recovery possibility (Chan et al., 2009), as well as environmental friendliness and stability for toxic influents (Tomei et al., 2021). Thus, research became interested in investigating several operational conditions of such anaerobic process and the routes to enhance its performance. One of the applications of the anaerobic digestion process is the anaerobic membrane bioreactors (AnMBR); this technology is advantageous concerning robustness, sludge retention, and resilience for harsh operational conditions (Muñoz Sierra et al., 2019; Aslam et al., 2022). However, these phenolic compounds seem to have severe implications on anaerobic bacterium communities that would influence the stability of the process, and for that, some means of enhancement should be explored (Garcia Rea et al., 2020; Jung et al., 2022).

In the last decade, research was conducted to understand better the syntrophic interaction between microbial communities representing different anaerobic processes (e.g., acetogenesis, methanogenesis). The standard mechanism of the reducing equivalents transfer in syntrophic interactions was based on hydrogen diffusion as an electron carrier, but lately, a more robust mechanism depending on direct interspecies electron transfer (DIET) has been investigated (Wang et al., 2021). Most research on conductive materials were conducted in batch-like experiments, but fewer were conducted in continuous flow processes, especially with AnMBR (Wang et al., 2021). The use of magnetite with phenolic wastewater was investigated, and the results showed an enhanced methane production rate,

conversion rate, and shift in the degradation pathway, thus showing promising results for continuous-flow applications (He et al., 2019; Jung et al., 2022).

On top of that, recent studies targeted membrane fouling control and mitigation using nano-particles (e.g., zeolites, magnetite, etc.). These nano-particle applications proved to reduce the soluble microbial products (SMP) and extracellular polymeric substances (EPS) concentration in sludge, thus increasing the fouled-cake layer's porosity. As a result, this reduced the flux deterioration rate and the frequency of cleaning cycles and enhanced the lifetime of the membrane (Rezaei & Mehmia, 2014; Hazrati et al., 2018; Zhou et al., 2019; Sabalanvand et al., 2021).

1.2 Knowledge gap and problem statement

DIET-related research showed promising results regarding enhancing the anaerobic degradation process, targeting process stability, resilience, and methane production (Xu et al., 2019; Wang et al., 2021). One of the potential applications would be with toxic aromatic compounds such as phenol and p-cresol, which were advised not to be accumulated in high concentration due to their inhibitory impacts on methanogens (Garcia Rea et al., 2022). Moreover, p-cresol was reported as a slow degrading compound compared to other aromatic compounds and VFAs (e.g. Phenol, acetate … etc.). (Veeresh et al., 2005). Thus, this study intended to investigate the impact of magnetite nanoparticles (as means of stimulating DIET) on enhancing the degradation of a synthetic-coal gasification-like stream with phenol & p-cresol. In addition, with membrane fouling being a major problem in membrane installations, another branch of study targeted the use of nano-particles to increase the formed-cake layer porosity, reduce the cake resistance, and by that enhancing the transmembrane pressure (TMP) and the working flux, and thus reducing the backwashing cycles (Zhou et al., 2019; Sabalanvand et al., 2021; Tomei et al., 2021).

Rarely presented in previous literature, the investigation of magnetite-stimulated DIET (Direct Interspecies Electron Transfer) in relation to phenol remains limited (Jung et al., 2022), and no reports have been found regarding its application to p-cresol. Furthermore, only a few studies have addressed the combined evaluation of magnetite utilisation in an AnMBR (Anaerobic Membrane Bioreactor) application concerning the anaerobic degradation of a mixture of phenolic compounds, including phenol and p-cresol, as well as the associated challenges of membrane fouling. Thus, the objectives of this research are as follows:

- Investigating the impact of magnetite on the p-cresol degradation process regarding the rate and the removal efficiency.
- Investigating the impact of magnetite in an anaerobic membrane bioreactor (AnMBR) regarding methane production rate and yield.
- Investigating the impact of magnetite on the sludge characteristics (PSD & SMP/EPS)
- Investigating the impact of magnetite on mitigating membrane fouling.

Thus, corresponding to these objectives, the research questions and the hypothesis are based on different magnetite dosage and sub-questions and are as follow:

- **RQ1**: What is the impact of a 20 mmol/L & 40 mmol/L of Fe_3O_4 on the anaerobic degradation p-cresol in AnMBR (representing a continuous flow reactor) and batch reactors, supplied in different experimental phases?

- RQ1.1: What is the impact of a 20 mmol/L & 40 mmol/L of Fe_3O_4 on the anaerobic degradation of p-cresol (supplied with phenol in a 1:1 concentration ratio) in an AnMBR?
- RQ1.2: What is the impact of a 20 mmol/L of Fe_3O_4 on the anaerobic degradation of p-cresol as a sole carbon source (representing a more stressed condition) in a batch experiment?

  Hypothesis: If magnetite is added to the AnMBR or batch reactors with a concentration of 20 mmol/L and with p-cresol as substrate, then the degradation rate will be enhanced under the influence of reaction acceleration toward products. And if the concentration is increased to 40 mmol/L, the degradation rate will be further enhanced.

- **RQ2**: What is the impact of a 20 mmol/L & 40 mmol/L of Fe_3O_4 on the methane production rate and methane yield in AnMBR and batch reactors?
  - RQ2.1: What is the impact of a 20 mmol/L & 40 mmol/L of Fe_3O_4 on the methane production rate and yield in AnMBR fed with a (1:1) concentration ratio of p-cresol & phenol?
  - RQ2.2: What is the impact of a 20 mmol/L & 40 mmol/L of Fe_3O_4 on the acetoclastic-specific methanogenic activity (SMA) in batch reactors fed with acetate as a carbon source?

    Hypothesis: If magnetite is added to the AnMBR with a concentration of 20 mmol/L and with phenol and p-cresol as main substrates, then the reactor methane production rate will be enhanced through the acetoclastic pathway under the assumption that acetoclastic species are enriched with DIET (as reported in literature). Furthermore, if the concentration is increased to 40 mmol/L, a higher production rate will be reached.

- **RQ3**: What is the impact of a 20 mmol/L & 40 mmol/L of Fe_3O_4 on the particle size and the SMP/EPS of the sludge in an AnMBR setup?
  - RQ3.1: What is the impact of a 20 mmol/L & 40 mmol/L of Fe_3O_4 on the particle size of the sludge in an AnMBR setup fed with a (1:1) concentration ratio of p-cresol & phenol?
  - RQ3.2: What is the impact of a 20 mmol/L & 40 mmol/L of Fe_3O_4 on the SMP/EPS concentration of the sludge in an AnMBR setup fed with a (1:1) concentration ratio of p-cresol & phenol?

    Hypothesis: If magnetite is added to the AnMBR with a concentration of 20 mmol/L and with phenol and p-cresol as main substrates, then the sludge will have less SMP/EPS concentration, less repulsion between biomass cells and thus better agglomeration. Furthermore, if the concentration is increased to 40 mmol/L, then a lower concentration of SMP/EPS will be expected and even better agglomeration.

- **RQ4**: What is the impact of a 20 mmol/L & 40 mmol/L of Fe_3O_4 on the fouling of the membrane in an AnMBR setup fed with a (1:1) concentration ratio of p-cresol & phenol?

  Hypothesis: If magnetite is added to the AnMBR with a concentration of 20 mmol/L with phenol and p-cresol as main substrates, then the SMP/EPS concentration of the sludge will be less, the formed membrane cake layer would be more porous and the fouling rate will be less. Moreover, if the concentration is increased to 40 mmol/L, then better fouling mitigation will be expected.

2 Literature Review

2.1 Phenolic compounds

2.1.1 Phenolic compounds characteristics

Phenolic compounds exist naturally and anthropogenically depending on their sources. The anthropogenic ones detected in the environment are mostly related to human activities such as the industrial field (Anku et al., 2017). Labelled as a pollutant group of concern, the United States Environmental Protection Agency (EPA) and the European Union (EU) recognise their damaging effects on the environment in both short and long terms (Mahugo-Santana et al., 2010; Anku et al., 2017). These compounds are commonly known for their toxicity, not only in their initial state but also for the intermediates produced under degradation effects upon interacting with other factors in nature (Kulkarni & Kaware, 2013). The chemical industry is one of the main producers and consumers of such a group; pesticides/ insecticides, wood distillation, disinfectant chlorine, and paper production are examples of such usage processes (Paasivirta et al., 1985; Anku et al., 2017). Environmental pollution with these compounds can come from natural events such as wildfires or anthropogenic resources such as benzene degradation or coal tar from coal-related activities. Anthropogenic pollution could come directly from poor waste management or indirectly from runoff under the influence of rainfall (Tsuruta et al., 1996; Anku et al., 2017). Phenolic compounds undergo reactions inside the human body and produce intermediates that can bond with proteins causing a serious effect on the human body; additionally, the introduction of such compounds can be through skin adsorption on contact (Schweigert et al., 2001; Anku et al., 2017).

Phenol. Phenolic compounds are organic compounds with a direct bond between their aromatic ring and the hydroxyl group. The classification of such groups could be based on their carbon chain, skeleton structure, distribution in nature, etc. Initially isolated in 1834, the well-known aromatic ring bonded with one hydroxyl group is labelled as phenol (C_6H_5OH). Phenol is a combustible compound soluble in polar solvents and hydrocarbons. It is also referred to as carbolic acid, phenic acid, benzo-phenol, or hydroxybenzene (Busca et al., 2008; Anku et al., 2017). According to its temperature, it can have a reactive influence on rubber, coatings, plastics, aluminium, magnesium, lead, and zinc. Moreover, it is commonly used in chemical industries, oil & gas and coal applications, lubricant production, and pharmaceutical products. Widely used in industries, phenol derivatives can also be produced, such as cresols and resins (35% of production). In addition, these derivatives are used in other applications such as the construction industry, fertilisers/ explosive/paint production, dye manufacturing, textiles, and appliances (Busca et al., 2008; Careghini et al., 2015; Anku et al., 2017). High concentrations of phenol are proven to have critical damage to the heart and kidney, burn-like effects on the skin, DNA damage and protein destruction, and in serious cases, comas and death. (Health U. D. O. and Services H., 1999; Busca et al., 2008; Anku et al., 2017). However, according to Busca et al. (2008), no reliable evidence concludes that phenol has carcinogenic potential. EPA has set a limiting standard of (< 1 ppb phenol) in surface water for water purification purposes (Busca et al., 2008).

P-cresol. Another distinguished phenolic member is a compound from the cresol family, and it is referred to as para-cresol (p-cresol) ($CH_3C_6H_4OH$), usually known as 4-methyl-phenol, 4-cresol, or p-hydroxytoluene. Commonly, this compound is formed either by fractional distillation or cumene process, or sulfonation, from coal tar, benzene, and toluene, respectively (Andersen, 2006). Compared to other cresols, p-cresol is the highest in terms of permeability, making its contact a high-risk potential (Supandi et al., 2020). One recorded resource for p-cresol pollution is landfill leachate and the residue of incineration activities of waste, as well as waste streams from industries such as cosmetics and

pharmaceuticals (Andersen, 2006; Anku et al., 2017). This compound is also introduced as a potential carcinogenic source when induced into living cells and is labelled as a priority pollutant by the EPA. The standard limit of p-cresol allowed in drinking water is around one µg/l, as advised by the World Health Organization (WHO) (Surkatti & El-Naas, 2014). P-cresol has the highest toxicity compared to the other isomers, and its accumulation in living cells is related to heart, kidney, and liver failures (Supandi et al., 2020). Andersen (2006) reported the brief results of an experiment on rats and mice, where a cresols mixture of 30,000 ppm was introduced to their diet. The experiment observed changes in liver and kidney characteristics regarding weight and function, atrophic impact on female reproductive organs, and other damage related to bone hypocellularity. In another experiment on hamsters, a sort of forestomach hyperplasia was noticed. In addition, an inhalation experiment was conducted on rats, where mixed cresols were introduced, by which weight loss, lung protein damage, and disturbance in the central nervous system were observed (Andersen, 2006).

2.1.2 Common concentrations and available removal technology

Common concentration. Regarding the estimated concentration in some wastewater streams, phenol has a wide concentration range depending on the source. Concentration could be in the range of (6-500 mg/L) as in refineries and could go up (9-6800 mg/L) as in coal processing, but in most other industrial streams, it is expected to have a maximum concentration of (1220-1600 mg/L) (Busca et al., 2008). According to Veeresh et al. (2005) review, the COD contributed by phenolic compounds ranged between 40-80%; depending on the type of industry; where in some cases, such as coal conversion and coke process, the COD of the waste stream was divided into 60% contributed by phenol and 30% by cresols. Fedorak & Hrudey (1986) reported the water quality of an effluent stream from a coal liquefication plant, whereas the phenol concentration reached a range of 4900 mg/l with a p-cresol of about 420 mg/l. It was also reported that p-cresol from the coal gasification process could reach a concentration of 880 mg/l (ATSDR, 2008). One common industry is coal gasification, and this process produces streams that contain a mixture of toxic compounds, such as phenols, resorcinol, cresols, xylenol, etc. It was found that coal gasification wastewater (CGW) contains an average phenol concentration of 2000 mg/l and a p-cresol concentration of about 250 mg/l (Ji et al., 2016).

Removal technologies. Due to their effects, phenolic compounds are a matter of concern in nature, so some techniques are adopted to reduce their impact. These techniques may be related to eliminating the component (e.g., by extraction & adsorption) or changing its properties (e.g., by polymerisation and degradation). The removal technique and technology selection should consider the problem's removal and the compounds' recovery as a source (Anku et al., 2017). The most common techniques and methods are presented in photocatalytic degradation, ozonation, oxidation, solid/liquid extraction, biological methods, adsorption, membrane separation, electro-Fenton-method, ion-exchange, and others (Busca et al., 2008; Anku et al., 2017). A summarised overview of the available technology-related experiments for phenol removal is given in Appendix (1). In-depth, biological methods are commercially known in the industrial stream treatment as being inexpensive relative to the operational costs, environmentally friendliness, and robustness in terms of mineralisation of pollutants, and these methods are either aerobic or anaerobic (Surkatti & El-Naas, 2014; Anku et al., 2017).

Biodegradation. Patterson (1975) demonstrated that biological oxidation can be conducted for dealing with phenol concentration in the range of 5-500 mg/l; a variety of microbial community strains were reported to be effective for that process as well (e.g., Pseudomonas Putida, Pseudomonas fluorescens, Trichosporon cutaneum, etc.), as well as fungi strains (Busca et al., 2008). Coal gasification wastewater (CGW) is reported by Ji et al. (2015) to be treated by activated sludge methods, batch reactors, anoxic/aerobic & anaerobic/anoxic/aerobic processes, expressing the variety of options and the

applicability of integration between them. Activated sludge methods in Rotating Biological Contactors (RBC) were investigated for phenol degradation application; the sludge reported was pre-acclimatized to 400 mg/l phenol, and oxygen supply was reported to be a sensitive parameter to the degradation rate (Busca et al., 2008). High removal results are reported in a moving bed bioreactor (MBBR) with a powdered activated carbon technology (PAC) in a pilot study on a Sasol coal/liquid plant and in another MBBR application, whereas phenol removal had successfully reached 89%, showing the suitability of such technology (Ratcliffe et al., 2006; Li et al., 2011). Other novel methods, such as Biomembrane aerobic reactors (BioAX) and membrane bioreactor hybrid powdered activated carbon (MBR-PAC), are also reported to be potential technologies that could be used for CGW treatment (Li et al., 2014; Jia et al., 2014).

At that time and before 1990, aerobic treatment was the dominant technique adopted for treating phenolic wastewater. Furthermore, breakthrough experiments were being published during that period, demonstrating the applicability of anaerobic methods and starting a new timeline where anaerobic techniques would be widely investigated (Veeresh et al., 2005). The first technologies investigated included an activated carbon anaerobic filter, a gravel media anaerobic filter, and an expanded bed (Suidan et al., 1981; Blum et al., 1985; Wang et al., 1986). These experiments demonstrated that phenol removal with anaerobic techniques could reach >90% (Veeresh et al., 2005). Later on, more research was conducted on other commonly used anaerobic digestors: Upflow anaerobic sludge blanket (UASB), sequencing batch reactors (SBR), and expanded granular sludge bed (EGSB) application, for coping with the inhibitory effect of certain streams (e.g., CGW), and the results were promising (Wang et al., 2010; Zhao et al., 2013; Yu et al., 2014).

2.2 Anaerobic digestion

2.2.1 Anaerobic process

Our main scope of interest is the anaerobic processes due to their lower operational costs than aerobic ones, the potential recovery of biogas and methane as energy sources, and the minimal sludge production (Chan et al., 2009). Being the common electron acceptor in aerobic processes, oxygen is absent in anaerobic conditions. Thus, other electron acceptors are needed to enclose the process. These electron acceptors mainly include organic matter (with acidogenic, fermentative, and methanogenic bacteria), sulfates (with sulfate reducers), and ferric iron (with iron reducers)…. etc.(Hammill & Crawford, 1996; Ghattas et al., 2017; Said et al., 2021).

Generally, the anaerobic process is conducted along a chain of 4 phases: hydrolysis, acidogenesis, acetogenesis, and methanogenesis phases. Firstly, the hydrolysis phase is concerned with breaking complex structures and organics (e.g., Proteins, fats & carbohydrates) into more easily-degraded forms (e.g., Monomers, amino acids & sugars), whereas fermentative hydrolytic bacteria are the common active microbial class in this phase (Lei et al., 2018; Aslam et al., 2022). In the second phase, the formed monomeric compounds are converted into short-chain structures (e.g., volatile fatty acids “VFA”, alcohols, hydrogen, carbon dioxide & acetic acid). This phase is labelled as acidogenesis and is commonly known for its fast kinetics compared to other phases, as the environmental conditions highly influence its active microbial communities (Visvanathan & Abeynayaka, 2012; Aslam et al., 2022).

Acetogenesis is the third stage of that chain of process, where acetic acid, carbon dioxide, and hydrogen are produced from the biodegradation of VFAs under the activity of acetogens (syntrophic). The bacterial communities in this phase are highly related. For example, VFAs are oxidised to hydrogen and acetate; meanwhile, uncommon reactions that can exist include the production of hydrogen/CO_2

from acetate oxidation by acetate oxidisers, and the conversion of hydrogen and carbon dioxide back to acetate by homoacetogenic bacteria. Unfamiliarly, homoacetogens are also reported to be able to consume sugars and alcohols for acetate formation (Xie et al., 2014; Aslam et al., 2022). Various species are reported to be active during that phase, such as *Clostridium* and *Acetobacterium* (Ketheesan & Stuckey, 2015). The final phase is methane production from acetic acid or H_2/CO_2. Two classes of methanogens are reported in that process: Aceticlastic and hydrogenotrophic. Aceticlastics are related to converting the acetate to methane, whereas it is reported that about 70% of the produced methane comes from that pathway (Aslam et al., 2022). On the other hand, hydrogenotrophic methanogens convert H_2/CO_2 to methane (Xie et al., 2014). *Methanosaeta* and *Methanosarcina* are reported as the most commonly found bio-species in the acetate conversion pathway (Ketheesan & Stuckey, 2015). To summarise, the performance of such processes can be monitored from methane production, giving insights into the degradability of substrates, over-loading conditions, and even emerging inhibitory conditions (Hussain & Dubey, 2017; Aslam et al., 2022). A conceptual overview of the process can be observed in Figure (1).

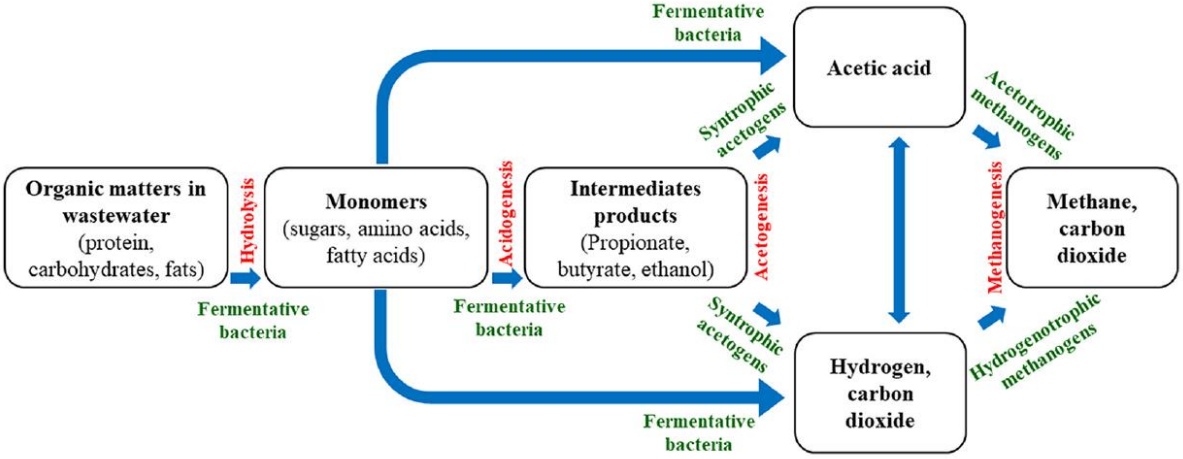

Figure (1) : The anaerobic conversion process of organics (Aslam et al., 2022)

2.2.2 Phenol Degradation pathways

Aerobic Degradation. For phenol aerobic degradation, phenol goes through hydroxylation/ oxygenation of the aromatic rings through the reduction of oxygen/water, whereas another hydroxyl group is added to the ring producing catechol under the influence of the dioxygenase enzyme (Xiaojian et al., 1991; Müller & Babel, 1994; Anku et al., 2017). Thus, as aromatic compounds (e.g., phenol) are degraded aerobically through conversion to catechol, they undergo one of two pathways (ortho or meta pathway), then the final compounds formed (cis-muconic acid, hydroxy-muconic semialdehyde) are consumed by the microbial communities through the Krebs-cycle process (van Schie & Young, 2000; Busca et al., 2008).

Anaerobic Degradation. One of the initial suggestions about anaerobic digestion was related to a stratification process and biological respiration. However, without a further relation to the limiting step, this theory did not sustain the debate on it (Said et al., 2021). For anaerobic degradation, it is a common degradation pathway for phenol to be converted to benzoate, then to cyclohexane carboxylic acid, through a dearomatization-hydrogenation process. Then, this ring structure is further fissioned to heptanoate, which is degraded further to acetate and then to methane. It should be noted that the rate-limiting step of such a pathway was argued to be the phenol-benzoate step (Kobayashi et al., 1989; Fang et al., 1996; Fang et al., 2004). However, that is not the only known pathway, a caproate-related pathway

that ends up with acetate was also reported, but the pathway scheme of degradation is reported only in thermophilic conditions and is not fully understood (Fang et al., 2006; Levén et al., 2012). In general, the degradation of phenolic compounds could proceed through mesophilic and thermophilic environments. Nevertheless, most of the published research, including the isolation of bacterium, is reported in the mesophilic environment (~37 ºC) (Levén et al., 2012). The temperature is presented as an effective parameter in the degradation of phenolic compounds, where research has shown that the degradation process is better stimulated under 50 ºC. Additionally, it is reported to affect the degradation pathway, whereas some intermediates (e.g., benzoic acid) are better traced in mesophilic conditions than in thermophilic (Karlsson et al., 1999; Fang et al., 2006; Levén & Schnürer, 2005 & 2006 & 2010).

Regarding the degradation insights, phenol and p-cresol go from a peripheral pathway into a central one that yields acetyl-CoA and eventually ends with methane production. The peripheral pathway of phenol is comprised of four stages. The first stage is related to phenyl-phosphate production from the phosphorylation of phenol; this process is catalyzed by phenyl-phosphate synthase (PPS). The second stage is the carboxylation to 4-hydroxybenzoate by utilizing the phenyl-phosphate carboxylase (PPC) catalyst. For the third stage, the 4-hydroxybenzoate-CoA ligase enzyme (HBCL) is used for the CoA-thioester conversion, utilizing it further through a reductively dehydroxylated reaction. And by that, and through the final stage, benzoyl-coenzyme A (CoA) is produced via catalyzing 4-hydroxybenzoyl-CoA reductase (HBCR) (Harwood et al., 1999; Nešvera et al., 2015). On the other hand, p-cresol is initiated by utilizing a p-cresol methylhydroxylase (CMH) catalyst to oxidize the methyl group typically found in cresols; this process produces an aldehyde form (4-hydroxybenzaldehyde). Then, through a carboxylation reaction to produce 4-hydroxybenzoate, the process is further converted through the previously discussed pattern. The overall degradation route for both phenol & p-cresol is illustrated in Figures (2)& (3) (Harwood et al., 1999; Nešvera et al., 2015; Tomei et al., 2021). Moreover, in case phenol and carbon dioxide are abundant in the environment (with relatively high concentrations), it was reported that the conversion route from phenol goes directly to 4-hydroxybenzoate by utilizing 4-hydroxybenzoate decarboxylase as a catalyst (Tomei et al., 2021). It should be noted that within this pathway, the reverse decarboxylation of 4-hydroxybenzoate back to phenol is also possible and reported through fermentative bacterium species (Harwood et al., 1999).

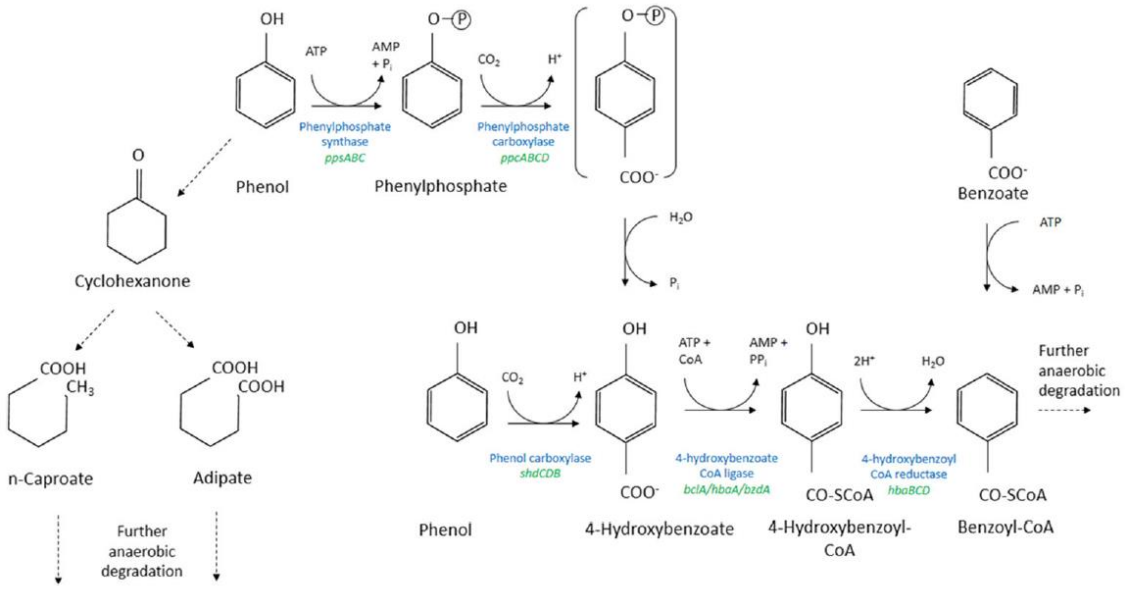

Figure (2): Detailed Anaerobic degradation pathways of phenol till the Benzoyl-CoA step (Tomei et al., 2021)

After the peripheral pathway ends with benzoyl-CoA, the central pathway is initiated. Benzoyl-CoA is reduced to 1,5-dienoyl-CoA (with the catalyzing of benzoyl-CoA reductase (BCR)). Then, 6-hydroxycyclohex-1-ene-1-carboxyl-CoA is produced using dienoyl-CoA hydratase (DCH) as a catalyst. An oxidation stage follows by utilizing b-hydroxyacyl-CoA dehydrogenase and producing 6-oxocyclohex-1-ene-1-carboxyl-CoA. Ring fission stages are then initiated by hydration and cleavage, ending with 3-hydroxypimelyl- CoA via 6-oxocyclohex-1-ene-1-carbonyl-CoA hydrolase. Then through β-oxidation processes, acetate products are cultivated. Appendix (2A) & (2B) represent graphical representations of the central pathway of benzoyl-CoA degradation (Harwood et al., 1999; Nešvera et al., 2015). Furthermore, various bacterium species are reported in an anaerobic environment for phenol/p-cresol degradation. Examples of the active bacterial population reported in mesophilic conditions include *Desulfotomaculum subcluster Ih, Syntrophorhabdaceae, Syntrophorhabdaceae Syntrophus*, and others (Zhang et al., 2005; Chen et al., 2008; Chen et al., 2009; Levén & Schnürer, 2010). A graphical representation of the methanogenic bacterium contributing to the degradation of phenol is described in Appendix (3)

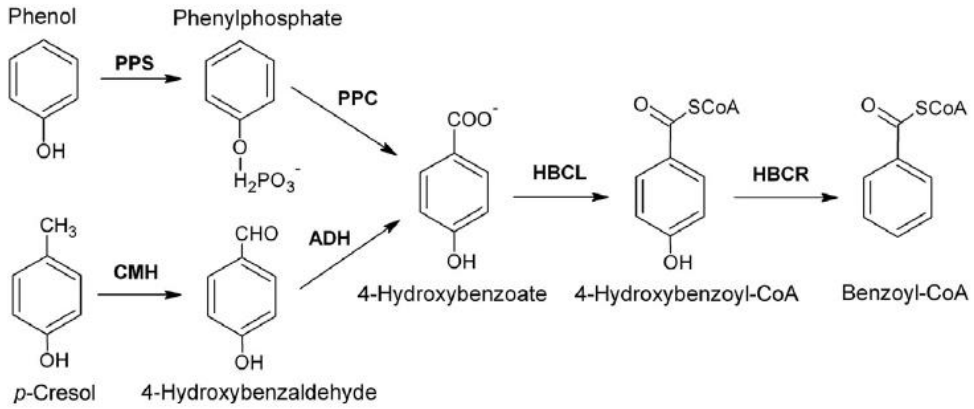

Figure (3): Simplified Anaerobic degradation pathways (peripheral) of phenol and p-cresol to Benzoyl-CoA. *Abbreviations of enzymes: PPS, phenyl-phosphate synthase; PPC, phenyl-phosphate carboxylase; HBCL, 4-hydroxybenzoate-CoA ligase; HBCR, 4-hydroxybenzoyl-CoA reductase; CMH, p-cresol methylhydroxylase; ADH; aldehyde dehydrogenase* (Nešvera et al., 2015)

2.2.3 Application regarding phenolic compounds

Phenolic degradation investigations were conducted in the anaerobic environment under a variety of conditions and bio-cultures: methanogens, denitrifying, sulfate reducers, optimised temperature, and recirculation ratios (Hwang & Cheng, 1991; Fang & Zhou, 1997; Lay & Cheng, 1998; Fang & Zhou, 1999; Puig-Grajales et al., 2003; Fang et al., 2004). Experimenting cresols with benzoate, Fang & Zhou (1997) demonstrated that cresols, presented as m- & o-cresols, had an insignificant impact on the benzoate methanogenesis; however, the cresols concentration was in the range of 225 mg/l. Using an easily biodegradable substrate, and inducing a co-metabolism process in the biomass culture, is considered a practical strategy in dealing with a hard-degrading substrate (e.g., Phenol). It is reported that adding some easily biodegradable compounds (such as glucose and sucrose) with phenolic compounds kept the methanogens in an "active phase" (Veeresh et al., 2005). For example, Tay et al. (2001) demonstrated the use of glucose in enhancing phenol removal that reached 98%, compared to 88% without glucose as a co-substrate. VFA's are also considered as additional carbon sources for p-cresol removal, whereas a complete removal of cresol was observed compared to only 80% removal in non-addition VFA cases (Kennes et al., 1997). Another experiment included phenol with p-cresol, in

which phenol had a more relative removal over p-cresol, and that p-cresol removal rate declined with phenol depletion. This further indicated that phenol was a co-substrate for cresol-non-acclimatized biomass (Fang & Zhou, 2000). Veeresh et al. (2005) review categorises co-substrates into readily degradable and phenols. In the first category, methane generation is commonly the rate-limiting step, while it is the formation of methane predecessors in the second. This is also related to the specific methanogenic activity (SMA) (relative to measuring the methane-producing capability), where it is found that for granules, the SMA and the ease of anaerobic degradation of phenolic compounds are as follows: acetate > benzoate > phenol> p-cresol (Veeresh et al., 2005).

The effect of the pre-acclimatized conditions of biomass and their effect on degradation was also reported by Garcia Rea et al. (2022), by which p-cresol had inhibitory effects on phenol-acclimatized biomass in AnMBR treating phenolic synthetic wastewater. However, the biomass adapted to p-cresol even when acclimatised to phenol, which was accounted for the fact that both compounds share the same degradation pathways (Fang & Zhou, 2000; Garcia Rea et al., 2022). Lay & Cheng (1998) concluded from their experiment that the adaptation of the sludge to the phenolic substrate was considered a necessity for optimised-operational conditions of the treatment unit. However, that would not discard the inhibition impact of such compounds on the sludge at high concentrations (Tay et al., 2000). Fang & Zhou (2000) also highlighted the importance of optimising the loading rate in the removal efficiency of reactors, where it was advised that high retention time should be adopted when dealing with increasing concentrations of phenolic compounds. This optimised retention time was concluded to be around 15 hrs in another experiment working with a UASB (Rincon et al., 2002).

As an overview of the used technology, UASB is one of the most common reactors known as an anaerobic application in industrial water treatment. An analysis of wastewater technologies adopted in the industrial sector found that 67% of the anaerobic reactors were UASBs (Habets, 1996). In another study, the researchers noted that UASB reactors reached as as high as 4000-5000 installations (van Lier et al., 2020). Specifically for phenolic wastewater treatment, other technologies are explored as well, such as CSTR, SBR, anaerobic activated carbon reactor (AnBAC), anaerobic immobilised fluidised bed reactor (AIFBR), EGSB, and AnMBR, whereas the microbial conditions for most of these experiments were based on a mesophilic environment (Tomei et al., 2021). Relative to their performance, Tomei et al. (2021) also reported that UASB, EGSB, and AnMBR-type systems showed more robust results in phenol removal than SBR & CSTRs. Nevertheless, UASB reactors are extensively investigated regarding phenolic compounds' removal under the influence of different operational parameters (e.g., HRT, salinity, co-substrate, etc.) (Tomei et al., 2021).

2.2.4 Anaerobic membrane bioreactor (AnMBR)

Membrane bioreactor technology is conceptually based on combining a filtration installation (membrane-based) with an activated sludge process (MBR). This integration enhances the process performance with fewer operational requirements and footprint traces (Judd, 2016). The advancement in that technology by using an anaerobic environment is called anaerobic membrane bioreactor (AnMBR), providing a promising enhancement in environmental aspects such as sludge handling, environmental friendliness, and energy production (Mei et al., 2016; Chen et al., 2019; Aslam et al., 2022). Anaerobic membrane bioreactors are advantageous in terms of full retention of the biomass, which stabilises the process and produces high-quality effluent. Conceptually, this is achieved by the separation of the hydraulic retention time (HRT) from the sludge residence time (SRT) and the flexibility of the operation control (Liu et al., 2018). This technology is implemented in different setups and configurations. With CSTR being the widely used setup for the bioreactor, other well-known configurations can be adopted with a membrane separation concept (e.g., UASB & AFBR). However,

UASB has an advantage over that technology due to its operational scheme of retaining the biomass at the bottom, resulting in a reduction in the fouling potential of the membrane (Aslam et al., 2022).

Configuration. Regarding the membrane configuration, there are two main modes: a side-stream or a submerged; and another integrated form can be constructed from these forms. A side-stream configuration places the membrane outside the bioreactor, by which the mixed-liquor is retained, and permeate water can be collected. Alternatively, the submerged mode of membranes conducts the separation step within the bioreactor volume. For the integral of both modes, an externally-submerged configuration is adopted by using a membrane within a tank but outside the reactor's main body. The advantage of such integration is related to maintenance and the applicability of isolating the membrane without disturbing the main biomass (Aslam et al., 2022); more insights about the setup and configuration are described in Figure (4).

Phenolic Application. As being addressed for its robustness in terms of contaminant removal & the stability of operation, AnMBR technologies are taking momentum in the investigation field. Despite that, very few researches were published on such an application in the phenolic compounds' removal, and most of them investigated the extreme conditions of operation (Muñoz Sierra et al., 2017; Muñoz Sierra et al., 2018(a); Muñoz Sierra et al., 2018(b); Muñoz Sierra et al., 2020), while in others co-metabolism was the highlight (García Rea et al., 2020; Garcia Rea et al., 2022). Muñoz Sierra et al., 2018(a) investigated the impact of harsh environment represented in an increasing pattern of the system salinity in an AnMBR; then, a modified version was conducted by adapting the setup to a thermophilic environment (Muñoz Sierra et al., 2020). García Rea et al. (2020) continued the research by searching for methods to enhance the removal efficiency by the supplementation of other carbon & energy sources. More recently, the investigation was further extended to include a mixture of phenol and p-cresol/ resorcinol as a stream influent to explore the inhibitory impacts of the compounds on the biomass (Garcia Rea et al., 2022). In an assessment with the UASB technology, AnMBR showed enhanced removal characteristics and resilience to extreme conditions, highlighting its promising potential compared to other technologies (Muñoz Sierra et al., 2019).

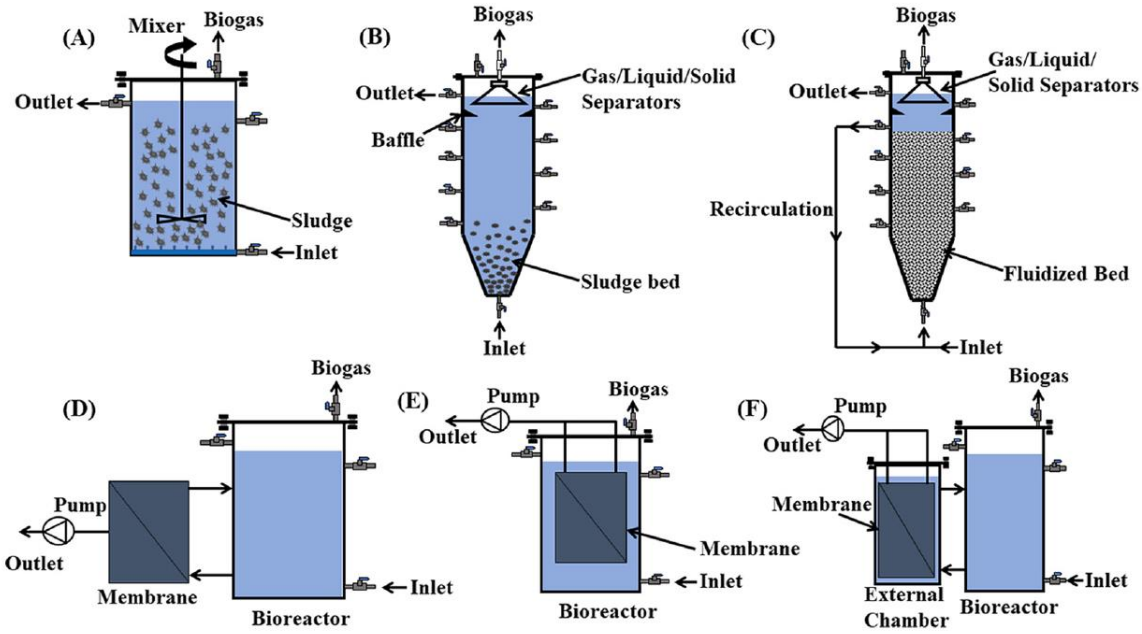

Figure (4): Common setup of anaerobic bioreactors such as completely stirred tank reactor 'CSTR' (A), upflow anaerobic sludge blanket 'UASB' (B), anaerobic fluidized reactor 'AFBR' (C); and the applicable membrane configuration: side-stream (D), submerged (E)), externally submerged (F) (Aslam et al., 2022)

2.3 Interspecies electron transfer

2.3.1 Process description

In anaerobic degradation, it is reported that acetogenesis and methanogenesis are the limiting-step that influence the performance of the whole process; This is due to their slow growth rate, inefficient syntrophic interaction, and their sensitivity to their environment (Wang et al., 2021). Within this phase, several factors lead to the failure of the process, such as the accumulation of volatile fatty acids (VFAs), the inhibition of toxic substances towards methanogens, and the disturbance in the interspecies electron transfer (Baek et al., 2018; Xu et al., 2019). To illustrate the role of electron transfer, a network between interspecies is conducted between fermentative (syntrophic) bacteria and methanogens to transfer electrons; two routes establish this network. The first route depends on hydrogen (or formate) as an electron shuttle for transferring electrons. This hydrogen is produced initially by the reduction of protons, which is then consumed by methanogens. This mechanism is referred to as indirect interspecies electron transfer (IIET) or as recently been labelled as hydrogen interspecies electron transfer (HIET). (Mcinerney et al., 2009; Stams & Plugge, 2009; Xu et al., 2019). One main problem with this mechanism is that the H2 reaction is unfavourable in standard conditions, and its initiation is highly dependent on the abundance of efficient hydrogen scavengers (e.g., methanogens) (Xu et al., 2019). The other route does not include mediators to work but, instead, a direct flow of electrons; thus, this method is commonly referred to as direct interspecies electron transfer (DIET). The transfer of electrons in this route is conducted by membrane cytochromes, conductive pili, or even conductive materials, schematically presented in Figure (5). DIET is reported to be a more favourable pathway for methanogens electron transfer than HIET, considering that this process is independent of hydrogen/formate concentration, so there is no energy needed for their formation (Xu et al., 2019; Wang et al., 2021). Thus, it was noted that DIET has a rapid electron transfer scheme, is thermodynamically feasible, and energy efficient, making it incorporated within several anaerobic sub-process (e.g., methanogenesis) (Lin et al., 2017; Mei et al., 2018; Wang et al., 2021). Wang et al. (2021) proceeded to review the independence of the DIET on hydrogen, as well as the applicability of the mechanism thermodynamically (Gibbs energy); a graphical representation of this review is presented in Figure (6).

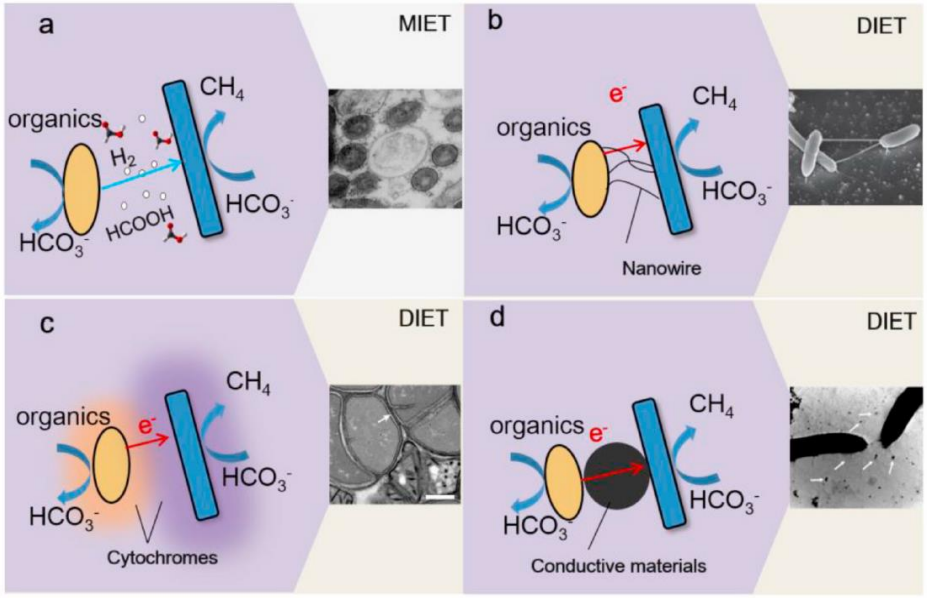

Figure (5): Schematic presentation of the proposed models of interspecies electron transfer mechanisms, describing the syntrophy between fermentative bacteria and methanogen; via (a) hydrogen/ formate, (b) nanowires (proposed model for pili-like structures), (c) cytochromes, (d) conductive materials (Wang et al., 2021).

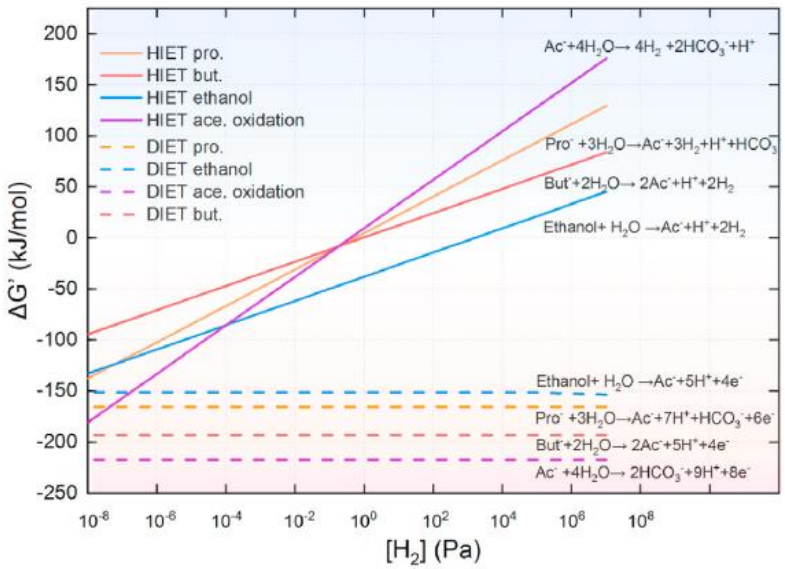

Figure (6): Thermodynamics of Organic acids (VFAs) oxidation and their dependence on the hydrogen partial pressure for the hydrogen and direct electron transfer mechanisms (HIET & DIET) (Wang et al., 2021).

2.3.2 Direct Interspecies electron transfer (DIET)

DIET connections are considered biogenic structures and are comprised of c-type membrane cytochromes and appendages-like-pili. And due to its potentials, the addition of conductive materials is also investigated as an external influence (a physical mechanism). Conductive and semi-conductive (e.g., iron oxides, magnetite) are reported to stimulate microbial interaction and progress the reaction rate relative to degradation and methane production. And due to their high conductivity, they are reported to be more effective than biological and carbon-based materials (Wang et al., 2021). In addition, research proposes that it helps with enhancing the process stability, resilience to harsh operational conditions, and shortening the initial lag time (Park et al., 2018; Martins et al., 2018; Xu et al., 2019). This process enhancement comes mainly from avoiding one of the main operational problems; VFA accumulation. As DIET enhances acetogenesis/ acetate oxidation/ methanogenesis, the VFA rate of conversion becomes more consistent, and thus the anaerobic process failure is avoided (Wang et al., 2021). To add, several authors suggested different models for the DIET mechanism; Appendix (4) represents the proposed schemes of those models. Moreover, several mechanisms can also work simultaneously. Working groups of nano-wires with cytochromes and cytochromes with conductive materials are suggested. DIET could also work in parallel with the hydrogen-induced transfer (HIET) to boost the overall transfer (Wang et al., 2021). On the other hand, Ueki et al. (2018) demonstrated that pili are essential for the cytochrome-based mechanism, while it is argued to be independent the other way around (Wang et al., 2021). Magnetite, as a strong candidate for conductive materials, was also reported for its stimulated DIET in the anaerobic degradation process and methane production (Yan et al., 2018; Peng et al., 2018), and its range of enhancing mechanisms either by DIET or by stimulating dissimilatory-iron reduction; under the presence of ferrous/ferric phases (Wang et al., 2021). Moreover, its reported magnetic properties, recyclability in operation (Baek et al., 2017), abundance, and relatively cheap cost (Wang et al., 2021) would make it preferable over others.

Application. A range of investigations was reported as a DIET-related application, relating different species with the ability to adapt to an induced DIET through conductive/semi-conductive material. Kato

et al. (2012) investigated the stimulation of electron transfer by magnetite nanoparticles and through an acetate-oxidation reaction between Goebacter with denitrifiers. Granular activated carbon (GAC) was also reported to enhance electron transfer between Geobacter metallireducens and Methanosarcina barkeri (Liu et al., 2012). Thus, the presence of Geobacter species is used to indicate and highlight the stimulation of the DIET process, such as Geobacter metallireducens, Geobacter sulfurreducens, and Geobacter hydrogenophilus, but not Geobacter bemidjiensis; along with Methanothrix strains (Methanothrix thermophile, Methanothrix concilii, and Methanothrix harundinacea) (Wang et al., 2021). However, a PCA analysis was conducted by Wang et al. (2021) to demonstrate that there was no direct relation between the DIET stimulation via conductive material and the abundance of Geobacter; instead, a correlation could be concluded with Methanosarcina species. The system substrate is also reported to affect the DIET process, as well as the active microbial strains; ethanol is utilised over glucose, propanol & butanol over propionate & butyrate as well (Wang et al., 2016; Li et al., 2018). Thus, more investigation is needed to understand this phenomenon and explore the range of substrates and their related microbial activity (Wang et al., 2021).

Phenolic Application. In a study investigating a synergetic impact of magnetite with zero-valent iron (ZVI), the authors observed that the combination of both materials induced an enhanced phenol degradation rate & cumulative methane production compared to magnetite only, ZVI only and control cases. Magnetite was argued to enhance phenol and benzoate degradation rates more than ZVI (in a methanogenesis-inhibited environment), but insignificantly. In addition, magnetite impacted the acetoclastic methanogenic and the homoacetogenic pathway, enhancing the conversion rate (He et al., 2019). Moreover, Jung et al. (2022) investigated the anaerobic degradation of phenol and benzoate with magnetite supplementation in a sequential batch experiment. The results showed a significant change in methane production rate and, thus, degradation in the case of magnetite addition for the phenol case. The change here, corresponding to a change in the methanogenic activity, was argued to be from the magnetite-induced DIET effect. On the other hand, there was an insignificant change for benzoate, which was accounted to the ease of degradation of that compound in the first place compared to phenol. The authors also performed a non-metric multidimensional scaling (NMDS) analysis, in which it proved that the magnetite induced a microbial shift in the active species, favouring species that can positively make use of the presence of the conductive material (e.g., magnetite) to enhance their conversion rate when the reaction is slow (Jung et al., 2022).

2.4 Membrane Fouling control

One of the major problems arising in membrane-related setups is the matter of fouling which reduces the quality of effluent and the filtration process's overall performance (Aslam et al., 2022). The fouling phenomenon results from different components deposited on the membrane surface. This could be identified by a steep increase in the transmembrane pressure (TMP), resulting in a throttled flux of the membrane, loss of energy, and efficiency (Xu et al., 2013; Deng et al., 2014). Regarding the fouling condition, the fouling phenomenon can be reversible or irreversible, or even a condition of both. Fouling that can be removed by physical means is referred to as 'reversible' ones, while fouling based on clogged pores that require a special form of treatment (e.g., chemical cleaning) is referred to as 'irreversible' fouling. Generally, the fouling is caused by pore blocking, cake layer development, organics adsorption, or concentration polarisation (Lin et al., 2010; Aslam et al., 2022). In-depth, solutes, colloids, cells (and others) are considered foulants, which contribute to different fouling mechanisms depending on their size. For example, if their size becomes smaller than the membrane pore size, they will induce pore-blocking, which in return and with the help of other foulants (EPS, flocs, etc.), will increase the potential of cake formation (Judd S., 2010; Chen et al., 2017).

Aslam et al. (2022) reported some strategies that could help in membrane fouling control, such as gas sparging & scouring, PAC and GAC fluidisation, electric field application, and physical/chemical cleaning. Santos et al. (2017) and Meng et al. (2009) highlighted the efficiency of combining chemical cleaning (acidic pH and sodium hypochlorite) and physical backwashing mechanisms, respectively, in retrieving membrane filtration capacity. However, it is highlighted that on a long-term basis, and even after using different strategies, part of the filtration potential will be irretrievable (Shahid et al., 2020). Concerning municipal wastewater treatment, the recent research conducted on sludge-related fouling investigated the potential reduction of such a phenomenon by modifying sludge and biomass characteristics and inducing scouring techniques (Liu et al., 2018)

As for the factors affecting the severity of fouling, operational factors are evaluated; mixed liquor suspended solids (MLSS), solid and hydraulic retention time (SRT & HRT), temperature, extracellular polymeric substance (EPS), soluble microbial products (SMP) and modes of operation are all different factors that impact the fouling condition (Le-Clech et al., 2006; Liu et al., 2018). For instance, Basile et al. (2015) noted that adopting a cross-flow as a mode of operation would help to reduce membrane fouling by inducing a higher flux/diffusion mechanism (Basile et al., 2015). Moreover, both SMP and EPS are microbial-related types of fouling, which are expected to be major contributors to AnMBR's fouling. EPS and SMP are macromolecules with three-dimensional porous forms, which are ideal for acting as a surface for cell attachment (Liu et al., 2018). EPS, in particular, is related to biomass's metabolic activity, besides excreted proteins & humic acid (Aslam et al., 2022). HRT and SRT are also included in fouling control. To illustrate, HRT reduction is reported to control SMP accumulation and further fouling. (Liu et al., 2018). Ouyang & Liu (2009) also experimented with varying the SRT (10, 40, no-sludge withdrawal), and it was found that the SRT of 10 days was the highest in terms of fouling, highlighting the potential of fouling reduction by increasing the solid retention again.

Relative to our scope, Sabalanvand et al. (2021) investigated the use of magnetite and silver nanoparticles for membrane fouling control in an MBR setup. The results showed that the nano-particles successfully enhanced the filtration flux and reduced its deterioration rate; the improvements were in the range of 30% & 40% for magnetite and silver, respectively. This was linked with the reduction in SMP and EPS values. They argued that these compounds were adsorped on the nano-particles and, thus, larger flocs were formed. This led to a more-porous cake layer on the membrane and, thus, a longer running time (Sabalanvand et al., 2021). Similar observations were reported by Zhou et al. (2019), where the additions of aluminium nitride enhanced the membrane permeability, TMP operating conditions, and membrane operation lifetime. The enhancement also included a delay in TMP building up and fewer cycles of cleaning needed over the experiment runtime (70 days). In addition, their argument about the source of the mitigation was also related to the decrease in EPS & SMP concentrations, and mainly polysaccharides by the supplementation of nano-particles. And other more research that investigated nano-particles on membrane-like technology and their effect on fouling mitigation, opening the door to a promising application in the future (Rezaei & Mehmia, 2014; Hazrati et al., 2018).

3 Experimental plan

3.1 Experimental setup

In order to better understand the impact of magnetite, the experiment was divided into two separate phases with different loading conditions; phase (I) and phase (II). In each phase, (2) identical modules of bioreactors were used, each of a total volume of 7 litres, and these reactors were equipped with an ultrafiltration membrane installation; more details about the membrane are presented in Table (1). These bioreactors had a theoretical working volume of 6.25 ± 0.25 L, labelled AnMBR-C& AnMBR-M. The mixed liquor was maintained at a specific temperature of 35± 1 ºC by using a water-bath system that keeps water recirculation in the reactor double wall. Moreover, the setup of each reactor had three flow pumps (feed, effluent, and recirculation) to control the flow.

The pressure was mainly monitored from the membrane installation side, whereas three sensors were installed on the influent, concentrate, and permeate (AE sensors, NL). These sensors had a pressure range between (-800 and +600 mbar) to capture normal positive pressure of operation and possible negative ones during backwashing. Similar sensors (of range 0~100 mbar) were also used to measure the pressure in the body of the main reactor (Garcia Rea et al., 2022). Through this system of sensors and as the membrane has a constant flux operation, the membrane's Transmembrane pressure (TMP) could be monitored, and the membrane condition and fouling status could be evaluated. Through a recirculation scheme, the membrane extracted the permeate stream, and a more concentrated stream of mixed liquor was to be retained and recirculated back to the reactor to stimulate a mixing process inside the reactor. A gas recirculation pump was also installed to recirculate the produced biogas from the headspace into the mixed liquor to enhance the mixing. On the other hand, the permeate was separated after the membrane and collected separately for analysis; the membrane installation worked with a cross-flow of 1 m/s as adopted by Garcia Rea et al. (2022). The schematic diagram of the setup is illustrated in Figure (7).

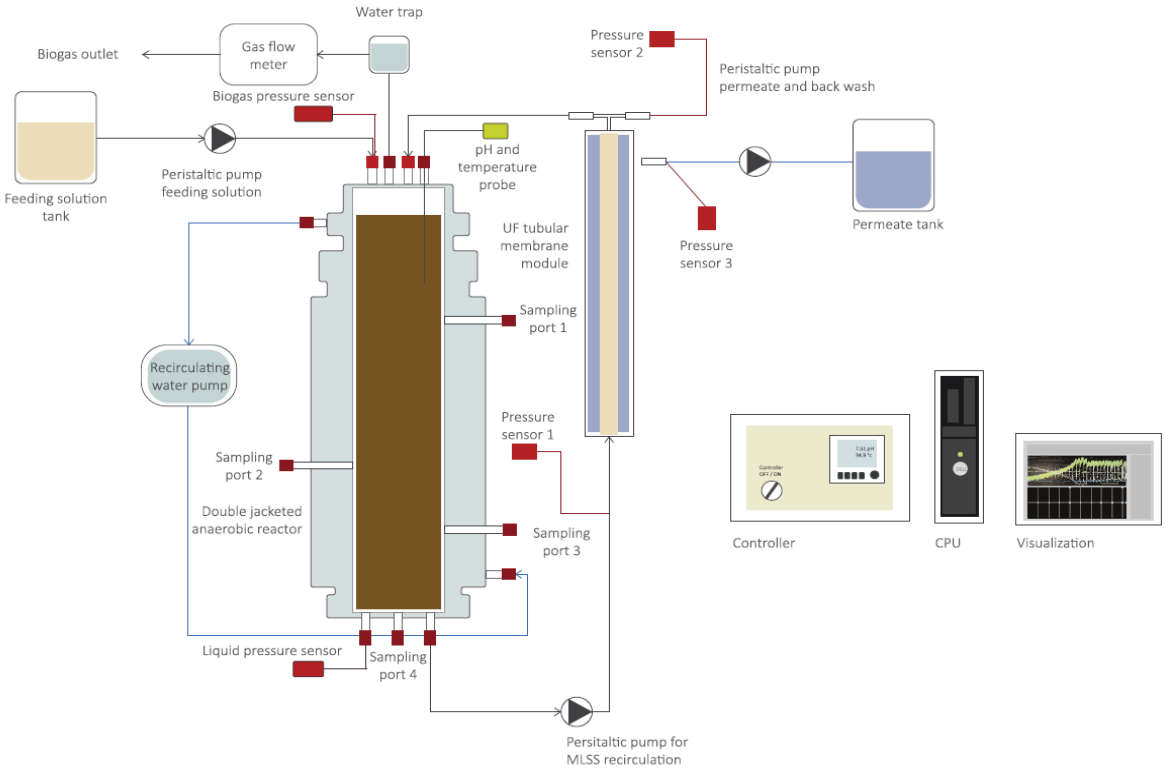

Figure (7): The Experiment setup of the AnMBR used with the schematic connections (Garcia Rea et al., 2022)

AnMBR-M was conducted as the main experiment by which magnetite was induced to enhance the degradation of both phenol and p-cresol. At the same time, AnMBR-C was the control experiment in which the degradation was achieved without magnetite supplementation. The biomass was retrieved from an industrial wastewater treatment facility (UASB) from Shell (Moerdijk, NL) that was acclimatised to only benzoate and acetate. Before the operation, both reactors started with biomass acclimatised on 200 mg/l phenol and 200 mg/l p-cresol, prepared in a previous start-up phase. Phase (I) had an initial VSS concentration of 5.83 ± 0.22 gVSS/L for AnMBR-C, compared to 5.77 ± 0.19 for AnMBR-M. In contrast, phase (II) had an initial value of 3.81± 0.12 gVSS/L for AnMBR-C and 3.37± 0.08 gVSS/L for AnMBR-M. Similar to Garcia Rea et al. (2020), the feed constituent had an acetate-compounds in the form of sodium acetate-trihydrate (Sigma Aldrich, USA) supporting the biomass with an equivalent of 1 gCOD/L. Additionally, sodium butyrate (Sigma Aldrich, USA) was added for an additional 1 gCOD/L supply of substrate, constantly supporting the reactor with a total of 2 gCOD/L of readily biodegradable carbon/ energy sources (CES); besides the loading conditions of the bioreactors with phenol and p-cresol on different stages, which is further described in Table (2). More insights about the operational conditions are presented in Appendix (5).

Essential nutrients and buffers were also fed to the reactor; micronutrients, macronutrients, phosphate buffer (A)& (B), and yeast extracts were introduced with the relative ratios of 0.76 mL, 1.5 mL, 2.2 mL, 3.4 mL, 50 mg per each g COD in the feed (Hendriks et al., 2018; Muñoz Sierra et al., 2018(a); García Rea et al., 2020); more details are described in Table (3). In addition to that, the TDS of the reactor was kept within the same order of magnitude, as adopted by Garcia Rea et al. (2022), but with a slight change by keeping the Na^+ concentration at 6 g/L for phase (I) and 6.5 g/L for phase (II), in which equivalent amounts of sodium chloride were added. The consideration of salinity in the experiment was regarded for its limited impact on the anaerobic process. Salinity inhibits biomass presented in salt stress, which hinders enzyme production, hampers cell activity, and influences plasmolysis (Dereli et al., 2012). More specifically, sodium was proven to affect acetoclastic methanogens activity (Rinzema et al., 1988).

The concentration of magnetite that was adopted in AnMBR-M was based on the VSS concentration. Two of the most recent research represented by Jung et al. (2022) and He et al. (2019) experimented the use of magnetite (as Fe_3O_4) to degrade phenol, and the used dosage was 6.66 and 6.52 mmol magnetite/ gVSS. Another previous research used a slightly higher ratio to deal with the phenol degradation process, inducing a dosage of 1.75 g magnetite/ g VSS (~7.5 mmol magnetite/ gVSS) (Yan et al., 2018). Based on those research, it was decided to adopt a dosage within the same range, making a total concentration of about 40.0 mmol magnetite (Fe_3O_4)/ L for phase (I) and 20.0 mmol magnetite (Fe_3O_4)/ L for phase (II). The added magnetite was a Sigma-Aldrich product of size (50-100 nm) representing an ultrafine size range, which is the range bigger than the nano-range (<20 nm) (Kohli, 2015), however, other references define the range of (1-100 nm) as nanoparticles (Lee & Lee, 2019).

Table (1): Installed membrane characteristics for the continuous flow experiment of the AnMBR (Garcia Rea et al., 2022)

Items	Unit	AnMBR-C /M
Ultrafiltration Pore size	nm	30
Module Type	-	PVDF module (Pentair, NL)
Flow scheme	-	inside-out
Length	cm	64
Diameter	cm	0.52
Cross-flow velocity	m/s	1 (~1830 L/d)

Table (2): The feed flow and the influent concentration regarding phenol and p-cresol for the continuous flow experiment and the corresponding volumetric loading rate

Phase	Stage	Estim. Days of operation	Feed flow (L/d)	Phenol		P-cresol	
				concent. (mg/L)	vLR * (mg /L/ d)	concent. (mg/L)	vLR * (mg /L/ d)
Phase (I)	Stage I	0-16	1	200	32.0	200	32.0
	Stage II	17-30	1	300	48.0	300	48.0
	Stage III	31-44	1	400	64.0	400	64.0
	Stage IV	45-58	1	600	96.0	600	96.0
	Stage V	59-73	1	900	144.0	900	144.0
Phase (II)	Stage V-a	83-86	0.4	900	57.6	900	57.6
	Stage V-b	87-90	0.6	900	86.4	900	86.4
	Stage V-c	91-100	0.8	900	115.2	900	115.2
	Stage V-d	101- 114	1	900	144.0	900	144.0
	Stage VI	115-126	1	1200	192.0	1200	192.0
	Stage VII	127-143	1	1600	256.0	1600	256.0

Table (3): Nutrients and buffer concentrations adopted in the experiment (García Rea et al., 2020)

Nutrients		Conc. (g/ L)	Nutrients		Conc. (g/ L)
Macro-Nutrients (1.5 mL/g COD)	NH_4Cl	170	Micro-Nutrients (0.76 mL/g COD)	EDTA-Na_2, $ZnCl_2$	1, 0.05
	$CaCl_2.2H_2O$	8		$MnCl_2.4H_2O$	0.5
	$MgSO_4.7H_2O$	9		$FeCl_3.6H_2O$	2
Buffer A (2.2 mL/ gCOD)	$K_2HPO_4.3H_2O$	45.6		$NiCl_2.6H_2O$, H_3BO_3	0.05, 0.05
Buffer B (3.4 mL/ g COD)	$NaH_2PO_4.2H_2O$	31.2		$CuCl_2.2H_2O$	0.03
Yeast (mg / g COD)		50		Na_2SeO_3, Na_2WO_4	0.1, 0.08
				$(NH_4)_6Mo_7O_2.4H_2O$	0.09
				$CoCl_2.6H_2O$	2

3.2 Sampling and Analysis

A working plan was developed to accurately maintain a well-defined record of the process operation regarding sampling and analysis. Gas, feed, permeate flows, and the operational conditions and parameters (pressure, temperature, etc.) were recorded daily for the whole working operation time plan. Generally, the collected samples were analysed in triplicates to reduce the impact of measurement errors. Biogas samples of 10 mL samples were collected every 2 days, and the analysis was conducted on the days in between, by which a gas chromatograph (Agilent Technology) was used for the analysis. The model used for the gas analysis is Agilent 7890A equipped with a thermal conductivity detector (TCD) with an (HP-PLOT Molesieve) column (19095P-MS6) with dimensions of 60 m × 530 µm × 20 µm (Garcia Rea et al., 2022). The analysis method is dependent on a gas carrier, by which Helium was used. The carrier total flow rate was 23 mL/min and a split ratio of 1:1 at a pressure of 14.8 psi and septum purge flow of 3 mL/min. The oven temperature and the detector were kept at 45 and 200 °C, respectively. For the TCD, the utility and makeup flows were kept at 30 and 5 mL/min, respectively. The analysis running time was evaluated at 10 min per sample.

The reactor pH and electrical conductivity were also observed weekly by measuring them from the biomass samples. pH is considered a good indicator if there is instability in the process and an

accumulation of volatile fatty acids (VFA). In addition, the chemical oxygen demand (COD) of the permeate, sludge and feed were monitored by HACH Kits and spectrophotometer, and the measurements were conducted frequently to monitor the concentration levels. Dilution of samples was also considered to avoid the interference of some compounds with the analysis (e.g., Cl^-).

VSS/TSS measurements were conducted biweekly to record the concentration in the main bioreactor volume, by which a volume of 15 mL was extracted. The measurement was conducted by preparing filter paper in an aluminium dish, burning it at 550 ºC to remove contaminants and then recording the dish weight. After that, mixed liquor samples of 5 mL were transferred to each plate through a vacuum process and then moved to a 105 ºC oven for more than 12 hours to remove any residual water. Then, the plates were removed, the weights were measured, and the total suspended solids (TSS) were evaluated. After that, furnacing the sample again at 550 ºC and the weight loss would be attributed to the loss in volatile suspended solids (VSS).

3.2.1 Phenolic Compounds and VFA

High-performance liquid chromatography (HPLC) (SHIMADZU) and GC (Agilent Technology) were used to analyse the phenolic compounds and volatile fatty acids (VFA) constituents, respectively; this sampling frequency was recorded 3 times a week for the permeate and once for the sludge. Sludge samples of 20 mL were collected for the COD, GC, and HPLC analysis. The feed was prepared by the end of the week after checking the removal efficiency (from GC & HPLC) to increase the organic loading rate.

As part of the anaerobic degradation process**, GC (VFA)** was used for the measurement of phenol, p-cresol and volatile fatty acids. Samples of 750 µl were prepared with 750 µl of 1-pentanol (320 mg/l) and 10 µl of formic acid (95%); according to the protocol (García Rea et al., 2020). The equipment model used was Agilent 7890A, supported with a flame ionisation detector (FID) and an (HP-PLOT/U) capillary column of dimensions (25 m x 320 mm x 0.5 mm) (García Rea et al., 2020). The analysis method used Helium as a carrier gas with a total flow rate of 45 mL/min. The oven, inlet and detector temperatures were maintained at 180, 225 and 240 ºC, respectively. The pressure of the inlet was kept at 11 psi with a 3 mL/min septum purge flow. On the other hand, the fuel flow of the detector, the utility flow and the makeup flow were kept at 30, 400 & 10 mL/min, respectively. The running time was chosen to be 14.7 min relative to the needed retention time of these compounds.

On the other hand, **HPLC** was conducted mainly to monitor 4-Hydroxybenzoic acid (4-HBA) and benzoate (the two main intermediates in the degradation process). In this analysis, a sample of 1.5 mL was prepared with 10 µl of formic acid (95%). The equipment was supported with a (Nucleodur 100-3 CN-RP) column, a Macherey-Nagel product, with dimensions of 125 mm and 3 mm for length and internal diameter, respectively. The analysis was conducted by two UV detectors, by which the first detector was working at a wavelength of 269 nm, addressed for 4-HBA detection. On the other hand, the other detector was operating at 225 nm of wavelength to detect benzoate. The measuring phase was conducted with a 0.4 mL/min flow with a starting concentration of 5% (v/v) acetonitrile. The addressed samples were collected from the filtered supernatant of the sludge and the permeate. In addition, the filtered supernatant was prepared by centrifuging the sludge sample on 18500 g for 10 mins (under standard temp. of 20 ºC), then filtered through 0.45 µm filters (Chromafil Xtra).

3.2.2 Specific Measurements

Other analyses that were conducted through the experiment included iron measurement, particle size distribution (PSD), and SMP/EPS. To begin with, Fe (II) was measured in the sludge to have some insights if the dissimilatory mechanism of reduction of Fe (III) to Fe (II) was contributing to the DIET process (Baek et al., 2017). Fe analysis was conducted biweekly to keep track of any changes in the iron (II) concentration. PSD and SMP/EPS were analysed with minimal withdrawal to maintain a constant sludge concentration throughout the loading phase.

SMP/EPS. Sludge samples (15 mL) were taken for SMP/EPS measurements, including protein and carbohydrates, to see the impact of magnetite on sludge characteristics and if there was a relationship between that and membrane fouling. The soluble microbial products and the extracellular polymeric substance were extracted by the mild-harsh heat method (Li & Yang, 2007) according to the protocol described by Guo et al. (2020). Firstly, a sample of mixed liquor was extracted from the bioreactor and centrifuged at 15,000 g at 4 ^{o}C for 15 min. The supernatant was collected and was later addressed as the SMP. The pellets/ concentrate was resuspended to their original volume using a 0.05% NaCl (w/v) and forming a sample with a temperature of 50 ^{o}C. For the extraction of the EPS, another cycle of centrifugation at 15,000 g and 4 ^{o}C (10 min) was adopted, by which the loosely bound EPS (LB-EPS) were acquired from the supernatant. Another resuspension of the concentrate with the 0.05% (w/v) NaCl was conducted; however, the solution was heated in a water bath for 30 mins while being stirred at around 400 rpm; the temperature was maintained at 60 ^{o}C. The supernatant, resembling the tightly bound-EPS (TB-EPS), was collected after centrifugation at 15,000 g and 4 ^{o}C for 15 min. In each of these samples, protein and carbohydrates were measured.

Protein was measured using a BIO-RAD kit adopted based on the Bradford assay method, where Brilliant Blue G-250 dye was used as a reagent with proteins. Bovine Serum Albumin (BSA) was used as the standard solution for the process calibration, by which samples of concentrations of 2, 1.5, 1, 0.75, 0.5, 0.25, and 0.125 mg/mL were used (Appendix (6B)). As described in the manual protocol, 100 µL of samples were used with 5 mL of dye reagent, then mixed, incubated for about 10-15 min at room temperature and analysed. A spectrophotometer was used to analyse the colour absorbance of the samples on a wavelength of 595 nm (BIORAD). On the other hand, carbohydrates were measured using the phenol-sulfuric acid method (colourimetric method), by which a calibration curve, conducted from a standard solution of different concentrations, was first produced (Appendix (6C)). Glucose (Sigma Aldrich, USA) was used as the standard for that process. As described by Zuriaga-Agustí et al. (2013), a sample of 1 mL was added to a mixture of 1 mL phenol (5%) with 5 mL of sulfuric acid (95%). The solution was left for 10 min to react, then it was mixed well through vertexing and again left at room temperature for 30 min. A spectrophotometer was used to analyse the colourimetric characteristics of the sample, by which the measurements were conducted on a wavelength of 490 nm (Dubois et al., 1956).

Particle size Distribution (PSD). Particle size distribution analysis was conducted, by extracting a 1 mL sludge sample, to give insights into the change in mixed liquor size under the effect of magnetite and to show if there was any agglomeration of biomass. The PSD was measured by a light scattering technology (laser diffraction) working within a range of 10.7 nm to 2000 µm. The analysis was conducted by a BlueWave-Microtrac product with a sample delivery controller (SDC). The equipment was operated by a tri-laser with a 2-detector system. Regarding the analysis method, it is conducted in 60-sec runtime by a flow rate of 20% with (3) deaeration cycles and (6) rinses cycles. Water was used as the fluid medium with a refractive index of 1.33.

3.2.3 Batch Experiments

SMA. The specific methanogenic activity test (SMA) was conducted to compare the impact of magnetite on the rate of methane/biogas production, particularly on the acetoclastic methanogenesis. The inoculum used was taken from the reactors and returned after the test's end. The preparation was conducted in 160- & 300-mL bottles, including extracting biomass samples from the AnMBR and adding the substrate and nutrients until the working volume reached 90 mL. This test's volume was kept small to avoid huge fluctuations in the mixed liquor concentration inside the reactor. As described in the literature, the inoculum ratio to COD was advised to be (2); but with a modified version for that, the COD was prepared to be 1 gCOD/L with a final VSS of 1.5 g/L (Spanjers & Vanrolleghem, 2016). The nutrients, including micro-, macro-, buffers and yeast, were added based on the same ratios described previously in section (3.1) "Experimental Setup", as well as keeping the salinity conditions as the main reactors. Samples with and without substrate (blank) were prepared in triplicates. The working conditions for this reaction were kept at 35 ºC and mixed at 150 rpm. To stimulate anaerobic conditions, a nitrogen flushing stage was conducted to eliminate the residual oxygen in the bottles' headspace by performing a 5 min flushing cycle. The methane production was evaluated based on the headspace pressure measurements using OxiTops (Xylem/ WTW product) and the manometric method presented by Hafner et al. (2020). The maximum production rate was assessed based on the steepest slope of the reaction in a comparative manner with the blanks and the magnetite-supplementation case. The evaluation of such slope was based on Python-fitting the data to the modified Gompertz model (Eq.(1) & Appendix (16)). The model fitting was optimized by three parameters represented by the specific methane potential (A), the maximum rate (U) & the lag phase (λ); and presented as follows:

$$P = A.\exp\{-\exp[\frac{Ue}{A}(\lambda - t) + 1]\}$$

Eq.(1)

P: cumulative specific methane production gCOD-CH4/gVSS
A: specific methane potential (gCOD-CH4/gVSS)
U: maximum methane production rate (gCOD-CH4/gVSS/d)
λ: lag phase (days)
t: cumulative time for methane production (days)

*Adopted from (Budiyono et al., 2010)

P-cresol degradation. A batch test was conducted in phase (II) to assess the degradation rate of biomass from both reactors towards p-cresol. The test was conducted in 300 mL bottles with a working volume of 200 mL. The biomass concentration of the reactors was evaluated to be used in the calculation of the degradation rate. Depending on the dilution factor, the VSS concentration used in the calculation were 3.03 & 3.14 for C-reactors and M-reactors, respectively. The used substrate included p-cresol as the main C-source with the additional micronutrients previously described. Duplicates were made from each reactor, by which the initial substrate concentration for C-reactors was 396.9 ± 14.3 mgPcr/L and 382.0 ± 13.8 mgPcr/L for M-reactors, resembling an approximately 1 gCOD/L. The degradation pattern of the samples was fitted by a substrate degradation version of the modified Gompertz model to evaluate the behaviour of the biomass, as mentioned as follows (Eq (2)):

$$S = S_0.\left\{1 - \exp\{-\exp[\frac{R_m e}{S_0}(\lambda - t) + 1]\}\right\}$$

Eq.(2)

S: substrate concentration mgPcr/gVSS
S_0: initial substrate concentration (mgPcr/gVSS)
R_m: max. substrate conversion rate (mgPcr/gVSS/d)
λ: lag phase (days)
t: cumulative time for methane production (days)

*Adopted from (Li, Gu, & Pan, 2005)

Magnetite Adsorption Capacity. An assessment of the adsorption capacity of magnetite was conducted, by which the adsorption of protein and total carbohydrates content were the objectives. Samples from the C-reactor's EPS-TB were taken for the experiment, whereas several dilutions were tested with 20 and 40 mmol/L magnetite concentrations. The equilibrium results were evaluated using adsorption isotherms (q_e & C_e) and fitted using Langmuir (Eq.(3)) and Freundlich models (Eq.(4)) (Abin-Bazaine et al., 2022). The best fit of the nonlinear form would be the main criteria for the selection of the models, and they are described as follow:

Langmuir isotherm model	**Freundlich isotherm model**
$q_e = \frac{q_m K_L C_e}{1 + K_L C_e}$ Eq.(3)	$q_e = K_F . C_e^n$ Eq.(4)
C_e: equilibrium concentration of adsorbate q_e: adsorption capacity at equilibrium (mg/g) q_m: maximum adsorption capacity (mg/g) K_L: Langmuir constant (L/mg)	C_e: equilibrium concentration of adsorbate q_e: adsorption capacity at equilibrium (mg/g) n: Freundlich exponent (in other references 1/n) K_F: Freundlich's constant (mg/g)

*Adopted from (Abin-Bazaine et al., 2022)

3.2.4 Statistical Analysis

T-test is a statistical significance test based on the comparison of means with the assumption of the same variance, and it could be further modified to different variance values, referring to Welch's t-test. False conclusions could exist within the analysis in multiple forms. Type (I) errors are related to the significance level (α), which describes a false positive or rejecting the null hypothesis while it's true. The probability of type (I) existence is the significance level (α). On the other hand, Type (II) errors are related to the statistical test power (1-β), which describes the false negative or, in another context, accepting the null hypothesis while it's wrong; Type (II) error calculation is based on (β) (Nakagawa & Cuthill, 2007). In addition, the significance level (α) and (β) are related in that the likelihood of Type (I) is inversely proportional to the probability of Type (II) (Mudge et al., 2012).

As in some parts of this research, we had to deal with small sample sizes; we had to consider the false conclusions that could be drawn because of that. According to the literature, the definition of a very small sample size is that of a size less than 5 ($N \leq 5$). Moreover, it is known that having small-size samples would have low power and thus a higher probability of having a type (II) error (de Winter, 2013). It should also be noted that t-tests are based on the assumption that the sample sets are normally distributed, which could be hard to test in small sets. And for that, several researchers addressed using non-parametric tests instead of the normal parametric t-test (de Winter, 2013). However, for the validity of the test, de Winter (2013) showed that the usage of the t-test is feasible with small sets (N=3) under the condition of a large effect size ($D \geq 6$).

To reduce the type (I) and (II) potential errors, Mudge et al. (2012) suggested a procedure that depends on determining the critical size effect, minimising the combined probabilities (ω), and producing a (ω vs α) relationship, in which the optimum significance level could be selected (Eq.(5)). The critical size effect will be addressed from Cohen's (d), and for simplification, a statistical software will be used for that (Nakagawa & Cuthill, 2007), while the combined averaged probability (ω) is described as (Mudge et al., 2012):

$$\omega = \frac{\beta + \alpha}{2} \quad \text{Eq.(5)}$$

It should be noted that this procedure was only adopted for cases where we have a small number of data ($N \leq 5$), where it would be expected to have relatively high type (II) errors; while in other cases, the ordinary Welch's t-test of unequal variance will be adopted with a significance level (α=0.05) (Mudge et al., 2012). For ease of use, Excel was used to analyse the basic characteristics of the data in terms of mean, variance, and typical t-test values (Welch's t-test). In contrast, SPSS (IBM SPSS Statistics 28.0) was used for the more detailed analysis when the used sample was of small size with the previously described procedure. Some additional definitions are described in Appendix (7).

Methodology of analysis. The methodology of analysis and whether Excel or SPSS was used was depending on the conditions of the datasets that we were analysing. The first parameter to take into consideration was the dataset size if it was over 5 or equal/lower than 5. In case of a dataset size over 5, the normal t-test or the modified Welch's version was adopted depending on the variance condition; by which Excel was used. On the other hand, the effect size was analysed whether it's less than 6 or over/equal to 6; as for the latter case, a normal t-test/Welch could be used. But for values less than (6), the error (ω) vs significance level (α) was evaluated, and the optimum (α) was selected. And in comparison to the (p) of the t-test, the significance testing could be concluded; using SPSS. It should be noted that the effect size does not only differentiate which route to be taken, but also gives an indication about the magnitude of the significance that was concluded in the latter case. While finding the optimum (α) could highlight a significance of a test, the (d) value could emphasise whether this significance is small/neglected or not (Figure (8)).

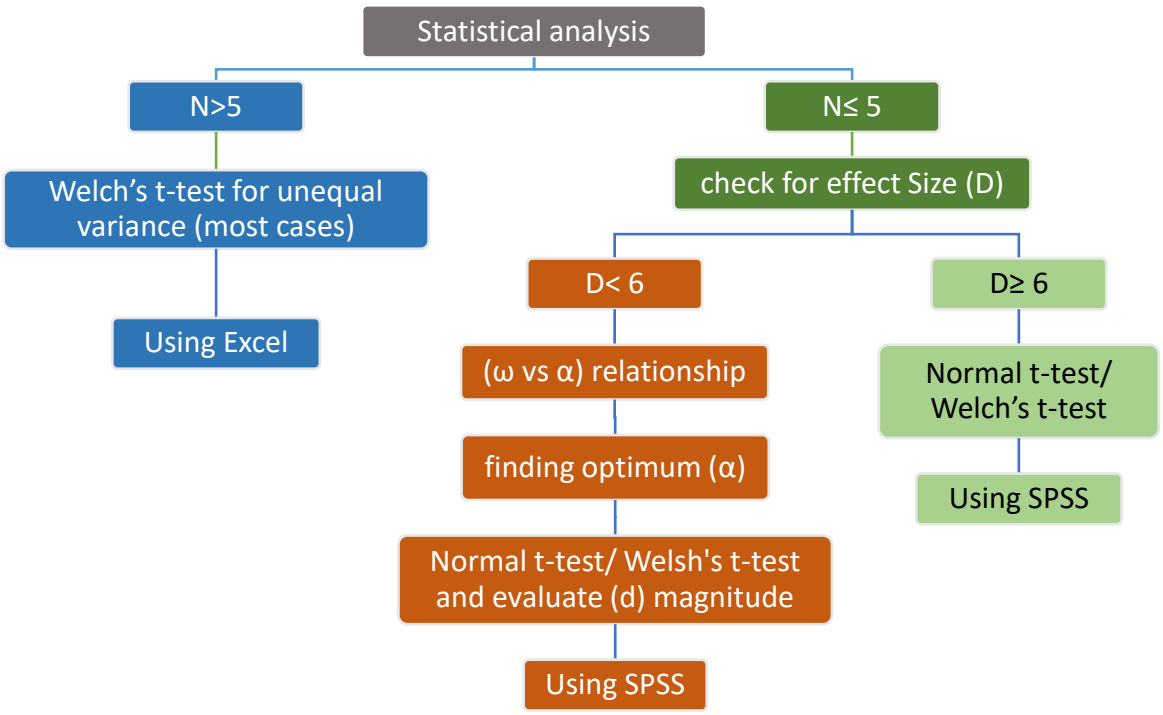

Figure (8): Methodology of using the statistical analysis that is mainly based on the dataset size and the effect size represented by Cohen's constant (d).

This summary was formulated based on the findings of Mudge et al. (2012) & de Winter (2013).

4 Results

4.1 Continuous Flow Experiment (AnMBR)

4.1.1 Reactors' working status

Phase (I). The operational parameters of both reactors were monitored and compared to eliminate any influence on the results that could be attributed to any change in the conditions. The pH of the reactors was kept around 7.09 ± 0.17 and 7.14 ± 0.16 for AnMBR-C and AnMBR-M, respectively (with no significant difference p>0.05; for Welch's t-test). The recorded pH and working volume of the reactors are presented in Figure (9). The fluctuations were maintained to have a minimum influence on the results and to be kept within the theoretical levels planned (6.25 ± 0.25 L) and addressed in the "Experimental Setup". The sludge retention time (SRT) for the whole phase of both reactors was calculated according to García Rea et al. (2020) and was evaluated at 754 days and 761 days for AnMBR-C and AnMBR-M, respectively. As mentioned in section 3.1, the VSS concentration of AnMBR-C was evaluated at 5.83 ± 0.22 gVSS/L, compared to 5.77 ± 0.19 for AnMBR-M on day-0. From day 36, the VSS concentration of AnMBR-C was observed to have lowered to an average value of 4.71± 0.07 gVSS/L until the end of phase (I). Similarly, within the same time frame, VSS concentration in AnMBR-M was around 4.80± 0.12 gVSS/L. Both reactors' VSS pattern seems similar throughout the experiment, and according to the optimised significance procedure, there was no significant difference between them (N1=N2= 5, d= 0.379, optimised α= 0.32, p=0.49, p> α, Appendix (8)); more details about the suspended solid's concentration is presented in Figure (10).

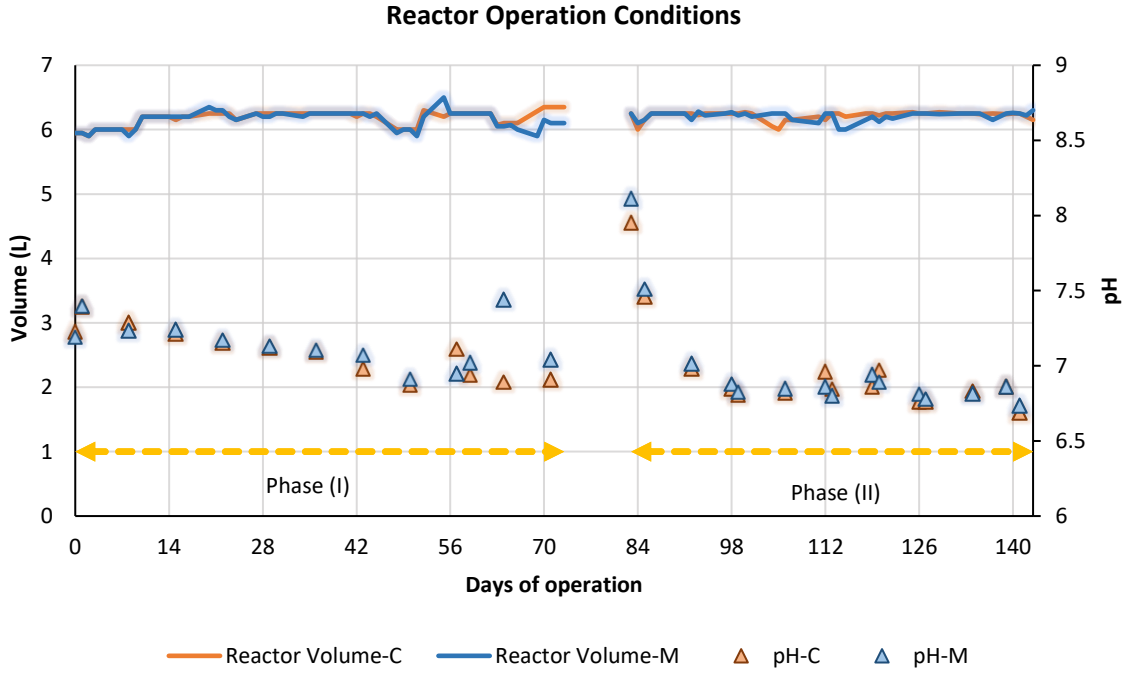

Figure (9): The pH and the working volumes of both reactors for phase (I) and phase (II)

Phase (II). After initiating the operation again in phase (II), the pH of both reactors started from a more alkaline point represented by 7.9 & 8.1 for AnMBR-C and AnMBR-M, respectively. This is mainly due to the declined acidic effect of the carbon dioxide released from the mixed liquor during sludge splitting and initialisation of the reactors; under the influence of the alkalinity. However, the pH of the reactors was 6.95±0.33 and 6.98±0.36 for AnMBR-C and AnMBR-M, respectively (with no significant

difference p>0.05; for Welch's t-test). Similar to phase (I), The evaluated SRT of both reactors was more than (600) days. For the initialisation of phase (II), the VSS concentration of AnMBR-C was 3.81± 0.12 gVSS/L, compared to 3.37± 0.08 for AnMBR-M on day 83. It should be noted that the sludge in phase (II) was collected from AnMBR-C by the end of phase (I) and split between both reactors, by which magnetite was resupplied to this new AnMBR-M sludge. Later on, during this phase, the VSS concentration of AnMBR-C was observed to have lowered to an average value of 3.49± 0.10 gVSS/L. Likewise, the VSS concentration in AnMBR-M was observed to be around 3.52± 0.02 gVSS/L. Furthermore, and similar to phase (I), the VSS concentration of both reactors seems to follow the same pattern, showing that there was no significant difference between them (according to the optimised significance procedure, N1=N2=5, d=0.120, optimised α=0.335, p=0.551, p>α, Appendix (8)).

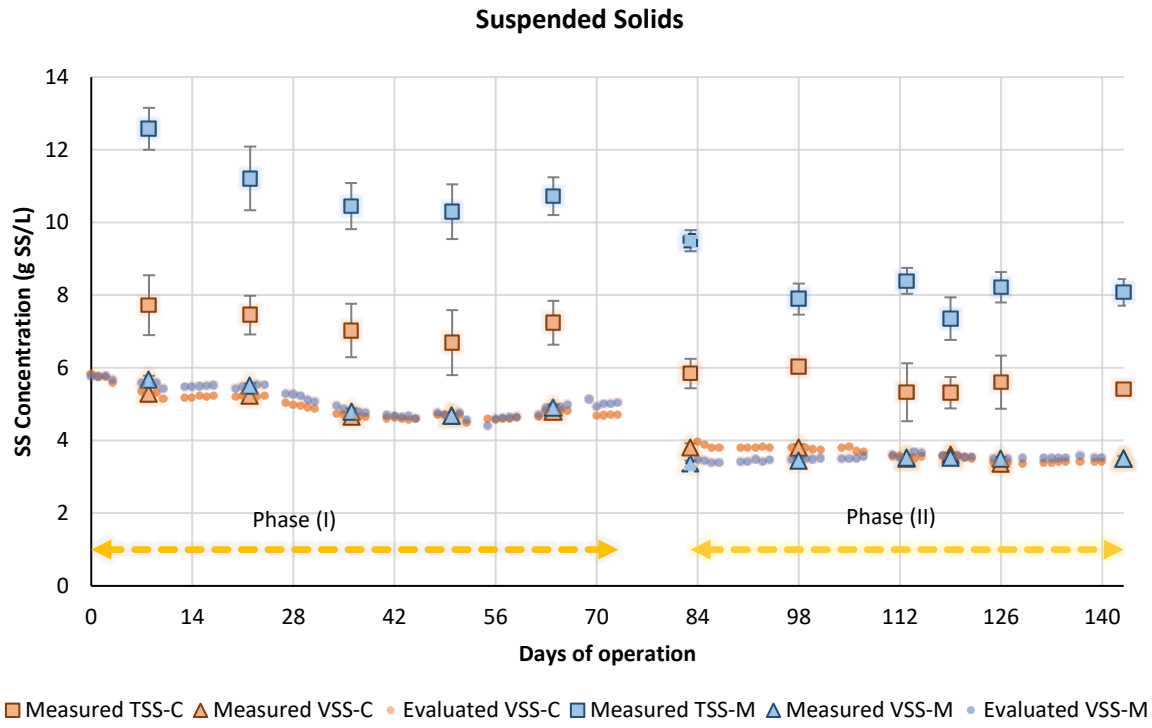

Figure (10): The suspended solids concentration (VSS & TSS) in both reactors for phase (I) and phase (II)
Note: The evaluated points in the VSS (g/L) is based on linear interpolation between the mass of VSS (g) divided by the volume of the reactor; subjecting it to any fluctuation in the level.

4.1.2 Loading conditions

Phase (I). As was mentioned in section 3.1, each loading stage took about 2 weeks before the next one was initiated. For AnMBR-C, stage (I) had an average working load of 87.1±8.0 mgCOD/ gVSS/d (5.8 mgPh/ gVSS/d & 5.8 mgPcr/ gVSS/d) corresponding to a COD removal of 94.8%. From day 17 to day 30, the average loading was 110.4 ±3.8 mgCOD/ gVSS/d (9.5 mgPh/ gVSS/d & 9.5 mgPcr/ gVSS/d) and then increased to an average of 138.0± 2.6 mgCOD/ gVSS/d (13.9 mgPh/ gVSS/d& 13.9 mgPcr/ gVSS/d) during stage (III). Regarding the COD removal, it was 97.2% for both stage (II) & (III). The loading reached 176.5 ±2.6 mgCOD/ gVSS/d (21.4 mgPh/ gVSS/d & 21.4 mgPcr/ gVSS/d) and 221.3± 2.2 mgCOD/ gVSS/d (31.1 mgPh/ gVSS/d & 31.1 mgPcr/ gVSS/d) during both stage (IV) and (V), respectively. The COD conversion seemed stable during these last two phases, with an average removal >98% for both.

Similarly, for AnMBR-M, the average loading rate was 86.6 ±6.3 mgCOD/ gVSS/d (5.8 mgPh/ gVSS/d & 5.8 mgPcr/ gVSS/d) for stage (I), then increased to 104.4± 2.5 mgCOD/ gVSS/d (9.0 mgPh/ gVSS/d & 9.0 mgPcr/ gVSS/d) in stage (II) and 134.8±5.9 mgCOD/ gVSS/d (13.6 mgPh/ gVSS/d & 13.6 mgPcr/ gVSS/d) in stage (III). The corresponding average COD removal was 95.4%, 97.7%, and 97.7% for stages (I), (II) and (III), respectively. In stage (IV), the loading reached 176.3 ±7.7 mgCOD/ gVSS/d (21.4 mgPh/ gVSS/d & 21.4 mgPcr/ gVSS/d) corresponding to COD conversion efficiency of 98.7%, while it reached 212.2± 11.8 mgCOD/ gVSS/d (29.8 mgPh/ gVSS/d & 29.8 mgPcr/ gVSS/d) at stage (V) with an average conversion of 97.4%. Although the average COD conversion of each stage seems quite similar, a deterioration in the COD removal performance was observed in AnMBR-M after day 66 (removal = 99%) till day 73 (removal= 94%). The loading conditions of both reactors and the deterioration are presented in Figure (11), and more details are in Appendix (9). In a similar observation, Garcia Rea et al. (2022) did reach a deterioration after surpassing the limit of 22 mgPcr/ gVSS/d (corresponding to 800 mg/L p-cresol concentration in the feed) in an experiment that included phenol kept at 2 g/L and an additional CES (acetate). This corresponded to a COD loading rate of about 1.6 gCOD/L/d, much higher than the one evaluated during An-M (~1.05 gCOD/L/d). Garcia's finding could verify the underloading status of the M-reactor and that the deterioration was likely related to the inhibition by p-cresol accumulation (Garcia Rea et al., 2022). This further suggested that the magnetite at this dosage did decrease the biomass organic loading capacity.

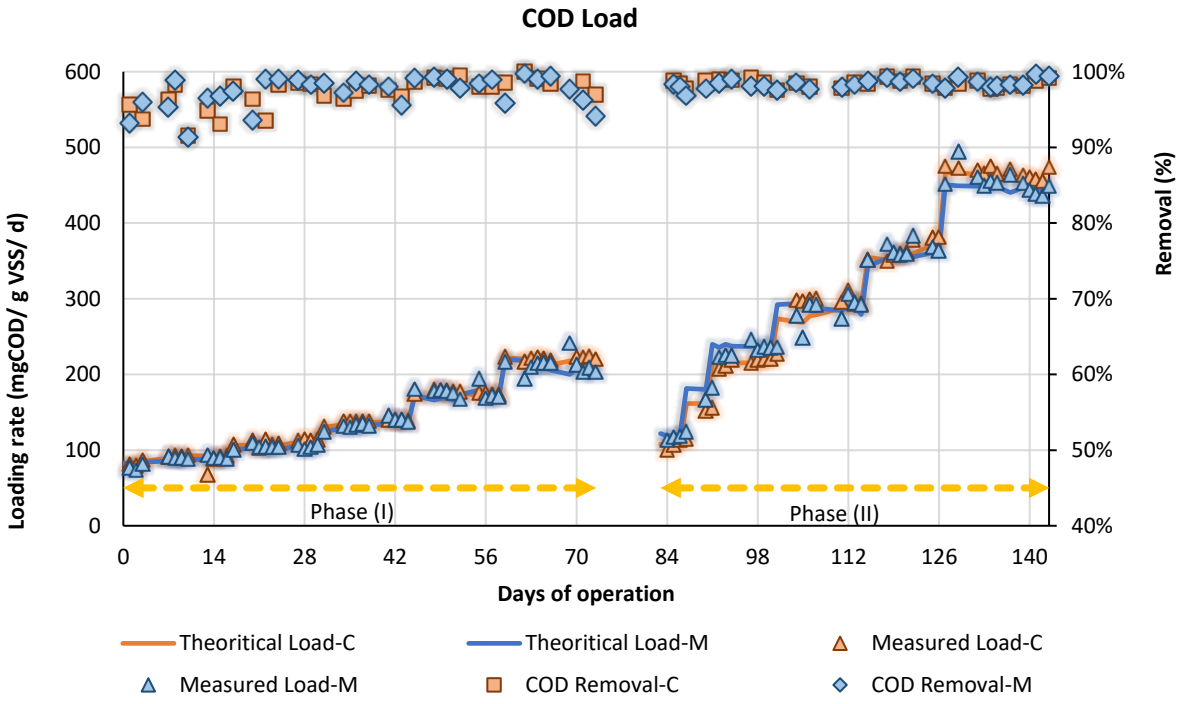

Figure (11): COD-specific loading rate and the corresponding removal percentage of both reactors for phase (I) and phase (II)

For **phase (II)** and the sludge's activation, the operation started with the same end-point concentration but with a lower volumetric loading rate (mg/L/d). The loading of stage (V-a) was initiated, for AnMBR-C, having an average of 106.8 ± 6.3 mgCOD/ gVSS/d (15.2 mgPh/ gVSS/d & 15.2 mgPcr/ gVSS/d) with a corresponding COD conversion of 98.6%. The loading was then increased to 132.8 ± 26.5 mgCOD/ gVSS/d (18.6 mgPh/ gVSS/d & 18.6 mgPcr/ gVSS/d) and further to 208.5 ± 21.6 mgCOD/ gVSS/d (29.3 mgPh/ gVSS/d & 29.3 mgPcr/ gVSS/d) during both stage (V-b) & stage (V-c), respectively. By the end of stage (V-c), the conversion of the system had recovered its capacity, as was maintained during the last stage of phase (I), stage (V). With the stable operation, the COD removal

percentage hit a minimum threshold of 98%. In stage (V-d), and as the flow reached the value of 1 L/d again, the average loading reached 290.4 ± 24.5 mgCOD/ gVSS/d (40.8 mgPh/ gVSS/d & 40.8 mgPcr/ gVSS/d), with a COD conversion of 98.1%. The conversion of the reactor was then tested at an average loading of 364.9 ± 13.0 mgCOD/ gVSS/d (55.6 mgPh/ gVSS/d & 55.6 mgPcr/ gVSS/d) during stage (VI), and the performance of it was marked at a COD conversion of 98.9%. While the performance of the reactor was stable, it was intended to increase the substrate concentration, by which it reached 467.1 ± 6.8 mgCOD/ gVSS/d (75.9 mgPh/ gVSS/d & 75.9 mgPcr/ gVSS/d) during stage (VII); with a conversion of COD of 98.4%.

Likewise, AnMBR-M had a COD loading of 116 ±2.75 mgCOD/ gVSS/d (16.3 mgPh/ gVSS/d & 16.3 mgPcr/ gVSS/d) in the initial stage of phase (II). Then, this rate was increased to an average of 145.5 ±29.7 mgCOD/ gVSS/d (20.4 mgPh/ gVSS/d & 20.4 mgPcr/ gVSS/d) by stage (V-b). Stage (V-a) had a COD conversion of 98.2%, comparable to stage (V-b), which slightly declined to an average of 97.3%. Further increase of the load in stage (V-c) didn't destabilise the conversion capacity of the system, by which COD conversion had risen to over 98%, corresponding to an average load of 225.8 ±19.0 mgCOD/ gVSS/d (31.7 mgPh/ gVSS/d& 31.7 mgPcr/ gVSS/d). In stage (V-d), AnMBR-M had a similar performance to AnMBR-C with COD conversion as high as 98%, while the loading was slightly lower (but within a deviation of 5% from the control), reaching a value of 279.1 ±23.1 mgCOD/ gVSS/d (39.2 mgPh/ gVSS/d & 39.2 mgPcr/ gVSS/d). Reaching the level of 7882 mgCOD/L substrate concentration, AnMBR-M had reached a loading of 364.4 ±10.1 mgCOD/ gVSS/d (55.5 mgPh/ gVSS/d & 55.5 mgPcr/ gVSS/d) with a conversion over 98% for stage (VI). Pushing the limits of the reactor further in stage (VII), the loading was increased to 453 ±15.3 mgCOD/ gVSS/d (73.8 mgPh/ gVSS/d & 73.8 mgPcr/ gVSS/d), and the reactor COD removal was stable at 98.6%. A graphical representation of the loading stages is presented in Figure (11) and Appendix (9).

4.1.3 Permeate Quality

From a general perspective in **phase (I)**, the permeate quality of AnMBR-C showed an insignificant difference compared to AnMBR-M with an average phase (I) effluent of 113.6 ± 62.5 mgCOD/L, while it was 120.4 ± 90.9 mgCOD/L for the latter one. The average COD conversion for the whole phase (for both reactors) was compared and was found similar according to Welch's t-test (97.2% ±0.0% & 97.3% ±0.0%, respectively). Moreover, the average p-cresol and phenol conversion percentages were also similar to the COD, evaluated at more than 99.0% for both reactors (showing insignificant differences in both substrate removal, $P>0.05$).

From day 0 till day 56, AnMBR-C showed traces of IC-6 (iso-caproate/ iso-hexanoate) compound with values ranging 1-5.6 mg/L, while there was no detection of such compound in AnMBR-M. IC-6 is known to be from the family of branched-chain fatty acids, preliminary correlated to growth and protein anaerobic utilisation (Sena et al., 2015; de Leeuw et al., 2019). From day 48 to the end of phase (I), AnMBR-C showed increasing p-cresol concentration in the effluent corresponding to less removal efficiency. The values peaked at around 18.8 mg/L on day 57 and declined again by the end of phase (I). It seemed that increasing the substrate concentration from 400 mg/L to 600 mg/L (+50% jump) had some deterioration impact on the biomass conversion capacity. However, the biomass had the capacity to overcome this inhibitory impact and recover in later stages. Benzoate was also detected on day 62, after the peak of the p-cresol, with a concentration of 24.7 mg/L. Despite that, it should be noted that the detection of benzoate was only once in the permeate, while it was not detected in the soluble part of the sludge samples. This might indicate that this was a false detection and that this value could be attributed to contamination in the HPLC equipment.

The situation of AnMBR-M was slightly different. This reactor showed no traces of (IC-6) as detected in AnMBR-C. This could be correlated to lower growth, as was previously mentioned. Similarly to AnMBR-C, from day 48 till the end of phase (I), more p-cresol was being detected, and the concentration peaked by the end of the phase, corresponding to the deterioration explained in section 4.1.2. The highest detected p-cresol concentration was on the end day of phase (I), with a value of 95.2 mg/L (<90% p-cresol conversion). In addition, trace concentrations of phenol and 4-HBA were detected from day 70. Also, benzoate concentrations were increasing in the system from day 64 till the end of phase (I), reaching values as high as 61.4 mg/L. AnMBR-M showed less removal performance compared to AnMBR-C regarding p-cresol. The accumulation of p-cresol in the process was likely related to less activity of the p-cresol degraders. According to the degradation pathway presented in Figure (3), p-cresol and phenol are converted to 4-HBA and then benzoate, and according to the findings of Fang & Zhou (2000) & Fang et al. (1996), the rate-limiting step was presented to be the phenol/p-cresol to benzoate step. In our observation, as p-cresol accumulated in the system and a minimal concentration of 4-HBA was detected, we could add up to Fang's finding that within the reported limiting step, the p-cresol to 4-HBA was more critical to be addressed as the limiting step. In addition, it was also observed by Fang & Zhou (2000) that, compared to other VFA and intermediates, benzoate was the most detected. Coinciding with these results, our observations included an accumulation of benzoate, suggesting that there was another rate-limiting step somewhere through the ring fission and the β-oxidation process.

According to Welch's t-test, comparing both reactors concerning the phenol and p-cresol conversion in **phase (II)** showed insignificant differences ($P>0.05$). The permeate quality for both reactors showed an average COD removal of over 98%, with the difference between them being insignificant (according to Welch's t-test, $p>0.05$). The permeate quality for AnMBR-C was marked at 131.4±48.6 mgCOD/L, compared to 132.6 ±47.5 mgCOD/L for the magnetite. P-cresol conversion percentage was evaluated at 99.5% and 99% for AnMBR-C & -M, respectively. While for phenol, both reactors had a 100% removal throughout the whole phase.

In AnMBR-C, p-cresol concentrations were detected in the permeate at the start of phase (II), and this concentration dropped to below 10 mg/L within a week. This is because the first few days were considered as reactivation for the biomass, where the total conversion capacity was not recovered yet. From day 94, trace levels of the IC-6 compound were detected until the end of the experiments, where the levels were below 10 mg/L. Also, p-cresol concentration was kept between 2.5-4.5 mg/L from day 94 till 114. During those 20 days, the concentration in the effluent never reached zero, indicating that the capacity limit of the sludge was being reached. However, the biomass recovered completely from day 115 till 143, where the p-cresol concentration was kept at zero. In addition, acetate was detected on day 101, even though the concentrations were as low as 11 mg/L, and the performance seemed to be enhanced in the following days. The detection of acetate and the incomplete degradation of p-cresol indicated the likelihood of a suppressed activity of biomass (p-cresol degraders and methanogens) by the increase of load within a small timeframe between stage (V-c) and stage (V-d). This reversible deterioration could be explained by the inhibitory impacts of phenol/p-cresol on methanogenic conversion, which in return could halt the upstream conversion process (Li Y. et al., 2018)

Likewise, AnMBR-M showed the same declining pattern of p-cresol concentration at the initialisation period, with values eventually dropping to less than 10 mg/L. The detection of IC-6 happened later than AnMBR-C, specifically on day 101 and until the end of the experiment, with concentrations varying from 3- 8 mg/L. Concerning p-cresol, such compound had been detected from day 92 until day 127, which showed that, compared with the control reactor, the p-cresol degraders in the magnetite reactor had lower conversion capacity. It should be noted that no VFAs were detected during phase (II), in

contrast to what was detected in AnMBR-C, which might indicate that methanogenic conversion capacity was higher. The graphical representation of the detected compounds and their corresponding concentration is presented in Figure (12).

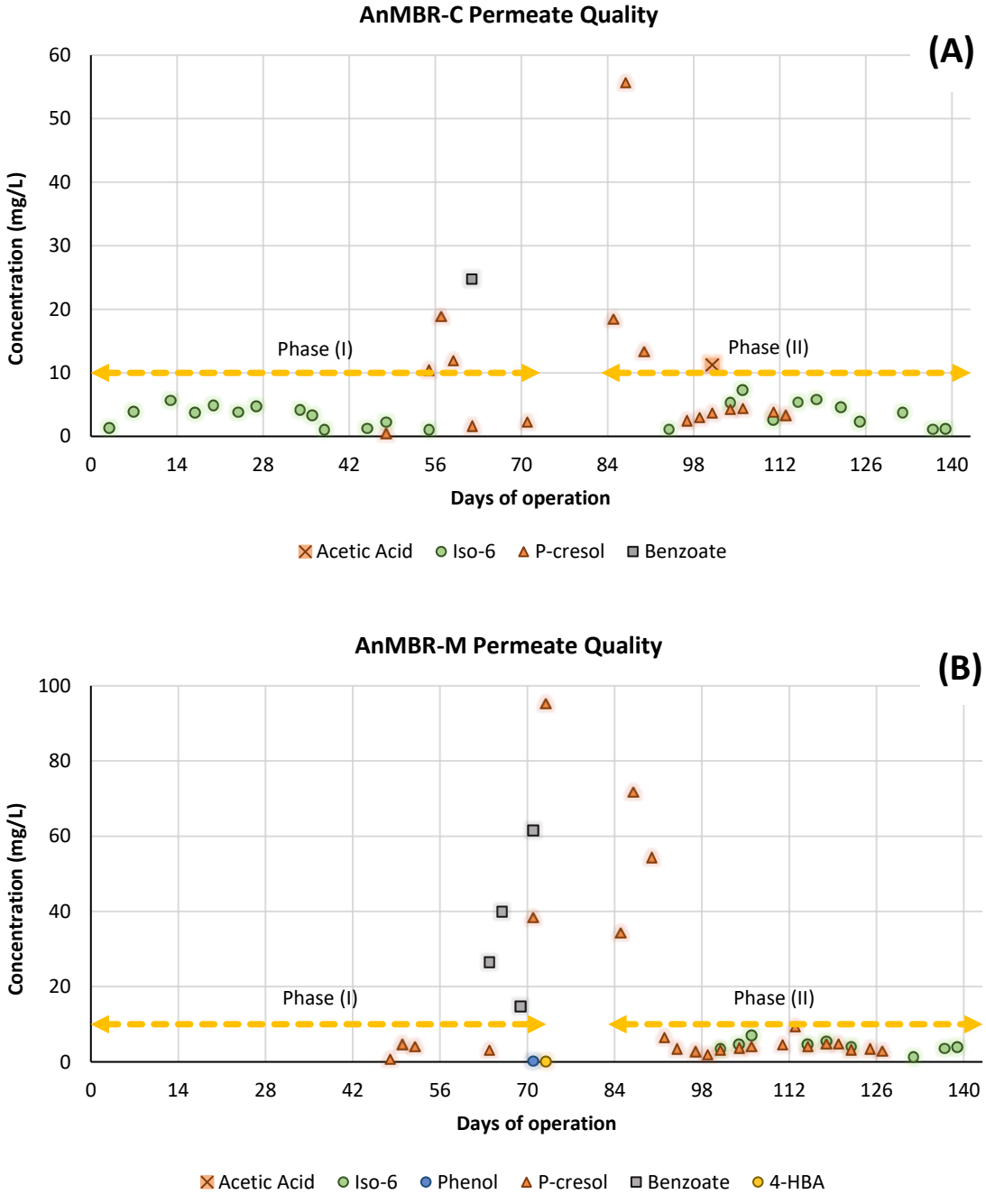

Figure (12): Permeate Quality of both reactors representing AnMBR-C (A) & AnMBR-M (B) for phase (I) and phase (II)

4.1.4 Methane Production

For the methane production of the reactors during **Phase (I)**, there was evident similarity between both reactors' performance. In stage (I), AnMBR-C started the methane production phase with 24.1 ± 1.9 mL/gVSS/d. Then an average range of 30.7 ± 3.0 mL/gVSS/d was obtained from day 17 to day 30. After that, and during stage (III), the production capacity was increased to 40.7 ± 2.8 mL/gVSS/d, before reaching a level of 52.2 ± 5.0 mL/gVSS/d during stage (IV). From day 59 till the end of phase (I), the average methane production was evaluated at 66.0 ± 5.1 mL/gVSS/d (Figure (13)). On the other hand, AnMBR-M started with producing an average of 23.0 ± 3.7 mL/gVSS/d for stage (I), and this value was increased to 28.9 ± 3.1 mL/gVSS/d in stage (II) and further to 38.4 ± 3.3 mL/gVSS/d in stage (III). The rate increased to 51.5 ± 4.5 mL/gVSS/d between day 45 to day 58. In stage (V), the specific methane production peaked at 71.8 mL/gVSS/d before declining on day 69 until it reached 41.6 mL/gVSS/d, corresponding to the deterioration in the COD conversion reported in section 4.1.2.

Referring to the whole phase, AnMBR-C had an average methane yield of 281.9 ± 35.4 mL CH_4/gCOD compared to 265.4 ± 38.6 mL CH_4/gCOD, for AnMBR-M, representing a lower yield by 6%. According to Welch's t-test ($p>0.05$), both datasets produced an insignificant difference ($P>0.05$). Reported values for phenol degradation with additional carbon and energy sources (CES) were in range of 270-280 mL CH_4/gCOD (Carbajo et al., 2010; García Rea et al., 2020). Similarly, the methane conversion was evaluated at 80.6%±1% gCH4-COD/$gCOD_{conv}$ for AnMBR-C and 75.8%± 1.2% gCH4-COD/$gCOD_{conv}$ for ANMBR-M, with no significant difference ($p>0.05$, for Welch's t-test). These values were also similar to other values presented in the literature, as 68% gCH4-COD/$gCOD_{conv}$ (García Rea et al., 2020) and > 85% gCH4-COD/$gCOD_{conv}$ (Lao, 2002; Scully et al., 2006).

Phase (II). After the initialisation process, methane production started from very low values and rose to reach values near the theoretical threshold of each stage. AnMBR-C obtained an average of 15.9 ± 3.1 mL/gVSS/d within the initial period. In a later stage, that production rate was increased to 29.6 ± 16.5 mL/gVSS/d. During stage (V-c), the production rate did reach an average value of 59.4 ± 7.3 mL/gVSS/d. In the later stage and between days 101-114, the production level was evaluated at 88.0 ± 8.0 mL/gVSS/d. Increasing the substrate concentration to 1200 mgPh/L + 1200 mgPcr/L, the methanogenic activity remained stable, and the production rate reached 105.2 ± 11.6 mL/gVSS/d. Pushing the limit of the reactor further, the production did increase to 129.9 ± 6.9 mL/gVSS/d at the last stage. To compare, AnMBR-M started with a lower production level of 11.9 ± 3.9 mL/gVSS/d, average. However, in a later stage, the gap in production between both reactors grew more significant and more prominent in favour of AnMBR-M. The methane production rose in stage (V-b) to 34.3 ± 21.5 mL/gVSS/d, and by the end of stage (V-c), reactor-M had a stage-production average of 75.7 ± 8.9 mL/gVSS/d. During stage (V-d), the threshold was pushed to 101.0 ± 10.5 mL/gVSS/d. Further production was maintained at stages (VI) and (VII), comprising an average methane rate of 120.9 ± 9.5 mL/gVSS/d and 143.0 ± 12.2 mL/gVSS/d.

Aside from stage (V-a), AnMBR-M maintained a 10%-28% higher methane production rate compared to AnMBR-C. On top of that, the average methane yield of AnMBR-M was higher than that of An-C's by about 15%, comprising an average phase yield of 324.8± 30. mL CH_4/gCOD and 284.3± 22.8 mL CH_4/gCOD, respectively. Both yield datasets showed a significant difference ($p<0.05$) relative to Welch's t-test. Methane production enhancement by magnetite was reported by several authors dealing with phenol as a substrate. The reported enhancement in the rate was presented between 9-68%; nevertheless, they rarely mentioned any significant enhancement in the methane yield (He et al., 2019; Jung et al., 2022). In contrast, Tang et al. (2021) observed a 10-14% enhancement in the methane yield after the magnetite supplementation for his phenol batches. According to our calculation, another significance was presented in the corresponding methane conversion with 81.2%±6.5% gCH4-

COD/gCOD$_{conv}$ for AnMBR-C and 92.8%±8.6% gCH4-COD/gCOD$_{conv}$ for AnMBR-M ($p<0.05$, for Welch's t-test). Similar values were again reported by Tang et al. (2021), with values ranging between 93-96.5 gCH4-COD/gCOD$_{conv}$ (evaluated from the methane potential). The comparison of the methane yield values of both reactors relative to some literature values is presented in Figure (14).

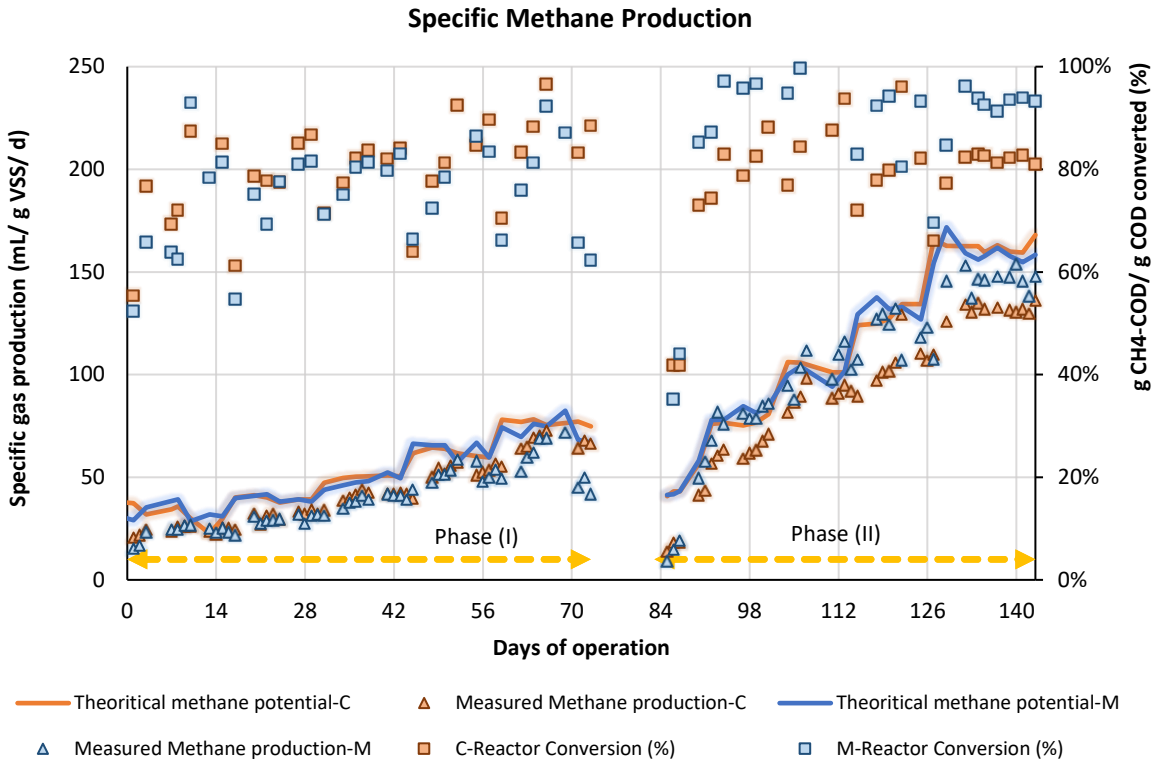

Figure (13): Specific methane production and the corresponding methane ratio in the COD converted of both reactors for phase (I) and phase (II)

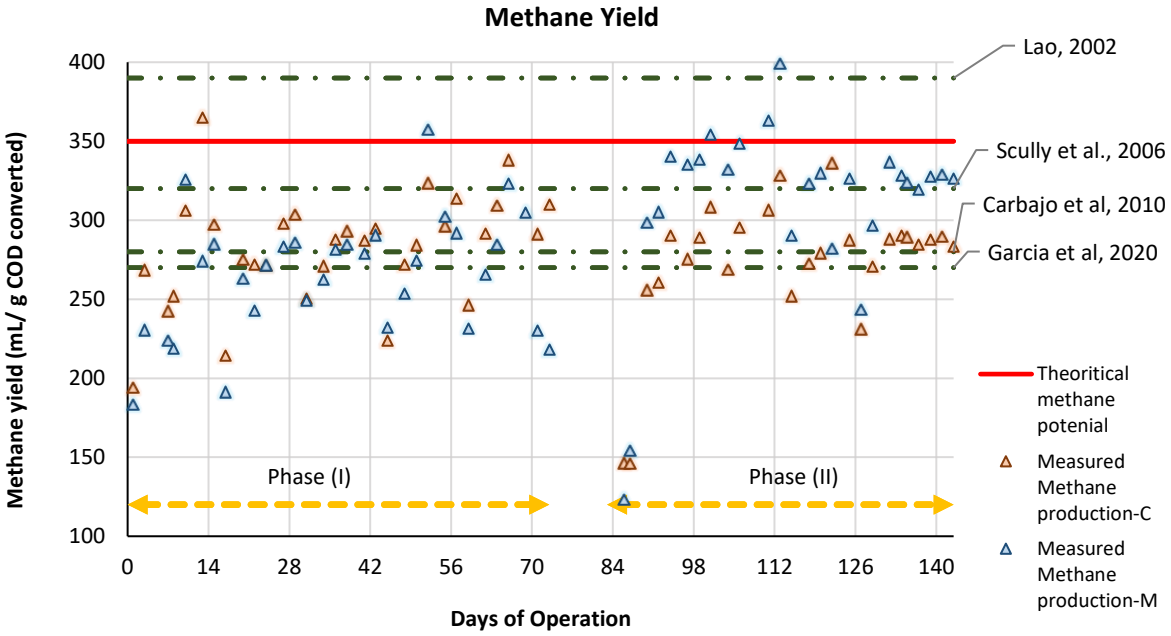

Figure (14): Methane yield of both reactors for phase (I) and phase (II), and the similar range of values in the literature

4.1.5 COD balance

During **phase (I)**, and as mentioned in section 4.1.3, the COD conversion showed an insignificant difference between reactors, while analysing the situation in more details showed a different conclusion. The calculated COD balance was conducted based on the contribution of methane-COD, effluent COD, soluble COD (sCOD), dissolved methane in the effluent, biomass growth, and COD-gap; with regard to the substrate COD. The substrate COD was evaluated based on the feed COD and the biomass in case of decay. Methane dissolved in the effluent was calculated depending on the partial pressure in the headspace and by Henry's law (Benjamin & Lawler, 2013). Firstly, and most importantly, the average methane production represented 79.2% ± 9% for AnMBR-C, compared to 74.8% ±10.6% for AnMBR-M. Aside from the last 3 days that represented the deterioration of An-M, the methane content in the COD balance showed no significant difference relative to An-C (according to Welch's t-test, $p>0.05$). Secondly, the effluent quality contributed with 2.8% ± 1.9% and 2.6% ±1.8% for reactor-C and -M, respectively. Biomass growth of AnMBR-C showed a better rate than AnMBR-M, evaluated at 3.4% ± 5.2% and 1.6% ±3.2% for the latter. The evaluation of such components produced a COD gap of 13.2% ± 9.8% for AnMBR-C, compared to 18.2% ±10.7% for AnMBR-M (Figure (15)). As the gap for An-M was 40% higher, it was analysed by Welch's t-test for significance. The test showed a significant difference between both datasets ($p<0.05$), suggesting that magnetite supplementation was attributing to electron losses by having mostly insignificant differences in each component of the COD balance that cumulatively produced a significant gap.

For **phase (II),** the average methane production was evaluated at 77.5%± 12.5% and 89.0%± 17.9% for AnMBR-C and AnMBR-M, respectively. The significance testing showed that there was a significant difference between both values within the timeframe of phase (II) (Welch's T-test, $P<0.05$). Moreover, the effluent quality was within the phase (I) levels with 1.5% ± 0.5% for reactor-C and 1.6% ±0.6% for M-reactor. Biomass growth of AnMBR-C showed a better rate than AnMBR-M, evaluated at 2.4%± 3.7%, and 2.0%± 2.0% for the latter. On the other hand, The COD gap was evaluated at 17.5% ± 13.8% for AnMBR-C, compared to 8.6%±16.6% for AnMBR-M. The data showed that the gap for An-M was 50% lower, and thus it showed a significant difference (according to Welch's t-test, $p<0.05$). These results showed that the flow of electrons (resembled by the COD balance gap) between different microbial communities was significantly enhanced by the likelihood of a stimulated DIET mechanism by the iron oxide nanoparticles resembled by the magnetite (Ambuchi et al., 2017; Tang et al., 2021).

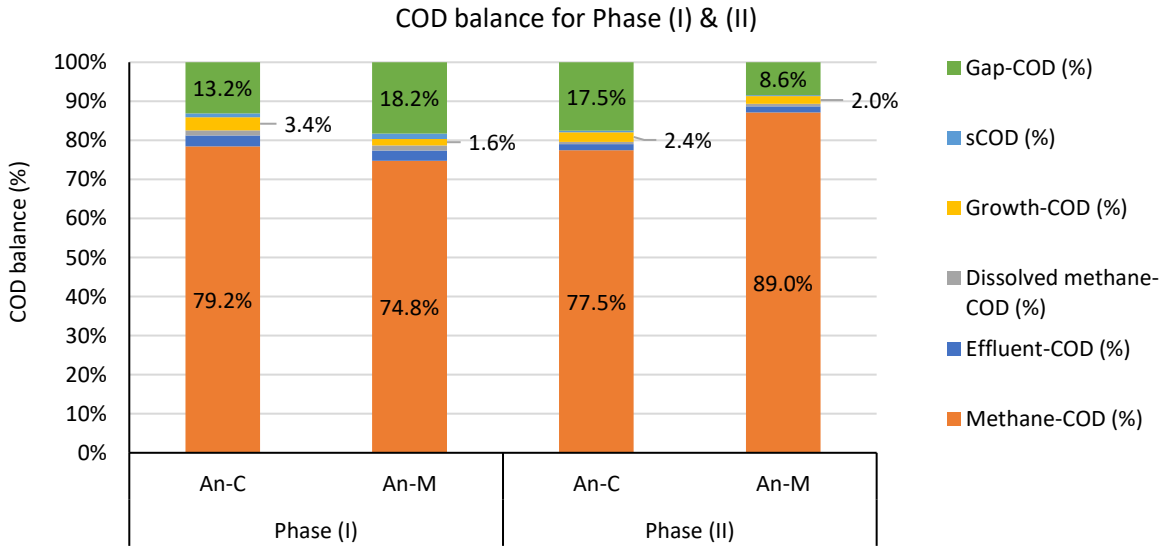

Figure (15): The Average COD balance of both reactors for phase (I) and phase (II)

4.1.6 Protein and carbohydrates

Concerning sludge characteristics, the protein and total carbohydrates were evaluated for AnMBR-C and AnMBR-M, whereas the An-M results were compared with reference to An-C. For phase (I), the SMP carbohydrates content reached the same level on day 56, with values around 7.5 mg/L (with a deviation of 3%), for both reactors. Regarding the EPS part, AnMBR-M showed 30% lower values for the EPS-LB, with carbohydrate content reaching 3.98 mg/gVSS compared to 5.71 mg/gVSS for AnMBR-C on day 56. Meanwhile, the EPS-TB showed a different phenomenon. Carbohydrates content in TB for AnMBR-M reached 12.36 mg/gVSS, compared to 9.22 mg/gVSS for AnMBR-C, levelling it to a 34% higher value. On the other hand, the protein content in SMP showed undetectable levels on day 56 for both reactors, showing the same similarity as for the carbohydrates content. The EPS-LB for An-M showed a value that was 69% lower than that detected in AnMBR-C, while the deviation between them in the tightly-bound EPS was minimal (9%). In general, the AnMBR-M showed lower content of protein & carbohydrates in EPS-LB than -M, with the exact content of both in SMP. However, it also showed similar values in the protein of EPS-Tb, but not the carbohydrates.

With the initiation of phase (II), the analysis taken from reactors needed to be more frequent to have more insights about the reactor. AnMBR-M showed lower carbohydrate content in the SMP between days 98 & 112 compared to AnMBR-C, and this deviation came from as high as -53% and dropped to only 4% by day 126. However, by day 139, this deviation increased again to -55%, with AnMBR-M carbohydrate content reaching as low as 4.48 mg/L. Similar to the same phenomenon in phase (I), carbohydrates in EPS-LB for AnMBR-M had an increasing deviation from AnMBR-C, whereas values went from being lower by 22% on day 98 to 40% lower on day 126 and further to 48% lower on the day 139. On the other hand, the EPS-TB showed a fluctuating trend; AnMBR-M showed higher values on days 98 & 112 and lower on days 126 & 139, compared to -C. For protein content, the SMP of AnMBR-M showed lower values after day 83 and until the end of the phase. The same could be concluded about the EPS-LB protein content. And again, the same fluctuating trend could be seen in the EPS-TB, with AnMBR-M showing higher values on days 98 & 112 & 139 and lower on days 126; insights about the values of raw data collected for SMP and EPS are described in Table (4).

Table (4): Protein and T. carbohydrates content in SMP and EPS of both reactors for phase (I) and phase (II)

Phases	Reactors	Day	SMP (mg/L)		EPS- LB (mg/g VSS)		EPS-TB (mg/gVSS)	
			Protein	T. Carb.	Protein	T. Carb.	Protein	T. Carb.
Phase (I)	AnMBR-C	0	9.57	2.46	7.15	0.75	22.31	8.10
		56	0.00	7.54	6.70	5.71	25.07	9.22
	AnMBR-M	0	13.79	3.70	10.44	1.18	27.70	7.77
		56	0.00	7.31	2.08	3.98	22.76	12.36
Phase (II)	AnMBR-C	83	15.19	8.18	14.20	6.35	38.51	15.42
		98	6.75	6.06	19.18	11.13	19.48	7.29
		112	21.38	12.49	17.57	12.85	23.55	9.66
		126	1.97	7.44	14.35	17.96	26.438	10.94
		139	9.57	9.90	16.51	24.69	24.80	21.54
	AnMBR-M	83	15.76	13.67	17.97	6.27	38.86	15.01
		98	5.91	5.32	12.93	8.66	25.94	10.42
		112	6.75	5.93	9.57	7.49	25.351	11.53
		126	0.56	7.71	11.11	10.70	20.456	7.69
		139	8.72	4.48	9.90	12.76	25.141	15.87

To generalise, the SMP of AnMBR-M had an average deviation of -29%± 29% for carbohydrates and -40%± 34% for protein. In addition, EPS-LB showed a consistent lower value for AnMBR-M, showing an average deviation of -38%± 11% for carbohydrates and -35%± 10% for protein. However, the EPS-TB for both carbohydrates and protein showed a less certain deviation of 2%± 35% and 5%± 23%, respectively (Figure (16)). With the high standard deviation values in the SMP & EPS-TB, it was not very clear if the magnetite had a positive or a negative influence, and for that, protein and carbohydrates data were statistically tested. According to the optimised significance procedure, there were insignificant differences between both reactors in SMP and EPS-TB, while it showed significance in the EPS-LB for both datasets of proteins and carbohydrates. The significance-testing results of the EPS and SMP are presented in Table (5). Ma et al. (2021) reported a similar observation, where the addition of magnetite reduced the SMP and EPS content regarding protein and carbohydrates compared to the control. He further attributed such reduction to a more syntrophic interaction between different microbial communities that could alleviate the toxicity of a saline environment.

Table (5): Significance testing results between both reactors regarding protein & carbohydrates content in SMP & EPS for phase (II)

		Optimum (α)	p	N	Conclusion
SMP	Protein	0.32	0.43	5, 5	Insignificant difference
	Carbohydrates	0.32	0.50	5, 5	Insignificant difference
EPS-LB	Protein	0.2	0.06	5, 5	Large significant difference (d>0.8)
	Carbohydrates	0.27	0.17	5, 5	Large significant difference (d>0.8)
EPS-TB	Protein	0.37	0.90	5, 5	Insignificant difference
	Carbohydrates	0.37	0.77	5, 5	Insignificant difference

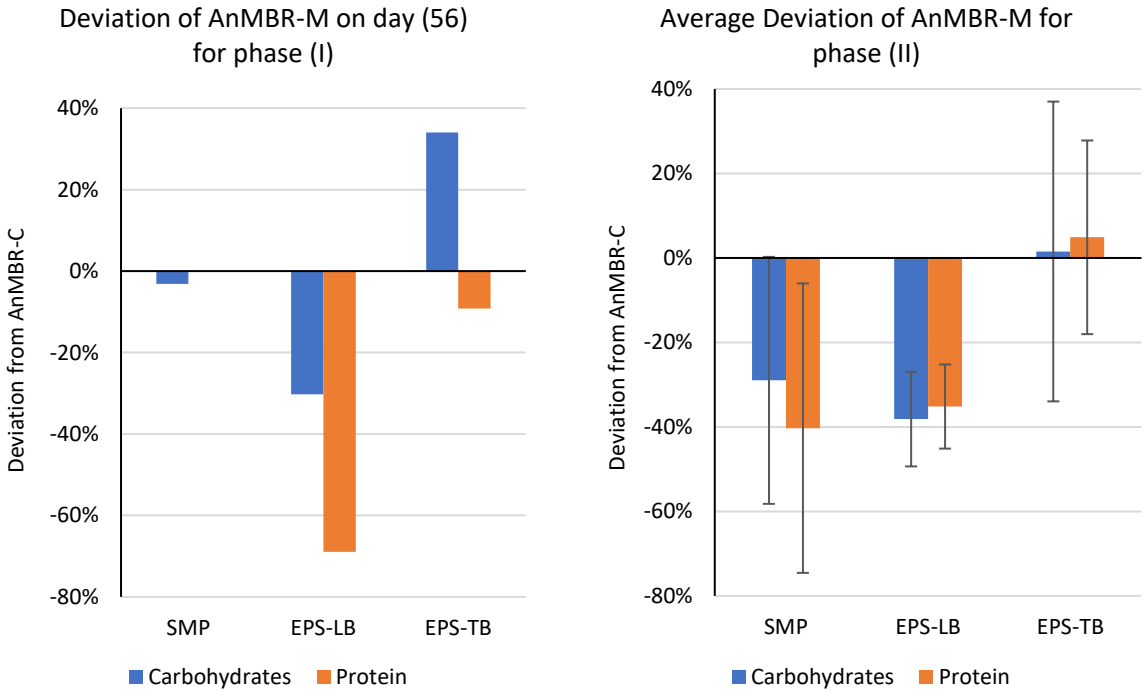

Figure (16): Average deviation of sludge characteristics of AnMBR-M with reference to AnMBR-C, represented with one day value for phase (I) (Left), and average values based on 4-day measurements for phase (II) (Right)

4.1.7 Particle size distribution (PSD)

The particle size distribution of the biomass was monitored for both reactors, and it showed observable fluctuations during operation. In phase (I), the d50 of AnMBR-C and AnMBR-M had the same value of 14.1 µm. Then the pattern kept increasing until day 56, reaching 15.5 µm and 15.2 µm for AnMBR-C and AnMBR-M, respectively. For both reactors, a decline in the size distribution was monitored on day 73; however, the decline was steeper in AnMBR-M. AnMBR-M showed a 73.5% reduction in the d50 compared to day 56, while AnMBR-C showed 26.1% compared to the same reference. The same pattern was observed in d10 and d90, as observed in Figure (17). This might indicate an inhibition effect of the increase in substrate concentration (600 to 900 mg/L phenol and p-cresol) between day 56 till the end of the phase. A similar phenomenon was observed by Li et al. (2018), where an increase in the smaller-sized-biomass was observed under the influence of increasing the phenol concentration and relative toxicity. However, as the reduction was more severe in AnMBR-M, it appeared that under these reactor conditions, biomass was suspectable to more toxicity.

On the other hand, d50 started with 10.8 µm for AnMBR-C and 3.7 µm for AnMBR-M; at the initialisation of phase (II). Although both reactors on that day were inoculated from the same biomass, the data showed that the smaller sizes in An-M could be correlated to the detected magnetite. As the detection of the equipment is based on the percentage of particles within each size bin, it was most likely that as the magnetite initially was in a scattered stage, it did influence the percentage detected in each size, shifting the whole distribution to a smaller size. During the whole phase timeframe, the PSD for An-C showed quite a stable size on days 98, 113, 126, and 139, where the average change of d50 relative to day 83 was -9%± 1%. On the contrary, AnMBR-M distribution showed an increasing trend after day 83. D50 for days 98, 113, 126, and 139 showed an increasing pattern, relative to day 83, of +12%, +40%, +62%, and +32%, respectively (Figure (17)). However, at the end of the stage, the distribution showed a decline in size, whereas from day 126 to day 139, a decline in d50 of -19% was monitored. This phenomenon was similar to the end of phase (I), where it could indicate the start of an inhibitory impact on the biomass.

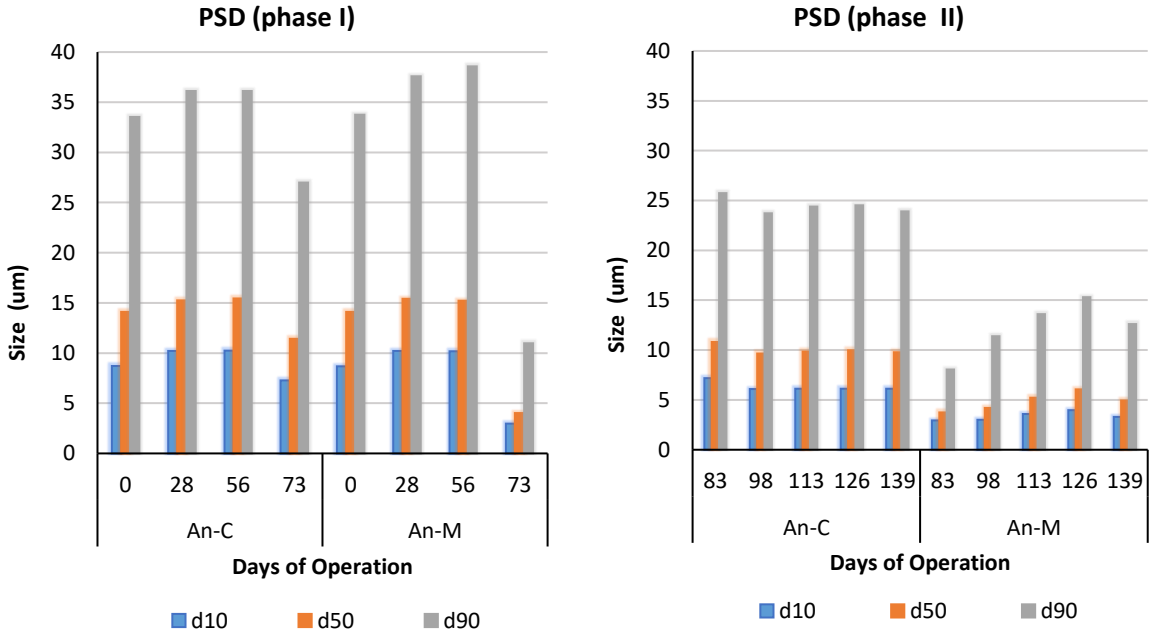

Figure (17): Particle size distribution (PSD) of both reactors in phase (I) (Left), and in phase (II) (Right)

Although there was an increasing trend in the particle size of AnMBR-C during phase (I), compared to phase (II), this could be attributed to the increase in size before reaching the optimum size under the specified operation conditions, just like the change in the VSS concentration in a reactor which is mainly dependent on the biomass environment including organic loading, temperature, pH and even the accumulation of inhibitory compounds (Show et al., 2004). The increase in particle size could also be attributed to a natural adaptation of the sludge towards the substrate, as bigger particle sizes were reported to have better phenol utilisation (Wang et al., 2020). To compare, AnMBR-M showed a similar trend to AnMBR-C during phase (I), while it showed a different trend during phase (II); this would likely indicate that there was a natural agglomeration of biomass in phase (I) in addition to the magnetite impact, while in phase (II) it would only be attributed to the magnetite. Gudkov et al. (2020) emphasised the influence of the nano magnetite particle concentration on the particle size distribution analysis. They showed that under the influence of a high concentration of nanoparticles (e.g. Fe & Cu) in a solution, the probability of collisions increased, leading to better agglomeration. Corresponding to our case, phase (I) had a higher magnetite concentration (40 mmol/L), leading to higher agglomeration potential compared to phase (II) and corresponding to 20 mmol/L. . Furthermore, this would likely be related to the fewer small particles being detected in PSD analysis in phase (I), thus less influence on the biomass size distribution compared to phase (II).

4.2 Batch Experiments

4.2.1 SMA

The specific methanogenic activity was tested in phase (I) and phase (II), whereas in each phase, the comparison between both reactors was evaluated. For phase (I), the SMA test was conducted on sludge taken on day 62 from the reactor under loading conditions equivalent to 900 mgPh/L + 900 mgPcr/L. The maximum SMA rate, yielded by the modified-Gompertz model, of An-M showed a 31% reduction in performance compared to the control, comprising an average value of 0.756 ± 0.186 gCOD/ gVSS/d and 0.522 ± 0.01 gCOD/ gVSS/d (Appendix (10)). The results showed a significant difference according to the optimised significance procedure ($N1=N2= 3$, $d= 1.784$, optimised $\alpha= 0.3$, $p=0.16$, $p< \alpha$, Appendix (8)).

On the other hand, for phase (II), the experiment was conducted on day 101 with sludge acclimatised under the loading conditions of stage (V-c). The previously-mentioned model produced rate of production for An-M within 7% of An-C (0.674 ± 0.048 gCOD/gVSS/d (AnMBR-C), 0.627 ± 0.034 gCOD/gVSS/d (AnMBR-M)); more insights about the SMA results are presented in Table (6). From a statistical perspective, the results showed a neglected-significant difference, which could be labelled as insignificant, according to the optimised significance procedure ($N1=N2= 3$, $d= 0.042$, optimised $\alpha= 0.31$, $p=0.235$, $p< \alpha$, Appendix (8)). Muñoz Sierra et al. (2017) reported an SMA result of 0.8 gCOD/gVSS/d at 6gNa+/L, in the range of the observed values in both phases. The reported values by Muñoz Sierra were under mesophilic conditions, comparable to this study. Other authors reported similar mesophilic-SMA levels for granular sludge treating phenol within the range of 0.64-0.75 gCOD/gVSS/d, by which their conditions included the use of additional carbon sources either during operation or reactor start-up (Tay et al., 2001; Fang et al., 1996).

Table (6): Maximum rate of methane production (SMA) by using acetate as sole substrate, and evaluated by curve-fitting of the data by modified Gompertz model for both reactors during phase (I) and phase (II)

Max Rate (gCOD/gVSS/d)	Phase (I)				Phase (II)			
	An-C		An-M		An-C		An-M	
	Max Rate	R^2	Max Rate	R^2	Max Rate	R^2	Max Rate	R^2
Sample 1	0.73	0.996	0.53	0.994	0.69	0.995	0.67	0.995
Sample 2	0.59	0.992	0.51	0.994	0.62	0.996	0.61	0.993
Sample 3	0.95	1.00	0.53	0.995	0.71	0.995	0.60	0.997
Average	0.76	-	0.52	-	0.67	-	0.63	-
St. deviation	0.19	-	0.01	-	0.05	-	0.03	-
Re. St. deviation	24.5%	-	1.9%	-	7.1%	-	5.5%	-

4.2.2 P-cresol degradation

The batch experiment conducted on the p-cresol yielded a significant difference between the results of both reactors (according to the optimised significance procedure, N1=N2= 2, d= 2.024, optimised α= 0.27, p=0.14, p< α, Appendix (8)). Surprisingly, reactor-C yielded a better rate of conversion for p-cresol with an average of 102.3± 28.6 mgPcr/gVSS/d, compared to an average rate of 12.9± 1.8 mgPCr/gVSS/d (Table (7) & Appendix (11)). It should be noted that the data of AnMBR-M showed a zero-order kinetics trend (linear-like graph), but it was fitted through the modified Gompertz model to be consistent with the analysis of AnMBR-C. Although AnMBR-M had an 87% lower conversion rate than AnMBR-C, it showed a similar range of values reported by Garcia Rea et al. (2022). He observed a range of 6.5-8.5 mgPcr/gVSS/d, corresponding to an initial concentration of 250-500 mg/l; however, it should be noted that the used sludge was unacclimatised to p-cresol, but only to phenol. Another reported value for acclimatised granular sludge was 27-31 mgPcr/gVSS/d, corresponding to an initial concentration of 159 mgPcr/L; biomass was taken from 2 reactors running under different operational conditions (feed: 300 & 380 mgPcr/L, HRT: 10 & 24 hrs) (Fang & Zhou, 2000). AnMBR-C conversion rate of p-cresol was even in the range of 3-4 times higher than the values reported by Fang & Zhou (2000) acclimatised granules, which could highlight the importance of the operational conditions and the added CES in producing biomass of high conversion.

Table (7): P-cresol maximum degradation rate by using p-cresol as sole substrate, and evaluated by curve-fitting of the data by modified Gompertz model for both reactors during phase (II)

Max Rate (mgPcr/ gVSS/d)	An-C		An-M	
	Max Rate	R^2	Max Rate	R^2
Sample 1	122	1.000	11.7	0.917
Sample 2	82	0.999	14.2	0.940
Average	102	-	12.9	-
St. deviation	29	-	1.8	-
Re. St. deviation	27.9%	-	13.7%	-

4.2.3 Magnetite Adsorption Capacity

The adsorption experiment showed that Freundlich's model could better describe the protein and carbohydrate data, with R2 of 98.8% & 92.6%, respectively. Protein had a higher (K_F) Freundlich constant/adsorption capacity value than carbohydrates, while it had a lower Freundlich exponent (n) (Table (8) & Appendix (12)). This indicated that protein has stronger adsorption bonding on magnetite than carbohydrates (np < ncarbs) (Nanta et al., 2018). Verifying that, proteins are described to have a strong binding tendency with iron oxide-magnetic nanoparticles through various mechanisms such as electrostatics interaction, hydrophobic interactions and coordinative and hydrogen bonds (Abarca-Cabrera et al., 2021).

Regarding the findings of the model, experimental research reported the adequacy of Freundlich isotherm in describing the adsorption of carbohydrates on magnetite nano-particles and specifically polysaccharides, while both isotherm models were described for protein (Abarca-Cabrera et al., 2021). However, it was argued that these models' use was inadequate for the nano-scale adsorption application due to their potential error (Abarca-Cabrera et al., 2021). According to the literature, a variety of adsorption capacities towards protein was addressed that could vary from low values as 25 mg/g to 570 mg/g (Abarca-Cabrera et al., 2021). A more specific experiment evaluated Freundlich parameters as 14.42 mg/g for (K_F) and 1.587 for (n) for adsorption of bovine serum albumin (BSA) on magnetite nanoparticles in a neutral environment (Rahdar et al., 2019). Similar values were addressed for polysaccharide adsorption on magnetite with (K_F) of 0.85 mg/g and (n) of 0.667 (Nanta et al., 2018). Considering our study relative to the literature, it was evident to mention that the different adsorption affinity and capacity were likely to be related to the interaction with the solution and the presence of other ion competition (Abarca-Cabrera et al., 2021).

Table (8): Adsorption isotherm parameters evaluated by curve fitting of Langmuir and Freundlich models

	Langmuir Model			**Freundlich Model**		
	q_m (mg/g)	K_L (L/mg)	R^2	n	K_F (mg/g)	R^2
Protein	6.461	0.585	77.5%	0.281	2.871	98.8%
Carbohydrates	4.101	0.284	86.5%	0.439	1.079	92.6%

5 Discussion

5.1 Alteration of sludge characteristics

During our operation, it was evident that magnetite adversely impacted the SMP and EPS (regarding both protein and carbohydrates). LB-EPS was reported to influence the bioflocculation of the sludge negatively (Li & Yang, 2007), aligned with what we could observe during the increasing trend of PSD and especially for AnMBR-M. In principle, The inverse relationship between the EPS-LB and the particle size was further verified by using Pearson correlation analysis, with values ranging between (r: -0.70 ~ -0.95) (Appendix (13)). Reports also emphasised the importance of having a high protein to carbohydrates ratio (P/C) in reducing the surface charge and repulsion, increasing surface hydrophobicity, and further stimulating particle cohesion (Zheng et al., 2005; Li et al., 2018). According to our calculation, an average drop of (90%) was recorded in the P/C ratios of EPS-LB by day 56 before the decline of the particle size on day 73. Although that was similar for both reactors, the P/C ratio in EPS-TB in AnMBR-M dropped (48%) between day 0 & day 56, while it stayed almost the same for AnMBR-C (only 1% drop). This could further explain the massive drop in the particle size observed on day 73 for AnMBR-M compared to -C. The production of smaller size particles would decelerate the degradation of aromatic compounds (that require cooperation between species and thus a more compact biomass) (Wang et al., 2020) and make them more susceptible to toxicity under the influence of diminished constraints on mass transfer (Muñoz Sierra et al., 2017). This might have started a positive feedback process of increasing biomass inhibition by the enda of phase (I), by the p-cresol accumulation.

One of the mechanisms of magnetite to reduce the SMP/EPS is the magnetite alteration of the sludge characteristics under the influence of the complex interaction between different microbial species (Ma et al., 2021). Another mechanism is its adsorption from the soluble and the attached part of the sludge. As was explained in section 4.2.3, the adsorption capacity of protein and carbohydrates could be theoretically large; however, the complex nature of the reactor environment might suppress it. Phosphate groups can bind on the surface of magnetic oxides, making a negative shell that is mainly selective regarding positively-charged compounds (Daou et al., 2007; Abarca-Cabrera et al., 2021). Also, the competition between proteins and carbohydrates and the possible formation of complexes could influence the adsorption process (Abarca-Cabrera et al., 2023).

Relative to our research, it was expected that the used phosphate buffer was the leading player in reducing the adsorption capacity of magnetite for protein and carbohydrates, which were then competing over the remaining sites. The longevity of such a process would be of question; however, as reviewed by Paulino et al. (2023), one of the efficient mechanisms of capacity recovery is regeneration under the influence of microbial communities and biofilms. The bio-regeneration can be very effective in freeing adsorption sites and renewing the adsorption process, cycle after cycle. However, the efficiency of the bio-regeneration process could be restrained under the influence of the relative size of nanoparticles with microbial communities and the relative inaccessibility of the adsorbent's micropores (Aktas & Cecen, 2007; Paulino et al., 2023).

5.2 Potential membrane fouling

In a constant flux system, it is common to monitor membrane fouling by measuring TMP (Rabie et al., 2001). However, due to sensor malfunction in phase (I), it was not feasible to acquire the TMP data; thus, the data collected were only from phase (II). According to our calculation, the fouling rate between both reactors showed an insignificant difference ($p>0.05$, for Welch's t-test), with a rate of 0.1 ± 1.3 mbar/d for AnMBR-C and 0.1 ± 1.8 mbar/d for AnMBR-M (Appendix (14)). Moreover, the permeability coefficient was calculated by dividing the flux by the TMP, and the values were 92.0 ± 15.8 L/m2/hr/bar for AnMBR-C and 85.4 ± 16.9 L/m2/hr/bar for AnMBR-M with no significant difference ($p>0.05$, for Welch's t-test). Although the membranes had been in operation for more than 4 months, it appeared like their fouling status was not that severe to be observed by the TMP; which could be related to the low flux operation of the membranes (1 L/d = 4.08 $L/m^2/hr$). In low flux operation (lower than critical flux), the development of a fouling-indicating cake layer takes long time, while the formation of the precedent gel layer starts immediately (Wang & Wu, 2009). Thus, other indicators should be analysed for better understanding.

In Wang et al. (2014) study, the fouling rate with and without adding nano-particles (NPs) showed insignificant differences, whereas the membrane resistance analysis showed different fouling behaviour. NP increased the pore blocking by ~250%, compared to a ~37% reduction in cake resistance, reducing the whole membrane resistance by about 20%. However, it should be noted that the nanoparticles' size was less than half of the membrane's nominal pore size, increasing the possibility of pore-blocking by nano-partciles. This phenomenon could explain the importance of the cake layer, which could act as a secondary barrier for the membrane pores, reducing the potential of pore blocking (Wang & Wu, 2009; Wang et al., 2014). According to our study, the EPS (especially the loosely-bounded) showed a significant difference between both reactors, indicating the possibility of a more porous, less-resistant cake layer formation (Johir et al., 2012; Wang et al., 2014). Thus, a more permeable layer would be expected, which would increase the chance of smaller size particles moving to the inside of the membrane, causing pore blocking. With the addition of NPs and the observation of smaller-size sludge flocs (especially by the end of phase (I)), the irreversible pore blocking could be the significant contributor to long-term fouling, as reported in the literature (Meng et al., 2007; Sabalanvand et al., 2021).

5.3 Deterioration mechanism

According to Ambuchi et al. (2017), microorganisms are subject to toxicity under certain factors. These factors are comprised of the presence of oxidative stress, metal catalysts, and membrane agitation. Oxidative stress under aerobic oxygen-rich conditions would be highly unlikely under the proper anaerobic environment, which mostly requires negative ORP values to operate (Ambuchi et al., 2017). In addition, using a high-purity nanoparticle product (>97%) would also eliminate the probability of impurities and the presence of a potential catalyst. This would leave us with the potential of cytotoxicity under the piercing influence of NP through the membrane. The membrane-damaging mechanism of NPs could be illustrated by membrane disruption, membrane permeability alteration, DNA damage …etc. (Lee & Lee, 2019). To our best knowledge, there were no records of anaerobic bacterial inhibition by magnetite; however, the cell's cytotoxicity could still be a potential (Lee & Lee, 2019). Lee & Lee (2019) emphasised that whether an enhancement or inhibition by metal NPs exists, the influence would be related to the type, size and shapes of NP, their time of exposure, and other conditions-related factors. Related to our study, with the reduction of the protective EPS, the sludge became more susceptible to the induced cytotoxicity by nanoparticle-membrane-piercing (Xu et al., 2022).

By the end of phase (I), AnMBR-M started deteriorating with a decline in methane production, indicating the inhibition of substrate degraders and methanogens. Although it could be argued that the cytotoxicity potential may have existed from the beginning, the substrate concentration could be the triggering factor. The deterioration of the reactor started after increasing the p-cresol from 600 to 900 mgPcr/L, which could be related to the reported methanogenic inhibitory limit (IC_{50}) of 730 mgPcr/L (Garcia Rea et al., 2022). However, it should also be noted that the biomass was already sensitive at that point, as the inhibition limit for phenol was already surpassed (inhibition levels = 400- 600 mgPh/L) (Yan et al., 2018). This methanogens inhibition started a feedback chain reaction with the phenol and p-cresol degradation, which had a different influence on each aromatic compound. Methanogens are proven to have no influence on the conversion process of phenol to benzoate, making benzoate accumulate in the system as a product of phenol (Cervantes et al., 2000). Although the process of phenol to benzoate is thermodynamically feasible (Eq (6)), the next step of benzoate to acetate conversion is not (Eq (7)). It was likely blocked from going further because the benzoate to acetate step heavily depends on hydrogen scavengers (Knoll & Winter, 1989; Cervantes et al., 2000). Also, Cervantes et al. (2000) highlighted that under a possible inhibition of methanogens, the overall metabolism of benzoate to methane was unlikely, despite being thermodynamically favoured (Eq. (8)).

On the other hand, p-cresol degradation depends on methanogens' bioactivity, as shown in the literature. Cervantes et al. (2000) monitored p-cresol degradation using methanogenic inhibitors, in which the experiment showed that p-cresol had a restricted conversion and most of the accumulation was from p-cresol itself (similar to our observation). However, he suggested that other unmonitored compounds (aside from benzoate and 4-hydroxybenzoate) might have also accumulated. The conversion of p-cresol to benzoate is unfavoured under standard conditions (Eq(9)), and a hydrogen scavenger is needed to stimulate such a reaction, by which 2 hydrogen moles are produced per one mole of p-cresol.

Table (9): Thermodynamics of phenol and p-cresol conversion process to benzoate (Eq (6) & Eq(9)), and benzoate conversion to acetate or methane (Eq (7) & Eq(8))

Reaction		**ΔG^o (kJ/reaction)**	**Eq.**
Phenol (Knoll & Winter, 1989)	$C_6H_6O + HCO_3^- + H^+ + H_2 \rightarrow C_7H_6O_2 + 2H_2O$	-45.6	(6)
Benzoate (Cervantes et al., 2000)	$C_7H_5O_2^- + 7H_2O \rightarrow 3CH_3COO^- + HCO_3^- + 3H^+ + 3H_2$	+70.4	(7)
Benzoate (Cervantes et al., 2000)	$C_7H_5O_2^- + 7.75H_2O \rightarrow 3.75CH_4 + 3.25HCO_3^- + 2.25\ H^+$	−124.1	(8)
P-cresol*	$C_7H_8O + H_2O \rightarrow C_7H_6O_2 + 2H_2$	+23.67	(9)

* Reaction formulated on the standard conditions with values adopted from (Thauer et al., 1977)

5.4 Magnetite impact on the process and DIET mechanism

Iron concentration was monitored and compared between both reactors throughout the operation. The results showed low iron concentration (Fe2+/Fe3+) in the reactor, suggesting that the dissimilatory iron reduction mechanism was unlikely to exist, which could be further explained by the persistent magnetite structure (Baek et al., 2017; Kang & Liu, 2021; Tang et al., 2021). In addition, Baek et al. (2019) emphasised the unlikely of iron ion solubilisation from magnetite under mesophilic anaerobic conditions, as it requires highly acidic conditions (pH<3). According to our study, the detected iron concentration could be directly related to the iron content in the nutrients, as Welch's t-test showed no

significant difference (P>0.05) between both reactors related to iron concentration (in both the permeate and the solubilised in sludge) (Appendix (15)). The dissimilatory iron reduction process has been presented as a robust mechanism that could utilise complex substrates, enhance the hydrolysis process (Peng et al., 2018), and even participate in the metabolising process of p-cresol, phenol and benzoate (Lovley & Lonergan, 1990). This suggested that the role of magnetite as an electron conduit promoting DIET would be the dominant process in case of evident enhancement and with the unlikelihood of the dissimilatory iron reduction process (Jung et al., 2022; Tang et al., 2021). Moreover, to understand the potential presence of the DIET mechanism, we had to consider the degradation pathway, the detected components in permeate, COD balance, methane production, SMA, and batch results.

Phase (I). Starting from the end product, the methane production was similar in AnMBR-C compared to AnMBR-M during phase (I) (section 4.1.4). In contrast, the SMA results (section 4.2.1) showed that the control reactor performed better than AnMBR-M. This indicated that the magnetite concentration of 40 mmol/L negatively affected the acetoclastic methanogens, which could be explained by the potential of cytotoxicity (Ambuchi et al., 2017; Lee & Lee, 2019). As the acetoclastic pathway appeared to partially contradict the methane as an end product, this suggested that either the hydrogenotrophic pathway or the DIET mechanism was participating. While acetoclastic methanogens were suppressed by 30%, acetate never accumulated in that reactor. It was possible that acetate was being converted to H_2 & CO_2 by acetate oxidizers. In an acetoclastic-stressed environment, magnetite enhanced the acetate conversion process through the syntrophic interconnection between acetate oxidation and methane reduction stages (Zhuang et al., 2018). With the biogas composition being similar between both reactors (insignificant difference, p>0.05), it was unlikely that there was an accumulation of H_2. This could be a possible explanation for enhanced hydrogenotrophic methanogenic activity alongside a syntrophic DIET mechanism induced by the magnetite nanoparticles to cover the methane production gap made by acetoclastic. Normal syntrophic acetate oxidation is thermodynamically unfavoured (Eq. (10)) and requires very active/abundant hydrogenotrophic species; this suggests the necessity of the DIET mechanism to alleviate acetate accumulation.

Analysing the upstream part, it was likely that magnetite had a negative influence on p-cresol under the influence of suppressed methanogenic activity, as was explained previously (Cervantes et al., 2000). Moreover, the COD balance indicated an insignificant difference in methane results, highlighting that methane (as the main electron terminal) was similar in both control and magnetite reactors. With fewer p-cresol donating electrons, it was possible to suggest that another substrate efficiently delivered them. Phenol conversion through magnetite-mediated DIET could be a possible mechanism, whereas the use of magnetite with this substrate was already addressed elsewhere (He et al., 2019; Tang et al., 2021; Jung et al., 2022). Another potential mechanism for phenol enhancement would be the abundance of carbon dioxide (from acetate oxidation). CO_2/HCO_3 could participate in phenol degradation by stimulating the initial carboxylation step, where it was reported that the absence of such compounds could halt the process (García Rea et al., 2020).

Reaction		ΔG^o (kJ/reaction)	Eq.
Syntrophic acetate conversion (Dolfing, 2001)	$CH_3COO^- + 4H_20 \rightarrow 4H_2 + 2HCO_3^- + H^+$	104.5	(10)
	$4H_2 + HCO_3^- + H^+ \rightarrow CH_4 + 3H_20$	-135.6	

During **phase (II),** AnMBR-M showed higher methane production compared to AnMBR-C (section 4.1.4) and its SMA showed an insignificant difference from the control one (section 4.2.1). This proved that the 20 mmol/L dosage of magnetite had a neutral impact on the acetoclastic methanogens. Lee et

al. (2019) reported the same neutral influence with the same magnetite concentration in a non-stressing environment. However, other reports indicated an acetate DIET enhanced conversion under a similar dosage (21.6 mmol/L) (He et al., 2019). The neutrality of the acetoclastic pathway and the lower COD balance gap suggested that DIET could be a strong candidate for process enhancement. As mentioned in section (4.1.5), the evident enhancement in the electron transfer suggested the likelihood of the magnetite acting as an electron conduit for stimulating DIET (Liu et al., 2012; Tang et al., 2021). The addition of magnetite to AnMBR-M showed that, for a longer duration compared to AnMBR-C, p-cresol was being detected in the permeate in phase (II). Alongside the batch results, which showed the declined p-cresol degradation rate compared to the control, it was clear that magnetite with dosage (20 mmol/L) negatively influenced the p-cresol degradation process. Using the same observation of the COD balance and the evident decline in p-cresol conversion, phenol was suggested to undergo enhanced conversion by syntrophic DIET collaboration to compensate for the process's undelivered electrons. A graphical representation of the potential enhancement is presented in Figure (18)

Although DIET enhancement in the syntrophic acetogenesis pathway was reported in the literature (Lee et al., 2019; Tang et al., 2021; Wang et al., 2021), there was no clear evidence to prove or decline it. In addition, the adverse influence of magnetite on the degradation of p-cresol was still unclear. A possible explanation could be the DIET selectivity. Jung et al. (2022) underlined the selectivity of the magnetite-DIET process, where an enhancement was observed with phenol as substrate but not with benzoate. It was suggested that the difference was because benzoate was a non-stressing, readily degradable substrate compared to phenol, although they both share the same pathway (Lee et al., 2019; Jung et al., 2022); however, this theory was not evidently verified. In addition, Jung et al. (2022) further highlighted the enrichment of certain bacteria and archaea in the magnetite-supplemented phenol batches. The selectivity of operation here was argued to be related to substrate complexity and other toxic levels of compounds, temperature and salinity (Zhuang et al., 2018; He et al., 2019).

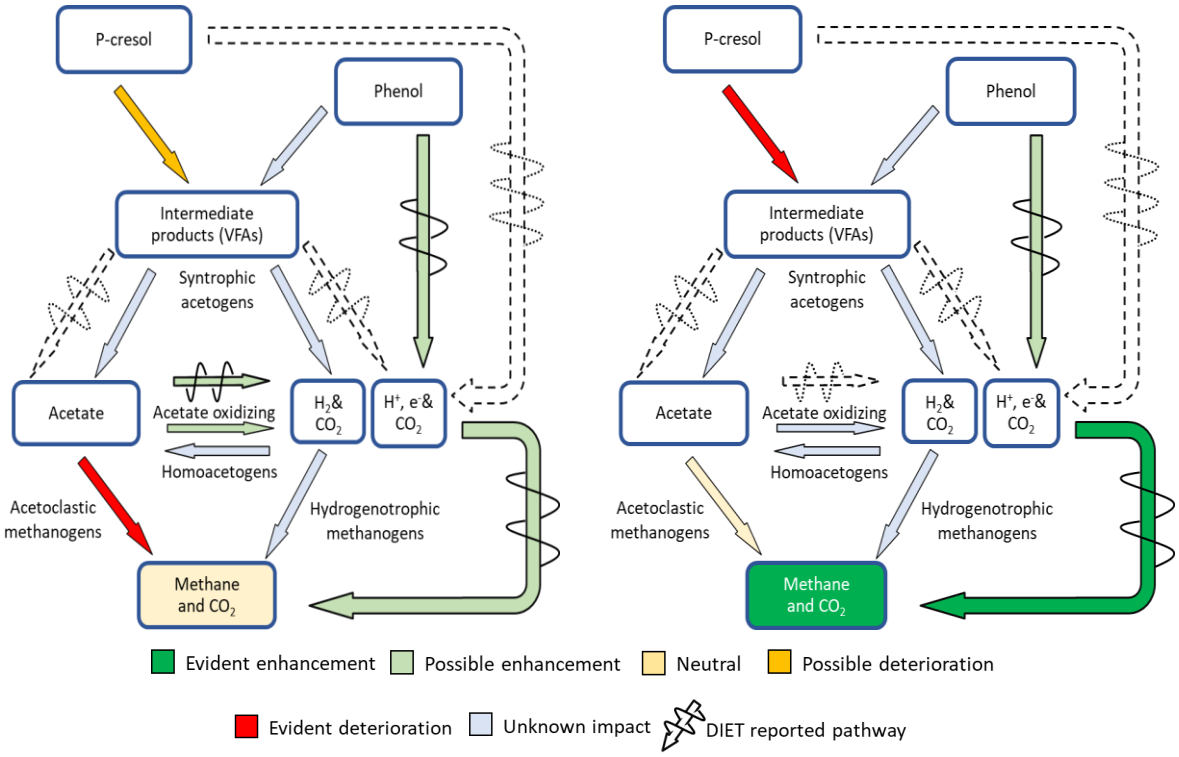

Figure (18): Potential enhancement and deterioration in the degradation pathway by the addition of magnetite for phase (I) (left), and phase (II) (right)

The stimulation of the DIET mechanism not only accelerated the flow of electrons (represented by methane production rate) but also impacted the number of electrons reaching methane as an electron terminal (represented by COD balance and methane yield). The accelerated flow could be explained by understanding the normal flow of electrons. Although the conductive pili/nanowires are shown to have high conductivity as a stand-alone structure, their network can have thousands of folds lower conductance (Gu et al., 2023). The reason behind that would be that the gap resistance between the unorganised network plays a vital role in this conductivity reduction (Gu et al., 2023). According to our case, the abundance of nano-sized conductive material (e.g. magnetite) in this gap areas could have alleviated part of this resistance, allowing a better flow of electrons.

On the other hand, the efficient recovery of electrons could be explained by understanding the possible cellular electron- consumption, whereas three possible mechanisms could be presented. The metabolism process includes the catabolic part, which is related to substrate oxidation and product reduction, and the anabolic part, which is related to biomass activities such as biomass growth, maintenance, and microbial-product production (Laspidou & Rittmann, 2002). Mechanism (1) would be related to the production of SMP/EPS. Labelled as an energy-intensive process, the production of EPS and SMP could reduce the available energy for biomass synthesis and yield (Laspidou & Rittmann, 2002; Wang et al., 2021). For phase (II), the magnetite had significantly impacted the production of EPS (especially EPS-LB), while the biomass growth showed an insignificant difference with the control reactor ($p>0.05$, Welch's t-test). There was likely a surplus of electrons that were not consumed either in the production of EPS or the biomass growth that could end up in the methane.

Mechanism (2) would be related to the energy requirements for the pili/nanowires. Although e-pili are essential for the DIET mechanism, the use of the magnetite as a conductive material could have reduced the need for the production of the same density of these biostructures, and correspondingly the energy consumed in their production would be reduced (Tang et al., 2021). Furthermore, energy is consumed for the extension of these pili or cytochromes structures for long-distance electron transfer. However, adding conductive materials could replace them for that application and thus reduce their energy requirements (Xu et al., 2022; Gu et al., 2023). Moreover, mechanism (3) would be related to the formation of Hydrogen as an intermediate. Hydrogen formation requires multi-enzymatic steps, making the production process energetically difficult (Wang et al., 2021). To illustrate, the redox potential (E_o') for cellular mediators such as (NAD^+/NADH) and (FaDH/ $FaDH_2$), which can be used for the reduction of protons to hydrogen, are evaluated at -320 mV and -220 mV. The energy implication comes from the fact that the reduction process to hydrogen (H^+/H_2) requires a higher redox magnetite (E_o' = -414 mV) (Stams & Plugge, 2009). With the potential of the DIET mechanism, the extensive production of hydrogen to act as an electron shuttle would not be required, as the syntrophic-DIET mechanism would stimulate the direct protons/ electrons intake to the methane production step (Wang et al., 2021).

5.5 Carbon and energy source (CES) influence

Compared to Garcia et al. (2022), the specific conversion of biomass addressed was exceeded in both reactors by reaching a maximum of 73.8-75.9 mgPcr/ gVSS/d (p-cresol concentration of 1600 mgPcr/L), while no failure appeared to happen under the total COD loading rate of 1.6 gCOD/L/d. This would not be related to the supplementation of magnetite rather than the operational conditions of the reactors. In addition, the inhibitory parts of the COD (p-cresol+ phenol) were participating with 80% of the total supply in the substrate by the end of phase (II), which happened to be the same ratio supplied by Garcia at his failure stage. This suggested that the stability of AnMBR-C (compared to Garcia et al. (2022)) could be attributed to the type of additional carbon and energy source (CES) supplied to the

process rather than its contribution ratio to the substrate COD (20%). In his study, as mentioned earlier, acetate was the additional CES used, while in our it was a (1:1) mixture of acetate and butyrate; however, in both studies, they were contributing with 2 gCOD/L in the substrate.

Under 1 mol of each (phenol and p-cresol) as substrate, 6.5 moles of acetate are produced, accompanied by 5 moles of hydrogen. Lowering both hydrogen and acetate concentration is needed to make the reaction thermodynamically favoured (García Rea et al., 2020; Garcia Rea et al., 2022). Moreover, the utilisation of both acetate & butyrate over acetate only showed enhancement in phenol degradation, according to García Rea et al. (2020). He argued that the enhancement could potentially be related to a syntrophic interconnection, by which acetoclastic or hydrogenotrophic methanogens would be included, with a further emphasis on the importance of hydrogen-consuming species (e.g. hydrogenotrophic methanogens) for the conversion of phenol (García Rea et al., 2020). In conclusion, this suggested that the failure reported by Garcia et al. (2022), compared to our AnMBR-C, could be related to a product inhibition by acetate that halted the process, further highlighting the importance of the CES in the process stability and in reaching high organic removal rates (Fang & Zhou, 2000; García Rea et al., 2020).

5.6 Microbial Analysis

A more straightforward way to understand the possible syntrophic collaboration of different species would be by analysing the microbial communities. However, due to the tight timeframe of our study, it was infeasible to complete. Despite that, certain species would be expected to be observed, depending on similar studies that included magnetite and similar substrate (e.g. Phenol, acetate, benzoate … etc.). DIET mechanism stimulated with magnetite have shown to stimulate the abundance of some acetoclastic methanogens like *Methanothrix* (He et al., 2019; Jung et al., 2022) and some hydrogenotrophic species such as *Methanospirillum* (Jung et al., 2022), *Methanolinea* and *Methanobacterium* (Ma et al., 2021). The stimulation of the aforementioned acetoclastic methanogens spp. in our case would be unlikely with the obtained SMA results under normal operation, however, they could still be abundant enough to participate in DIET mechanism. Other reported bacterium that could be enriched with magnetite supplementation are *Desulfomicrobium* as acetogenic species in a saline environment (Ma et al., 2021), *Clostridium* as flexible acetate oxidising/ homoacetogens species (He et al., 2019), *Peptoclostridium* as strict acetate oxidising (Jung et al., 2022), and the commonly reported *Geobacter* (Ma et al., 2021; Jung et al., 2022)

In magnetite application, complex collaborations between different species (mainly methanogens and syntrophic bacteria) were identified in the literature. Correlations were suggested between *Methanolinea & Geobacteraceae, Desulfomicrobium, Sphaerochaeta* (Ma et al., 2021), *Clostridium* with hydrogenotrophic methanogens (He et al., 2019), *Geobacter* (as a phenol degrader) with methanogens (e.g. *Methanosaeta & Methanospirillum)* (Rotaru et al., 2014; Jung et al., 2022), and *Peptoclostridium* with *Geobacter* (Jung et al., 2022). This interaction was suggested to help in alleviating the potential stress impact of the environment in terms of salinity and the substrate-fed (Ma et al., 2021).

6 Conclusion and Recommendations

Regarding the anaerobic degradation process, magnetite adversely affected the **p-cresol degradation rate**, independent of the concentration. On the other hand, different concentrations had different influences on methane production and the acetoclastic methanogens. In low magnetite dosage (e.g. 20 mmol/L), **methane production** was increased by 10% to 28%, while there was an insignificant effect on the acetoclastic methanogenic pathway. However, the higher dosage (e.g. 40 mmol/L) adversely impacted the acetoclastic pathway and had an insignificant impact on methane production. The latter case, with the possible inhibitory impact of the high dosage of magnetite on the acetoclastic, was attributed to the possibility of NP-induced cytotoxicity (e.g. by membrane piercing). Although the 40 mmol/L had some implications on the activity of acetoclastic, the bacterium community might have adapted to the acetoclastic-stressed conditions by stimulating the hydrogenotrophic pathway, DIET, and the corresponding acetate oxidising pathway. For both phases and based on the COD balance, it was possible that the lower degradation rate of p-cresol (and corresponding to it the lower rate of electrons delivery) could have been compensated by an enhancement in the degradation rate of the other main substrate phenol (and corresponding to it the higher rate of electrons delivery).

The stimulation of the DIET mechanism **accelerated the electron flow**, verified by the methane production and the un-detection of VFAs. The abundance of a conductive material between the nanowires was suggested to increase the conductance of the nanowire network and reduce the potential resistance. On the other hand, the **higher efficiency in electron recovery** was verified by the COD balance and the methane yield. Three mechanisms were suggested to contribute to the higher efficiency of the electron recovery, such as: (1) the lower production of EPS/SMP, (2) the unnecessity of energy investment in e-pili/nanowires production and extension, and (3) the conserved energy in the reduction process of proton to hydrogen. However, it should be noted that the scale of impact of these mechanisms was still unknown.

Magnetite changed the **sludge characteristics** regarding the particle size and the protein and carbohydrate concentration in SMP/EPS; however, the main key mechanism was still unclear for the latter part. With the magnetite supplementation, the protein and carbohydrate content appeared to decline, with a more significant influence on the EPS-LB. In addition, this alteration in sludge characteristics was suggested to enhance the flocculation of the biomass, as well as change the long-term operation of the membrane of the reactors by imposing more **irreversible pore-blocking fouling**. The increase in magnetite concentration from 20 mmol/L to 40 mmol/L would also be expected to increase the risk of this irreversible fouling. In summary, the sensitivity of the biomass to the chosen **magnetite dosage** was evident, suggesting that it was preferable to use the dosage of 20 mmol Fe_3O_4/L instead of 40 mmol/L. This choice would help mitigate the potential adverse impacts of the higher dosage on biomass and the risks of membrane fouling, as addressed. Aside from the magnetite, selecting the **additional carbon and energy source (CES)** and relative ratio in the substrate COD seemed essential in alleviating the inhibition of phenol and p-cresol and increasing their toxicity threshold. Compared to the latest publication, using a (1:1) ratio of acetate and butyrate showed better results than using acetate only. The reason behind that was suggested to be related to the potential process inhibition by products' accumulation, which in this case would be the acetate.

The addition of magnetite in p-cresol & phenol wastewater showed adverse effects on the degradation process. At the same time, the enhancement in methane production was less substantial than addressed in the literature. Thus, the further application of such conductive iron oxide in such wastewater **would not be recommended**. While the reason behind the unsuitability of magnetite towards the p-cresol degradation is still unknown, further investigations would be recommended. Some of these recommendations would be as follow:

- Optimizing the magnetite dosage needed for enhancing the process and reducing any possible inhibition impacts related to high dosages, as well as investigating the impact of dosage to VSS ratio (e.g. mmol/gVSS) on the process.

- Optimizing the relative size of the magnetite with respect to the biomass size to reduce the potentials of cytotoxicity imposed by the small particles through membrane piercing. As well as benefit from that in the agglomeration of the sludge and minimising the chances of increased membrane fouling by pore-blocking associated with NPs.

- Investigating in-depth the proposed mechanisms regarding better electron recovery efficiency to understand their significance and their scale of impact.

- Analysing both acetoclastic methanogens and hydrogenotrophic pathways with the syntrophic acetate oxidizers to prove or decline the proposition of DIET-stimulated methane evidently.

- Analysing the microbial communities included in both reactors to see the abundance of certain species that could be directly related to DIET and direct conversion of substrates. Also, use this analysis to understand the most vulnerable species to the high magnetite concentration that may have been toxication.

- Investigating the use of magnetite with p-cresol in methanogenic-stressed conditions using inhibitors (e.g. BES) to understand the significance of magnetite in possible shifting of the degradation pathway.

7 Bibliography

Lao, S.-g. (2002). Mechanisms of granular activated carbon anaerobic fluidized-bed process for treating phenols wastewater. *Journal of Environmental Sciences*, 132-135.

Abarca-Cabrera, L., Fraga-García, P., & Berensmeier, S. (2021). Bio-nano interactions: binding proteins, polysaccharides, lipids and nucleic acids onto magnetic nanoparticles. *Biomaterials Research*, 1-18.

Abarca-Cabrera, L., Xu,, L., Berensmeier, S., & Fraga-García*, P. (2023). Competition at the Bio-nano Interface: A Protein, a Polysaccharide, and a Fatty Acid Adsorb onto Magnetic Nanoparticles. *Appl. Bio Mater*, 146-156.

Abin-Bazaine, A., Trujillo, A., & Olmos-Marquez, M. (2022). Adsorption Isotherms: Enlightenment of the Phenomenon of Adsorption. In M. Ince, & O. Ince, *Wastewater Treatment.* IntechOpen. doi:doi: 10.5772/intechopen.104260

Ambuchi, J., Zhang, Z., Shan, L., Liang, D., Zhang, P., & Feng, Y. (2017). Response of anaerobic granular sludge to iron oxide nanoparticles and multi-wall carbon nanotubes during beet sugar industrial wastewater treatment. *Water Research*, 87-94.

Andersen, A. (2006). Final Report on the Safety Assessment of Sodium p-Chloro-m-Cresol, p-Chloro-m-Cresol, Chlorothymol, Mixed Cresols, m-Cresol, o-Cresol, p-Cresol, Isopropyl Cresols, Thymol, o-Cymen-5-ol, and Carvacrol. *International Journal of Toxicology*, 29-127.

Anku, W., Mamo, M., & Govender, P. (2017). Phenolic Compounds in Water: Sources, Reactivity, Toxicity and Treatment Methods. In M. Soto-Hernandez, M. Palma-Tenango, & M. d.-M. (Eds.), *Phenolic Compounds - Natural Sources, Importance and Applications.* (pp. 420-443). IntechOpen. doi:https://doi.org/10.5772/66927

Aslam, A., Khan, S., & Shahzad, H. (2022). Anaerobic membrane bioreactors (AnMBRs) for municipal wastewater treatment- potential benefits, constraints, and future perspectives: An updated review. *Science of the Total Environment (802)*, 149612.

ATSDR. (2008). *Toxicological Profile for Cresols: POTENTIAL FOR HUMAN EXPOSURE.* Atlanta, Georgia: Agency for Toxic Substances and Disease Registry (ATSDR).

Baek, G., Jung, H., Kim, J., & Lee, C. (2017). A long-term study on the effect of magnetite supplementation in continuous anaerobic digestion of dairy effluent – Magnetic separation and recycling of magnetite. *Bioresource Technology, 241*, 830-840.

Baek, G., Kim, J., Kim, J., & Lee, C. (2018). Role and potential of direct interspecies electron transfer in anaerobic digestion. *Energies 11*, 107.

Basile, A., Cassano, A., & Rastogi, N. (2015). Advances in membrane technologies for water treatment: materials, processes and applications. . *Elsevier.*

Benjamin, M. M., & Lawler, D. F. (2013). GAS TRANSFER FUNDAMENTALS. In *WATER QUALITY ENGINEERING: Physical/Chemical Treatment Processes* (pp. 162-165). United States of America: JohnWiley & Sons, Inc.

BIORAD. (n.d.). Quick Start™ Bradford Protein Assay. Hercules, CA, USA.

Blum, D., Hergenroeder, R., Parkin, G., & Speece, R. (1985). Anaerobic treatment of phenol degradability, toxicity. *Proceedings of the 1985 Specialty Conference* (pp. July 1–5). Northeastern University, Boston, MA: O'Shaughnessy, J.C. (Eds.),.

Budiyono, Widiasa, I., Johari, S., & Sunarso. (2010). The Kinetic of Biogas Production Rate from Cattle Manure in Batch Mode. *International Journal of Chemical and Biological Engineering*, 39-44.

Burn, S. (2014). Resource recovery from wastewater: a research agenda for Australia. *IWA Publishing*.

Busca, G., Berardinelli, S., Resini, C., & Arrighi, L. (2008). Technologies for the removal of phenol from fluid streams: A short review of recent developments. *Journal of Hazardous Materials, 160*, 265-288.

Carbajo, J., Boltes, K., & Leton, P. (2010). Treatment of phenol in an anaerobic fluidized bed reactor (AFBR): continuous and batch regime. *Biodegradation (21)*, 603–613. doi:10.1007/s10532-010-9328-1

Careghini, A., Mastorgio , A., Saponaro, S., & Sezenna, E. (2015). Bisphenol A, nonylphenols, benzophenones, and benzotriazoles in soils, groundwater, surface water, sediments, and food: a review. *Environmental Science and Pollution Research*, 5711-5741.

Cervantes, F., van der Velde, S., Lettinga, G., & Field, J. (2000). Quinones as terminal electron acceptors for anaerobic microbial oxidation of phenolic compounds. *Biodegradation 11*, 313-321.

Chan , Y., Chong , M., Law , C., & Hassell, D. (2009). A review on anaerobic–aerobic treatment of industrial and municipal wastewater. *Chemical Engineering Journal*, 1-18.

Chen, C., Wu, J., & Liu, W. (2008). Identification of important microbial populations in the mesophilic and thermophilic phenol-degrading methanogenic consortia. *Water Res. 42*, , 1963-1976.

Chen, C.-L., Wu, J.-H., Tseng, I.-C., Liang, T.-M., & Liu, W.-T. (2009). Characterization of active microbes in a full-scale anaerobic fluidized bed reactor treating phenolic wastewater. . *Microbes Environ. 24*, , 144-153.

Chen, R., Nie, Y., Hu, Y., Miao, R., Utashiro, T., Li, Q., . . . Li, Y.-Y. (2017). Fouling behaviour of soluble microbial products and extracellular polymeric substances in a submerged anaerobic membrane bioreactor treating low-strength wastewater at room temperature. *J. Membr. Sci. 531*, 1-9.

Chen, R., Wen, W., Jiang, H., Lei, Z., Li, M., & Li, Y.-Y. (2019). Energy recovery potential of thermophilic high-solids co-digestion of coffee processing wastewater and waste activated sludge by anaerobic membrane bioreactor. *Bioresour. Technol. 274*, 127–133.

Daou, T., Begin-Colin, S., Greneche, J., Thomas, F., Derory, A., & Bernhardt, P. (2007). Phosphate Adsorption Properties of Magnetite-Based Nanoparticles. *Chem. Mater (19)*, 4494-4505.

de Leeuw, K., Buisman, C., & Strik, D. (2019). Branched Medium Chain Fatty Acids: Iso-Caproate Formation from Iso-Butyrate Broadens the Product Spectrum for Microbial Chain Elongation. *Environ. Sci. Technol.*, 7704-7713.

de Winter, J. (2013). Using the Student's t-test with extremely small sample sizes. *Practical Assessment, Research, and Evaluation, Vol. 18*(Article 10). doi:https://doi.org/10.7275/e4r6-dj05

Deng, L., Guo, W., Ngo, H., Zhang, J., Liang, S., Xia, S., . . . Li, J. (2014). A comparison study onmembrane fouling in a sponge-submergedmembrane bioreactor and a conventional membrane bioreactor. *Bioresour. Technol. 165*, 69–74.

Dereli, R., Ersahin, M., Ozgun, H., Ozturk, I., Jeison, D., van der Zee, F., & van Lier, J. (2012). Potentials of anaerobic membrane bioreactors to overcome treatment limitations induced by industrial wastewaters . *Bioresource Technology (122)*, 160-170.

Dubois, M., Gilles, K., Hamilton, J., Rebers, P., & Smith, F. (1956). Colorimetric method for determination of sugars and related substances. *Anal. Chem. 28*, 350–356.

Fang, H., & Zhou, G. (1997). Anaerobic degradation of benzoate and cresol isomers in sulfate-rich wastewater. *Water Science Technology, 36*, 7-14.

Fang, H., & Zhou, G. (1999). Interactions of methanogens and denitrifiers in degradation of phenols. *Environmental Engineering, 125*, 57-63.

Fang, H., & Zhou, G. (2000). Degradation of phenol and p-cresol in reactors. *Water Science Technology, 42*, 237-244.

Fang, H., Chen, T., Li, Y., & Chui, H. (1996). Degradation of phenol in wastewater in an upflow anaerobic sludge blanket reactor. *Water Research, 30 (6)*, 1353-1360.

Fang, H., L. D., Zhang, T., & Liu, Y. (2006). Anaerobic treatment of phenol in wastewater under thermophilic condition. *Water Res.*, 427-434.

Fang, H., Liu, Y., Ke, S., & Zhang, T. (2004). Anaerobic degradation of phenol in wastewater at ambient temperature. *Water Science Technology, 49*, 95-102.

Fedorak, P. M., & Hrudey, S. E. (1986). ANAEROBIC TREATMENT OF PHENOLIC COAL CONVERSION WASTEWATER IN SEMICONTINUOUS CULTURES. *Water Research, 20*, 113-122.

Garcia Rea, V., Bueno, B., Cerqueda-García, D., Mu˜noz Sierra, J., Spanjers, H., & van Lier, J. (2022). Degradation of p-cresol, resorcinol, and phenol in anaerobic membrane bioreactors under saline conditions. *Chemical Engineering Journal (430)* , 132672.

García Rea, V., Muñoz Sierra, J., Aponte, L., Cerqueda-Garcia, D., Quchani, K., Spanjers, H., & van Lier, J. (2020). Enhancing Phenol Conversion Rates in Saline Anaerobic Membrane Bioreactor Using Acetate and Butyrate as Additional Carbon and Energy Sources. *Frontiers in Microbiology*, Article 604173.

Ghattas, A., Fischer, F., Wick, A., & Ternes, T. (2017). Anaerobic biodegradation of (emerging) organic contaminants in the aquatic environment. *Water Research (116)*, 268-295.

Gudkov, S., Baimler, I., Uvarov, O., Smirnova1, V., Volkov, M., & Semenova, A. (2020). Influence of the Concentration of Fe and Cu Nanoparticles on the Dynamics of the Size Distribution of Nanoparticles. *Frontiers in Physics, Vol (8)*.

Guo, H., Felz, S., Lin, Y., van Lier, J., & de Kreuk, M. (2020). Structural extracellular polymeric substances determine the difference in digestibility between waste activated sludge and aerobic granules. *Water Research (181)*, 115924.

Gupta, S., Ashrith, G., Chandra, D., Gupta, A., Finkel, K., & Guntupalli, J. (2008). Acute phenol poisoning: a life-threatening hazard of chronic pain relief. *Clin. Toxicol 46*, 250-253.

Habets, L. (1996). Overview of industrial anaerobic wastewater treatment. *Industrial Anaerobic Wastewater Treatment Conference.* London: SCI.

Hafner, S., Astals, S., Buffiere, P., Lojborg, N., Holliger, C., Koch, K., & Weinrich, S. (2020). Calculation of Methane Production from Manometric Measurements. *Standard BMP Methods document 201, version 2.6.*, 1-5.

Hammill, T., & Crawford, R. (1996). Degradation of 2-sec-butyl-4,6..dinitrophenol (dinoseb) by Clostridium bifermentans KMR-1. *Appl. Environ. Microbiol. (62)*, 1842 (LP)-1846.

Harwood, C. S., Burchhardt, G., Herrmann, H., & Fuchs, G. (1999). Anaerobic metabolism of aromatic compounds via the benzoyl-CoA pathway. . *FEMS Microbiology Reviews, 22*, 439-458.

Hazrati, H., Jahanbakhshi, N., & Rostamizadeh, M. (2018). Fouling reduction in the membrane bioreactor using synthesized zeolite nano-adsorbents. *Journal of Membrane Science*, 455-462.

He, C., Lin, W., Zheng, X., Wang, C., Hu, Z., & Wang, W. (2019). Synergistic effect of magnetite and zero-valent iron on anaerobic degradation and methanogenesis of phenol. *Bioresource Technology*, 121874.

Health U. D. O. and Services H. (1999). *Toxicological Profile for Asbestos. Update.* Atlanta, US: Agency for Toxic Substances and Disease Registry.

Hendriks, A. T., Van Lier, J. B., & De Kreuk, M. K. (2018). Growth media in anaerobic fermentative processes: The underestimated potential of thermophilic fermentation and anaerobic digestion. *Biotechnol. Adv., 36*, 1-13. doi:doi: 10.1016/j.biotechadv.2017.08.004

Hussain, A., & Dubey, S. (2017). Specific methanogenic activity test for anaerobic degradation . *Appl Water Sci 7 (2)*, 535-542.

Hwang, P., & Cheng, S. (1991). Treatment of p-cresol with a recirculating UASB reactor using the concept of kinetic control. *Water Science Technology, 24*(5), 133-140.

Ji, Q., Tabassum, S., Hena, S., G. Silva, C., & Yu, G. (2016). A review on the coal gasification wastewater treatment technologies: past, present and future outlook. *Journal of Cleaner Production, 126* , 38-55.

Ji, Q., Tabassum, S., Yu, G., Chu, C., & Zhang, Z. (2015). A high efficiency biological system for treatment of coal gasification wastewater – a key in-depth technological research. *Royal society of Chemistry, 5*, 40402-40413. doi:DOI: 10.1039/c5ra04215a

Jia, S., Han, H., Hou, B., Zhuang, H., Fang, F., & Zhao, Q. (2014). Treatment of coal gasification wastewater by membrane bioreactor hybrid powdered activated carbon (MBRePAC) system. *Chemosphere, 117*, 753-759.

Judd, S. (2010). The MBR Book: Principles and Applications of Membrane Bioreactors for Water and Wastewater Treatment. *Elsevier.*

Judd, S. (2016). The status of industrial and municipal effluent treatment with membrane bioreactor technology. *Chem. Eng. J. 305,* , 37–45.

Jung , S., Kim, M., Lee, J., Shin, J., Gu Shin, S., & Lee, J. (2022). Effect of magnetite supplementation on mesophilic anaerobic digestion of phenol and benzoate: Methane production rate and microbial communities. *Bioresource Technology*, 126943.

Kang, X., & Liu, Y. (2021). Performance and mechanism of conductive magnetite particle-enhanced excess sludge anaerobic digestion for biogas recovery. *RSC Advances*, 35559–35566.

Karlsson, A., Ejlertsson, J., Nezirevic, D., & Svensson, B. (1999). Degradation of phenol under meso- and thermophilic, anaerobic conditions. *Anaerobe 5,*, 25-35.

Kato, S., Hashimoto, K., & Watanabe, K. (2012). Microbial interspecies electron transfer via electric currents through conductive minerals. *Proc Natl Acad Sci Unit States Am (109)*, 10042-10046.

Kennes, C., Mendez, R., & Lema, J. (1997). Methanogenic degradation of p-cresol in batch and in continuous UASB reactors. *Water Research, 31 (7)*, 1549-1554.

Ketheesan, B., & Stuckey, D. (2015). Effects of hydraulic/organic shock/transient loads in anaerobic wastewater treatment: a review. *Crit. Rev. Environ. Sci. Technol. 45 (24),*, 2693–2727.

Kobayashi, T., Hashinaga, T., Mikami, E., & Suzuki, T. (1989). Methanogenic degradation of phenol and benzoate in acclimated sludges. *Water Science Technology, 21*, 55-65.

Kohli, R. (2015). Chapter 1 - Sources and Generation of Surface Contaminants and Their Impact. In R. Kohli, & K. Mittal, *Developments in Surface Contamination and Cleaning* (pp. 1-49). William Andrew Publishing.

Kulkarni, S., & Kaware, D. (2013). Review on research for removal of phenol from wastewater. *International Journal of Scientific and Research Publications*, 1-4.

Lay, J., & Cheng, S. (1998). Influence of hydraulic loading rate on UASB reactor treating phenolic wastewater. *Environmental Engineering (ASCE), 124 (9)*, 829-837.

Le-Clech, P., Chen, V., & Fane, T. (2006). Fouling in membrane bioreactors used in wastewater treatment. *J. Membr. Sci. 284 (1–2)*, 17–53.

Lee, J., Koo, T., Yulisa, A., & Hwang, S. (2019). Magnetite as an enhancer in methanogenic degradation of volatile fatty acids under ammonia-stressed condition. *Journal of Environmental Management, 241*, 418-426.

Lei, Z., Yang, S., Li, Y.-Y., Wen, W., Wang, X., & Chen, R. (2018). Application of anaerobic membrane bioreactors to municipal wastewater treatment at ambient temperature: a review of achievements, challenges, and perspectives. *Bioresour. Technol. 267*, 756-768.

Levén, L., & Schnürer, A. (2005). Effects of temperature on biological degradation of phenols, benzoates and phthalates under methanogenic conditions. *Int. Biodegr. Biodeter. 55*, 153-160.

Levén, L., & Schnürer, A. (2010). Molecular characterisation of two anaerobic phenol degrading enrichment cultures. *Int. Biodegr. Biodeter (64)*, 427-433.

Levén, L., Nyberg, K., & Schnürer, A. (2012). Conversion of phenols during anaerobic digestion of organic solid waste- A review of important microorganisms and impact of temperature. *Journal of Environmental Management*, S99-S103.

Levén, L., Nyberg, K., Korkea-Aho, L., & Schnürer, A. (2006). Phenols in anaerobic digestion processes and

inhibition of ammonia oxidising bacteria (AOB) in soil. *Sci. Tot. Environ. 364,*, 229-238.

Li, C., Tabassum, S., & Zhang, Z. (2014). A novel environmental biotechnological aerobic process (BioAX) for the treatment of coal gasification wastewater. *RSC Adv, 4*, 57580-57586.

Li, H., Han, H., Du, M., & Wang, W. (2011). Removal of phenols, thiocyanate and ammonium from coal gasification wastewater using moving bed biofilm reactor. *Bioresour. Technol., 102*, 4667-4673.

Li, H., Han, K., Li, Z., Zhang, J., Li, H., Huang, Y., & al., e. (2018). Performance, granule conductivity and microbial community analysis of upflow anaerobic sludge blanket (UASB) reactors from mesophilic to thermophilic operation. *Biochem Eng (133)*, 59-65.

Li, J., Gu, J.-D., & Pan, L. (2005). Transformation of dimethyl phthalate, dimethyl isophthalate and dimethyl terephthalate by Rhodococcus rubber Sa and modeling the processes using the modified Gompertz model. *International Biodeterioration & Biodegradation (55)*, 223-232.

Li, X., & Yang, S. (2007). Influence of loosely bound extracellular polymeric substances (EPS) on the flocculation, sedimentation and dewaterability of activated sludge. *Water Research (41)*, 1022-1030.

Li, Y., Tabassum, S., Chu, C., & Zhang, Z. (2018). Inhibitory effect of high phenol concentration in treating coal gasification wastewater in anaerobic biofilter. *Journal of Environmental Sciences (64)*, 207-215.

Lin, H., Xie, K., Mahendran, B., Bagley, D., Leung, K., Liss, S., & Liao, B. (2010). Factors affecting sludge cake formation in a submerged anaerobicmembrane bioreactor. *J.Membr. Sci 361*, 126-134.

Lin, R., Cheng, J., Zhang, J., Zhou, J., Cen, K., & Murphy, J. (2017). Boosting biomethane yield and production rate with graphene: the potential of direct interspecies electron transfer in anaerobic digestion. *Bioresour Technol 239*, 345–352.

Liu, F., Rotaru, A., Shrestha, P., Malvankar, N., Nevin, K., & Lovley, D. (2012). Promoting direct interspecies electron transfer with activated carbon. *Energy Environ Sci (5)*, 8982.

Liu, Y., Zhang, X., Ngo, H., Guo, W., Wen, H., Deng, L., . . . Guo, J. (2018). Specific approach for membrane fouling control and better treatment performance of an anaerobic submerged membrane bioreactor. *Bioresour. Technol. 268*, 658–664.

Lovley, D., & Lonergan, D. (1990). Anaerobic Oxidation of Toluene, Phenol, and p-Cresol by the Disssimilatory Iron-Reducing Organism, GS-15. *APPLIED AND ENVIRONMENTAL MICROBIOLOGY*, 1858-1864.

Mahugo-Santana, C., Sosa-Ferrera , Z., Torres-Padrón, M., & Santana-Rodríguez, J. (2010). Analytical methodologies for the determination of nitroimidazole residues in biological. *Analytica Chimica Acta, 665*, 113-122.

Martins, G., Salvador, A., Pereira, L., & Alves, M. (2018). Methane production and conductive materials: a critical review. *Environ. Sci. Technol. 52*, 10241–10253.

Mcinerney, M., Sieber, J., & Gunsalus, R. (2009). Syntrophy in anaerobic global carbon cycles. *Curr. Opin. Biotechnol (20)*, 623–632.

Mei, R., Nobu, M., Narihiro, T., Yu, J., Sathyagal, A., Willman, E., & al., e. (2018). Novel Geobacter species and diverse methanogens contribute to enhanced methane production in media-added methanogenic reactors. *Water Res 147*, 403–412.

Mei, X., Wang, Z., Miao, Y., & Wu, Z. (2016). Recover energy from domestic wastewater using anaerobic membrane bioreactor: operating parameters optimization and energy balance . *Energy 98*, 146–154.

Meng, F., Chae, S.-R., Drews, A., Kraume, M., Shin, H.-S., & Yang, F. (2009). Recent advances in membrane bioreactors (MBRs): membrane fouling and membrane material. *Water Res. 43 (6)*, 1489–1512.

Mudge, J., Baker, L., Edge, C., & Houlahan, J. (2012). Setting an Optimal a That Minimizes Errors in Null Hypothesis Significance Tests. *PLoS ONE 7(2):*, e32734. doi:doi:10.1371/journal.pone.0032734

Müller , R., & Babel , W. (1994). Phenol and its derivatives as heterotrophic substrates for microbial growth—An energetic comparison. *Applied Microbiology and Biotechnology, 42*, 446-451.

Muñoz Sierra, J. D., Lafita, C., Gabaldón, C., Spanjers, H., & van Lier, J. B. (2017). Trace metals supplementation in anaerobic membrane bioreactors treating highly saline phenolic wastewater. *Bioresour. Technol, 234*, 106-114.

Muñoz Sierra, J. D., Oosterkamp, M. J., Wang, W., Spanjers, H., & van Lier, J. (2018(a)). Impact of long-term salinity exposure in anaerobic membrane bioreactors treating phenolic wastewater: performance robustness and endured microbial community. *Water Res. (141)*, 172-184.

Muñoz Sierra, J. D., Wang, W., Cerqueda-Garcia, D., Oosterkamp, M. J., Spanjers, H., & B., v. L. (2018(b)). Temperature susceptibility of a mesophilic anaerobic membrane bioreactor treating saline phenol-containing wastewater. *Chemosphere 213*, 92-102.

Muñoz Sierra, J., García Rea, V., Cerqueda-García, D., Spanjers, H., & van Lier, J. (2020). Anaerobic conversion of saline phenol-containing wastewater under thermophilic conditions in a membrane bioreactor. *Front Bioeng Biotechnol 8*, 565311.

Muñoz Sierra, J., Oosterkamp, M., Wang, W., Spanjers, H., & van Lier, J. (2019). Comparative performance of upflow anaerobic sludge blanket reactor and anaerobic

membrane bioreactor treating phenolic wastewater: Overcoming high salinity. *Chem Eng J 366*, 480-490.

Nakagawa, S., & Cuthill, I. (2007). Effect size, confidence interval and statistical significance: a practical guide for biologists. *Biol. Rev., 82*, 591-605. doi:doi:10.1111/j.1469-185X.2007.00027.x

Nanta, P., Kasemwong, K., & Skolpap, W. (2018). Isotherm and kinetic modeling on superparamagnetic nanoparticles adsorption of polysaccharide. *Journal of Environmental Chemical Engineering*, 794-802.

Nešvera, J., Rucká, L., & Pátek, M. (2015). Catabolism of Phenol and Its Derivatives in Bacteria: Genes, Their Regulation, and Use in the Biodegradation of Toxic Pollutants. In *Advances in Applied Microbiology* (pp. ISSN 0065-2164). Elsevier Inc.

Ouyang, K., & Liu, J. (2009). Effect of sludge retention time on sludge characteristics and membrane fouling of membrane bioreactor. *J. Environ. Sci. 21 (10),* , 1329–1335.

Paasivirta, J., Humppi, T., Karjalainen , A., Knuutinen , J., Maĕntykoski, K., Paukku, R., . . . Vihonen, H. (1985). Polychlorinated phenols, guaiacols and catechols in environment,. *Chemosphere, 14*, 469-491.

Park, J., Kang, H., Park, K., & Park, H. (2018). Direct interspecies electron transfer via conductive materials: a perspective for anaerobic digestion applications. *Bioresour. Technol. 254*, 300–311.

Patterson, J. (1975). *Treatment Technology for Phenols in Wastewater Treatment Technology.* Ann Arbor, MI: Ann Arbor Science.

Peng, H., Zhang, Y., Tan, D., Zhaoa, Z., Zhaoa, H., & Quana, X. (2018). Roles of magnetite and granular activated carbon in improvement of anaerobic sludge digestion. *Bioresource Technology*, 666-672.

Puig-Grajales, L., Rodriguez-Nava, O., & Razo-Flores, E. (2003). Simultaneous biodegradation of a phenol and 3,4 dimethylphenol mixture under denitrifying conditions. *Water Science Technology, 48 (6)*, 171-178.

Rahdar, S., Rahdar, A., Ahmadi, S., & Trant, J. (2019). Adsorption of bovine serum albumin (BSA) by bare magnetite nanoparticles with surface oxidative impurities that prevent aggregation. *Canadian Journal of Chemistry*, 577-583. doi:dx.doi.org/10.1139/cjc-2019-0008

Ratcliffe, M., Rogers, C., Merdinger, M., Prince, J., Mabuza, T., & Johnson, C. (2006). Treatment of high strength chemical industry wastewater using moving bed biofilm reactor (MBBR) and powdered activated carbon (PAC) Technology. *Proc. Water Environ. Fed*, 1677-1694.

Rezaei, M., & Mehmia, M. (2014). The influence of zeolite (clinoptilolite) on the performance of a hybrid membrane bioreactor. *Bioresource Technol.*, 25-31.

Rincon, N., Chacin, E., Marin, J., Moscoso, J., Fernandez, L., Torrijos, M., . . . Fernandez, N. (2002). Optimum time of hydraulic retention for the anaerobic treatment of light oil production wastewater. *Rev. Tec. Fac. Ing. Univ. Zulia, 25(2)*, 90-99.

Rinzema, A., van Lier, J., & Lettinga, G. (1988). Sodium inhibition of acetoclastic methanogens in granular sludge from a UASB reactor . *Enzyme Microb. tech. 10 (1)*, 24-32.

S&P Global. (2022). *Chemical Economics Handbook – Phenol.* S&P GLobal.

Sabalanvand, S., Hazrati, H., Jafarzadeh ·, Y., Jafarizad, A., & Gharibian, S. (2021). Investigation of Ag and magnetite nanoparticle effect on the membrane fouling in membrane bioreactor. *International Journal of Environmental Science and Technology*.

Said, K., Ismail, A., Abdul Karim, Z., Abdullah, M., & Hafeez, A. (2021). A review of technologies for the phenolic compounds recovery and phenol removal from wastewater. *Process safety and Environmental Protection, 151*, 257-289.

Santos, F., Ricci, B., Neta, L., & Amaral, M. (2017). Sugarcane vinasse treatment by two-stage anaerobic membrane bioreactor: effect of hydraulic retention time on changes in efficiency, biogas production and membrane fouling. *Bioresour. Technol. 245*, 342–350.

Schweigert , N., Zehnder, A., & Eggen , R. (2001). Chemical properties of catechols and their molecular modes of toxic action in cells, from microorganisms to mammals. *Environmental Microbiology*, 81-91.

Scully, C., Collins, G., & O'Flaherty, V. (2006). Anaerobic biological treatment of phenol at 9.5–15 1C in an expanded granular sludge bed (EGSB)-based bioreactor. *Water Research (40)*, 3737-3744.

Sena, S., Sirobhushanam, S., Hantaka, M., Lawrence, P., Gatto, C., & Wilkinson, B. (2015). Short Branched-Chain C6 Carboxylic Acids Result in Increased Growth, Novel 'Unnatural' Fatty Acids and Increased Membrane Fluidity in a Listeria monocytogenes Branched- Chain Fatty. *Biochim Biophys Acta*, 1406-1415. doi:doi:10.1016/j.bbalip.2015.07.006.

Shahid, M., Kashif, A., Rout, P., Aslam, M., Fuwad, A., Choi, Y., . . . Kumar, G. (2020). A brief review of anaerobic membrane bioreactors emphasizing recent advancements, fouling issues and future perspectives. *J. Environ. Manag. 270*, 110909.

Show, K.-Y., Tay, J.-H., Yang, L., Wang, Y., & Lua, C.-H. (2004). Effects of Stressed Loading on Startup and Granulation in Upflow Anaerobic Sludge Blanket Reactors. *JOURNAL OF ENVIRONMENTAL ENGINEERING*, 743-750.

Spanjers, H., & Vanrolleghem, P. (2016). RESPIROMETRY. In M. van Loosdrecht, P. Nielsen, C. Lopez-Vazquez, & D. Brdjanovic, *EXPERIMENTAL*

METHODS IN WASTEWATER TREATMENT (pp. 169-171). IWA Publishing.

Stams, A., & Plugge, C. (2009). Electron transfer in syntrophic communities of anaerobic bacteria and archaea. *Nat. Rev. Microbiol. 7*, 568–577.

Stams, A., Plugge, C., de Bok, F., van Houten, B., Lens, P. D., & al., e. (2005). Metabolic interactions in methanogenic and sulfate-reducing bioreactors. *Water Science Technology, 52*, 13-20.

Suidan, M., Cross, W., Fong, M., & Calvert, J. (1981). Anaerobic carbon filter for degradation of phenols. *Journal of Environmental Engineering (ASCE), 107*, 563-579.

Sullivan, G., & Feinn, R. (2012). Using Effect Size—or Why the P Value Is Not Enough. *Journal of Graduate Medical Education*, 279-282. doi:http://dx.doi.org/10.4300/JGME-D-12-00156.1

Sunil, K., & Jayant, K. (2013). Review on research for removal of phenol from wastewater. *Int. J. Sci. Res. Publ. 3*, 1-5.

Supandi, A., Nunotani, N., & Imanaka, N. (2020). Effective p-cresol removal through catalytic liquid-phase oxidation under moderate conditions using Pt/CeO2-ZrO2-SnO2/SBA-16 as a catalyst. *JOURNAL OF ASIAN CERAMIC SOCIETIES, 8*, 116-122.

Surkatti, R., & El-Naas, M. (2014). Biological treatment of wastewater contaminated with p-cresol using Pseudomonas putida immobilized in polyvinyl alcohol (PVA) gel. *Journal of Water Process Engineering*, 84-90.

Tang, Y., Li, Y., Zhang, M., Xiong, P., Liu, L., & Bao, Y. (2021). Link between characteristics of Fe(III) oxides and critical role in enhancing anaerobic methanogenic degradation of complex organic compounds. *Environmental Research*, 110498.

Tay, J., He, Y., & Yan, Y. (2000). Anaerobic biogranulation using phenol as the sole carbon source. *Water Environ.Res., 72*, 189-194.

Tay, J., He, Y., & Yan, Y. (2001). Improved anaerobic degradation of phenol with supplemental glucose. *Environmental Engineering (ASCE), 127 (1)*, 38-45.

Tay, J.-H., He, Y.-X., & Yan, Y.-G. (2001). IMPROVED ANAEROBIC DEGRADATION OF PHENOL WITH SUPPLEMENTAL GLUCOSE. *JOURNAL OF ENVIRONMENTAL ENGINEERING, 127*((1)), 38-45.

Tomei, M., Angelucci, D., Clagnan, E., & Brusetti, L. (2021). Anaerobic biodegradation of phenol in wastewater treatment: achievements and limits. *Applied Microbiology and Biotechnology (105)*, 2195-2224.

Tsuruta , Y., Watanabe, S., & Inoue , H. (1996). Fluorometric determination of phenol and pcresol in urine by precolumn high-performance liquid chromatography using 4-(Nphthalimidinyl) benzenesulfonyl chloride. *Analytical Biochemistry, 243*, 86-91.

Ueki, T., Nevin, K., Rotaru, A., Wang, L., Ward, J., & al., e. (2018). Geobacter strains expressing poorly conductive pili reveal constraints on direct interspecies electron transfer mechanisms. *mBio*, 9.

van Schie, P., & Young, L. (2000). Biodegradation of phenol: mechanlsms and applications. *Bioremediation Journal, 4*, 1-18.

Veeresh, G., Kumar, P., & Mehrotra, I. (2005). Treatment of phenol and cresols in upflow anaerobic sludge blanket (UASB) process: a review. *Water Research, 39*, 154-170.

Visvanathan, C., & Abeynayaka, A. (2012). Developments and future potentials of anaerobic membrane bioreactors (AnMBRs). *Membrane Water Treatment 3* , 1-23.

Vogel, T., Criddle, C., & McCarty, P. (1987). E.S Critical Reviews: transformations of halogenated aliphatic compounds. *Environ. Sci. Technol (21)*, 722-736.

Wang, J., Wu, B., Sierra, J., He, C., Hu, Z., & Wang, W. (2020). Influence of particle size distribution on anaerobic degradation of phenol and analysis of methanogenic microbial community. *Environmental Science and Pollution Research* , 10391–10403.

Wang, L., Nevin, K., Woodard, T., Mu, B., & Lovley, D. (2016). Expanding the diet for DIET: electron donors supporting direct interspecies electron transfer (DIET) in defined co-cultures. *Front Microbiol* , 7.

Wang, W., Han, H., Yuan, M., & Li, H. (2010). Enhanced anaerobic biodegradability of real coal gasification wastewater with methanol addition. *Journal of Environmental Science., 22*, 1868-1874.

Wang, Y., Suidan, M., & Rittman, R. (1986). Anaerobic treatment of phenol by an expanded-bed reactor. *WPCF, 58*(3), 227-233.

Wang, Z., Wang, T., Si, B., Watson, J., & Zhang, Y. (2021). Accelerating anaerobic digestion for methane production: Potential role of direct interspecies electron transfer. *Renewable and Sustainable Energy Reviews* , 111069.

Xiaojian , Z., Zhansheng , W., & Xiasheng, G. (1991). Simple combination of biodegradation and carbon adsorption—The mechanism of the biological activated carbon process. *Water Research, 25*, 165-172.

Xie, Z., Wang, Z., Wang, Q., Zhu, C., & Wu, Z. (2014). An anaerobic dynamic membrane bioreactor (AnDMBR) for landfill leachate treatment: performance and microbial community identification. *Bioresour. Technol. (161)*, 29–39.

Xu, H., Chang, J., Wang, H., Liu, Y., Zhang, X., Liang, P., & Huang, X. (2019). Enhancing direct interspecies electron transfer in syntrophic-methanogenic associations with (semi)conductive iron oxides: Effects

and mechanisms. *Science of the Total Environment*, 133876.

Xu, M., Wen, X., Huang, X., Yu, Z., & Zhu, M. (2013). Mechanisms of membrane fouling controlled by online ultrasound in an anaerobic membrane bioreactor for digestion of waste activated sludge. *J. Membr. Sci. 445*, 119–126.

Yan, W., Sun, F., Liu, J., & Zhou, Y. (2018). Enhanced anaerobic phenol degradation by conductive materials via EPS and microbial community alteration. *Chemical Engineering Journal, 352*, 1-9.

Yang, Z., Xu, X., Guo, R., Fan, X., & Zhao, X. (2015). Accelerated methanogenesis from effluents of hydrogen-producing stage in anaerobic digestion by mixed cultures enriched with acetate and nano- sized magnetite particles. *Bioresource Technology, 190*, 132-139.

Young, L., & Rivera, M. (1985). Methanogenic degradation of four phenolic compounds. *Water Research, 19 (10)*, 1325-1332.

Yu, G., Zhang, Z., Ji, Q., Zhu, H., & Sheng, J. (2014). Experimental study on the treatment of wastewater from crushed coal pressuring and gasification by EGSB-contact oxidation process. *Ind. Water Treat., 34*, 55-59.

Zhang, T., Ke, S., Liu, Y., & Fang, H. (2005). Microbial characteristics of a methanogenic phenol-degrading sludge. *Water Sci. Technol (52)*, 73-78.

Zhao, H., Zhu, H., Ji, Q., Yu, G., & Zhang, Z. (2013). Technological processes of hydrolytic acidification for coal gasification wastewater treatment. *Water Purif. Technology, 32*, 45-50.

Zhou, G., & Fang, H. (1997). Co-degradation of phenol and m-cresol in a UASB reactor. *Bioresource Technology, 61*, 47-52.

Zhou, L., Ye, B., & Xia, S. (2019). Assessment of membrane bioreactor fouling with the addition of suspended aluminum nitride nanoparticles. *Chemosphere 237*, 124473.

Zuriaga-Agustí , E., Bes-Piá, A., Mendoza-Roca, J., & Alonso-Molina, J. (2013). Influence of extraction methods on proteins and carbohydrates analysis from MBR activated sludge flocs in view of improving EPS determination. *Separation and Purification Technology (112)*, 1-10.

8 Appendix

8.1 Appendix (1): Phenol-treating technologies in literature

Appendix (1): A review of phenol-treating-technology and its experimental conditions (Busca et al., 2008)

Technique	Temperature range (◦C)	Pressure	pH	Reactor	Additional chemicals	Additional energy supply	Performances (ex.)
Distillation	95–180	~1 atm	As such	Distillation column	No	No	Complete separation possible
Liquid-liquid extraction	(I) 20–50; (II) 60–180 (regeneration)	~1 atm	As such	(I) washing column; (II) distillation column	DIPE or MIBK (recycled)	No	*K*d (*W*ph in MIBK/*W*ph in H_2O) ~100 at 30◦C
Adsorption (AC)	20–50	~1 atm	~Neutral	Fixed bed column	AC	No	Adsorption capacity 200– 400 mgph/ gAC
Adsorption (resins, inorganics)	(I) 20–50; (II) 20–50 (regeneration)	~1 atm	~Neutral	Fixed bed column	PV-PDS resin; regeneration solution	No	Adsorption capacity 80–100mg_{ph}/ g_{AC} (resins); adsorption Capacity <200 mg_{ph}/ g_{AC} (silicalite)
Enzymatic oligomerization/ adsorption	20–50	~1 atm	Slightly acidic	Fixed enzyme bed on support; adsorption bed	Enzyme/support; Chitosan	No	C◦ph 0.02 g/l; tyrosinase 46 U/ml; chitosan 50 g/l; >phenol removal 90%
Pervaporation	20–50	~1 atm/ 1–20 Torr	As such	Membrane module	Membrane	Vacuum production	PEBA: enrichment factor 4–60 permeate flux 0–0.3 kg_{ph}/(m2 h)
Membrane extraction (ex. MTBE)	20–50	~1 atm	As such	Membrane module	Membrane Solvent	Solvent regeneration	C◦$_{ph}$ 0–5 g/l; feed flow 1–8 cm3/s; depletion degree 50–100% (MTBE)
WAO	180–315	20–160 Atm	Slightly acidic	Bubble column, stirred reactor, jet-agitated reactor	Air, an acid	No (stirring)	COD◦ 10–100 g/l, T 15–120 min, COD conv 75–90%
SWAO	400–650	250–350 Atm	As such	Bubble column, stirred or jet-agitated reactor	Air	No	TOC conv 99.99%; Residual TOC < 3.5ppm
CWAO	100–200	3–35Atm	As such	Pressurized slurry TR; fixed trickle bed	Air/catalyst	No	Noble metal or metal oxide cat.; COD◦ 10–100 g/l, TOC conv > 80–99%; *t*>20min

Ozonation	20–50	~1 atm	Basic	Bubble column, ejector	O_3, a base (a catalyst)	No (or ozone production)	Liquid flow 0.8m3/h, O_3-O_2 gas flow 0.5 Nm^3/h, $C°_{Ph}$ 6 10−5 g/l; phenol Conv 100% after 30–80 min, ejector, semi-batch
CWPO-Fenton oxidation	20–50	~1 atm	Acidic	Stirred slurry reactor, fixed bed reactor	H_2O_2, $FeSO_4$, an acid	No	$C°_{ph}$s 0.1 g/l; $C°_{H2O2}$ 10−2 ml/l; C◦ Fe^{2+} 2.5; 10−4 ml/l, 5 h, TOC Conv. >90%.
Enzymatic peroxidation	20–50	~1 atm	As such	Supported enzyme in a fixed or fluid bed, fixed bed for polymer separation	Enzyme, support, H_2O_2, an acid	No	$C°_{ph}$ 0.1 g/l; $C°_{H2O2}$ 0.034 g/l; flow rate 5–10 ml/min; phenol conversion 50–80%
Indirect Electrooxidation (electro-Fenton)	20–50	~1 atm	Acidic	Electrochemical cell	O_2, catalyst (e.g., $FeSO_4$), an acid	≤1V	COD◦ < 1000 ppm; COD_{final} <10ppm
Anodic oxidation	20–50	~1 atm	As such	Electrochemical cell	Expensive electrodes (BDD)	4–15V	TOC◦ 0.02 g/l; TOC Conv 60–100%, *t* 10–20 h
Photocatalytic oxidation (UV)	20–50	~1 atm	As such	Photochemical cell (slurry or fixed bed)	TiO_2	$h\nu(\lambda < 400$ nm)	C◦ph 0.04 g/l; t 300 min; TOC conv > 90%
Photocatalytic oxidation (vis)	20–50	~1 atm	As such	Photochemical cell (slurry or fixed bed)	N-doped TiO_2; TiO_2-carbon	Solar light	N-TiO_2, $C°_{ph}$ 0.06 g/l; t 120 min, phenol conv 27%
SCWG	~600	250–350 Atm	As such	Pressurized stirred tank reactor	No	No	C◦ph 5%; in the presence of Ni, t 45 min; phenol conv 100% (H_2, CH_4, CO_2, benzene)
PCD	20–50	~1 atm	Basic	Discharge reactor	Soda	30 kV	$C°_{ph}$ 0.05 g/l; NaOH 210 mmol/l; t 40 min; phenol conv 100%
GDE	20–50	~1 atm	Sightly acidic	Discharge reactor	An acid, Pt electrodes	900V	$C°_{ph}$ 0.3 g/l; C_{ph} 100 and TOC conv 60% *t* 80 min
Biological degradation	20–50	~1 atm	As such	Slurry or fixed bed reactor	Microbial cultures, fungi (support)	No	$C°_{ph}$ 0.4 g/l; removal rate 1.30 gph/l d

- WAO (Wet Air oxidation); CWAO (Catalytic wet air oxidation); CWPO (Catalytic wet peroxide oxidation); SCWG (Supercritical water gasification); PCD (pulsed corona discharge); GDE (glow discharge electrolysis)

8.2 Appendix (2): Central pathway for the degradation of phenol and p-cresol

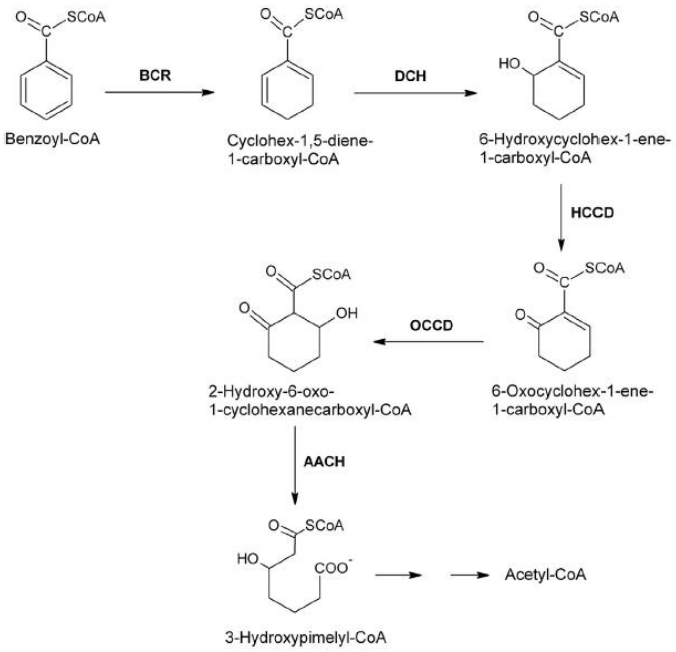

Appendix (2A): Anaerobic degradation pathways (central) of phenol and p-cresol. *Abbreviations of enzymes: BCR, benzoyl-CoA reductase; DCH; dienoyl-CoA hydratase; HCCD, 6-Hydroxycyclohex-1-ene-1-carboxyl-CoA dehydrogenase; OCCD, 6-oxocyclohex-1-ene-1-carboxyl-CoA hydrolase; AACH, alicyclic acid-CoA hydrolase* (Nešvera et al., 2015)

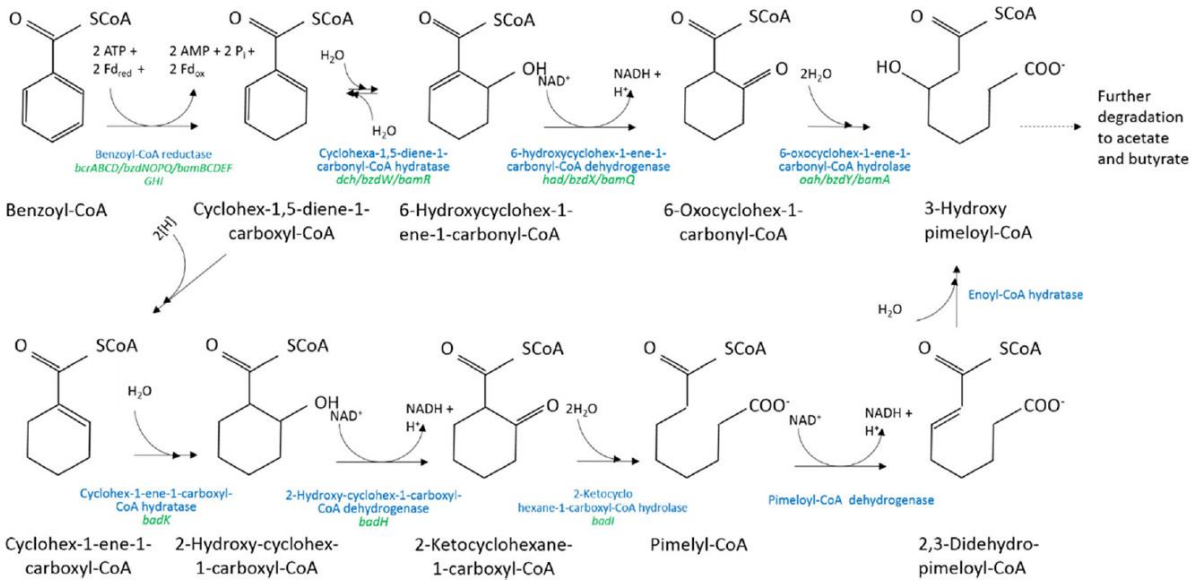

Appendix (2B): Anaerobic degradation pathway for benzoyl-CoA and derivatives (Tomei et al., 2021).

8.3 Appendix (3): Methanogenic degradation of phenol to benzoate

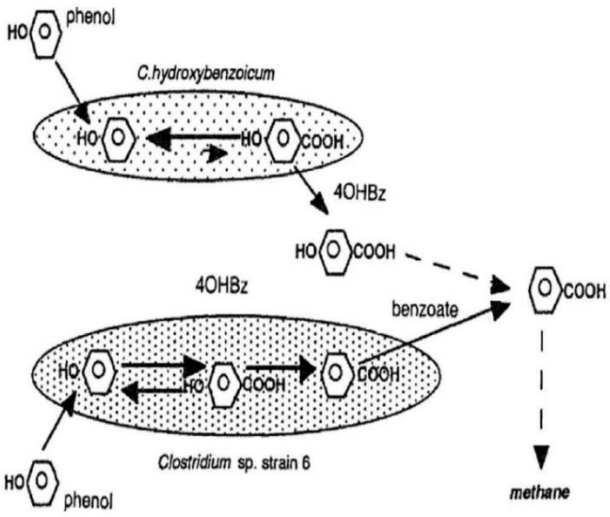

Appendix (3): A graphical representation of the methanogenic degradation of phenol to benzoate by two strains of Clostridium sp. (van Schie & Young, 2000; Said et al., 2021)

8.4 Appendix (4): Examples of electron transfer mechanisms

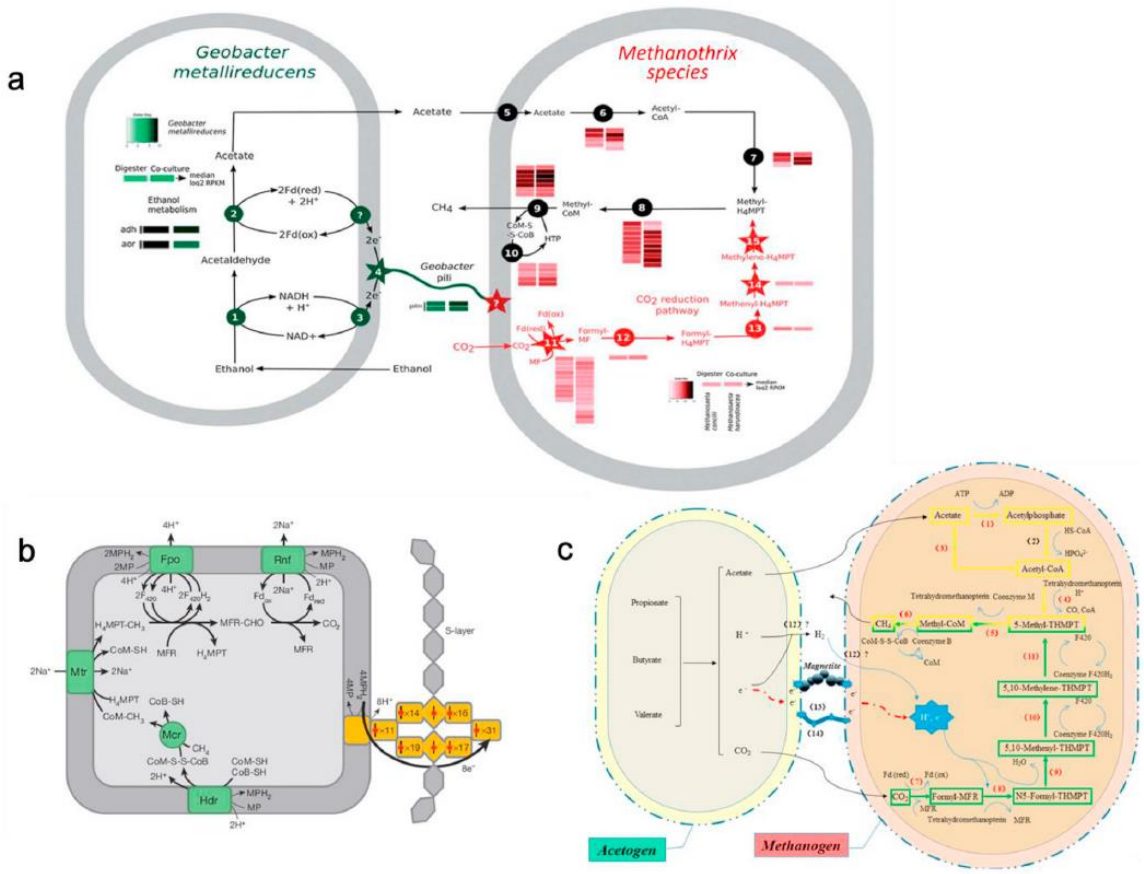

Appendix (4): The suggested different electron transfer mechanisms between different species and their suggested redox reaction and electron flow path via (a) pili structures, (b) cytochromes, (c) magnetite as a conductive material (Wang et al., 2021)

8.5 Appendix (5): Detailed operational conditions

Phase (I). Through the operation period of phase (I) the tank working volumes were fluctuated around 6.17± 0.12 L and 6.15 ± 0.13 L for AnMBR-C and AnMBR-M, respectively (with no significant difference $p>0.05$, for Welch's t-test). The deviation from the theoretical designed volume (6.25) would be mainly attributed to the extracted sludge for sampling and some minor pumping. Regarding the conductivity of the reactors, AnMBR-C had an average conductivity of 24.95 ± 1.14 mS/cm, compared to 24.38 ± 1.00 mS/cm for AnMBR-M (with no significant difference $p>0.05$, for Welch's t-test). According to our calibration curve, that is presented in Appendix (6), these values correspond to 6.06 & 5.91 g Na^+/L, for C & M respectively. Both Reactors were fed with a measured average flow of 1.001± 0.047 L/d and 1.003± 0.05 L/d, for AnMBR-C and AnMBR-M, respectively (with no significant difference $p>0.05$, according to Welch's t-test).

Phase (II). The status of phase (II) wasn't much of a different from phase (I). the tank volumes were maintained around 6.22± 0.07 L and 6.21 ± 0.07 L for AnMBR-C and AnMBR-M, respectively (with no significant difference $p>0.05$, for Welch's t-test). For the conductivity of the reactors, AnMBR-C had an average conductivity of 26.80 ± 0.82 mS/cm, compared to 26.92 ± 0.75 mS/cm for AnMBR-M (with no significant difference $p>0.05$, for Welch's t-test); corresponding to 6.53 & 6.57 g Na^+/L, for C & M respectively. As was mentioned, in the duration of day (83- 100), both Reactors were fed with stepped increase in the feed flow under keeping the inhibitory concentration constant from stage V in phase (I). From day (101) till day (143), AnMBR-C had an average feed flow of 1.015± 0.04 L/d, in comparison to an average flow of 0.995± 0.06 L/d for AnMBR-M (with no significant difference $p>0.05$, for Welch's t-test).

8.6 Appendix (6): Examples of the used calibration curves

This appendix presents the calibration curves constructed for several objectives (e.g., salinity... etc)

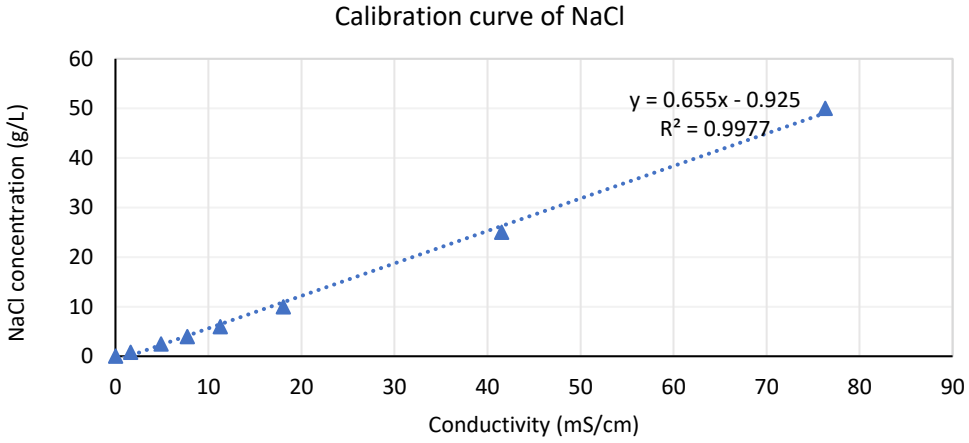

Appendix (6A): Calibration curve for the NaCl concentration of the reactor

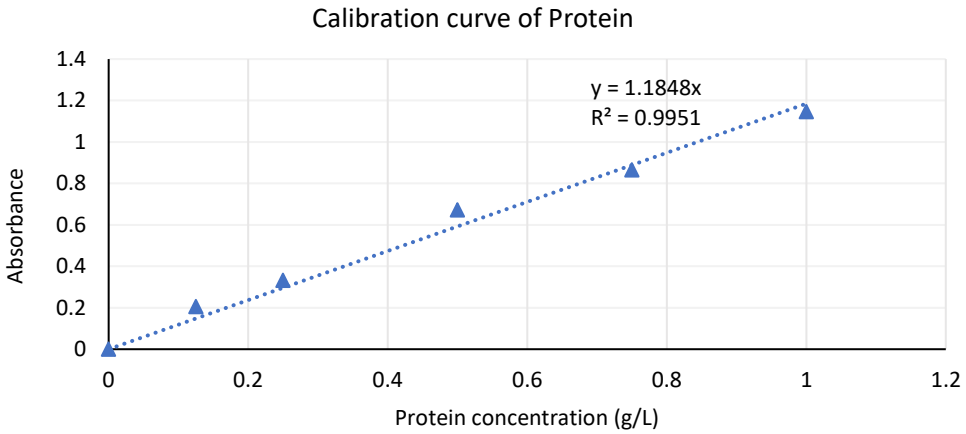

Appendix (6B): Calibration curve for the protein concentration of the reactor

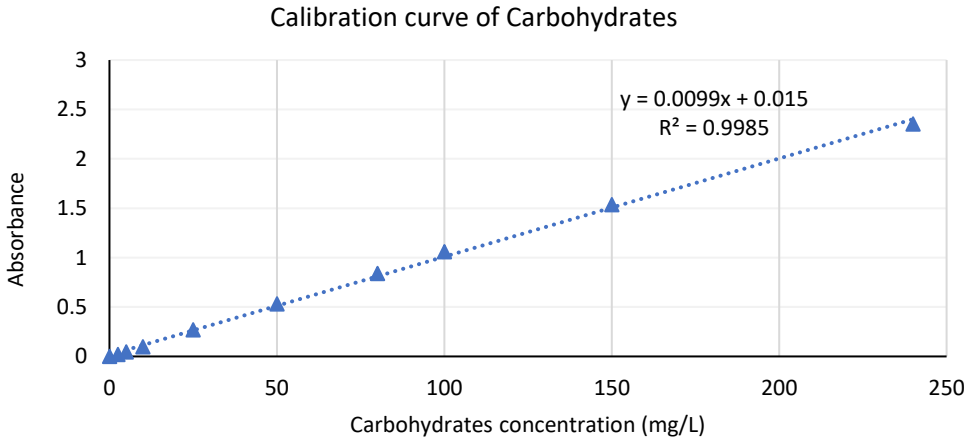

Appendix (6C): Calibration curve for the protein concentration of the reactor

8.7 Appendix (7): Statistical background information

Definitions and further insights. One of the main parameters to evaluate in a statistical analysis is the Power or as referred to as the Statistical power. This value describes the ability of the analysis to detect the significance between groups, when there is real difference. Having a high power with a real difference between datasets, increases the chance of detecting it, and vice versa. And this latter false value is labelled by the type (II) error, which is the probability of falsely accepting the null hypothesis (falsely no significant difference) (Sullivan & Feinn, 2012). Ultimately, to enhance the conclusion of studies, the statistical power is intended to be increased or even maximized; by which several methods could be adopted such as: dealing with groups having a more distinguished differences, increasing sample sizes and increasing the significance level (Sullivan & Feinn, 2012).

The effect size is described as a scale of identifying the significant different between two datasets; and it can be presented in absolute or relative values. Cohen's (d) value, as one of the widely used effect size equation, could emphasize that this significance is small and can be neglected, according to Cohen's scale (Sullivan & Feinn, 2012). The effect size is calculated based on mean difference between the datasets, divided by the standard deviation. Cohen's described scale, highlighted values of (d=0.2) to be small, (d=0.5) to be medium, and (d=0.8 to be large; where it could be further expended that any values that could lie outside of this region is either very small (d<0.2) or very large (d>0.8) (Sullivan & Feinn, 2012).

8.8 Appendix (8): Optimised significance procedure's results

This appendix represents the datasets that were tested according to their statistical significance with the optimised procedure.

Phase (I)

- VSS during the whole phase

		type (I)		Type (II)		
P-two sided	**Cohen's (d)**	**alpha**	**Power**	**beta**	**omega**	**Status**
0.488	0.3797	0.05	0.097	90%	0.4765	Insignificant
0.49	0.3797	0.3	0.408	59%	0.446	Insignificant
0.49	0.3797	0.35	0.458	54%	0.446	Insignificant
0.49	0.3797	0.4	0.507	49%	0.4465	Insignificant
0.49	0.3797	0.8	0.845	16%	0.4775	significant

optimum Alpha 0.32 P 0.49
The conclusion: **Insignificant difference** P > α

- SMA (900 ppm)

		type (I)		Type (II)		
P-two sided	**Cohen's (d)**	**alpha**	**Power**	**beta**	**omega**	**Status**
0.094	1.784	0.05	0.249	75%	0.4005	Insignificant
0.16	1.784	0.25	0.738	26%	0.256	significant
0.16	1.784	0.3	0.794	21%	0.253	significant
0.16	1.784	0.35	0.837	16%	0.2565	significant
0.16	1.784	0.8	0.98	2%	0.41	significant

optimum Alpha 0.3 P 0.16
The conclusion: **significant difference** P < α
(d) conclusion: **big difference** D > 0.8

Phase (II)

- VSS during the whole phase

		type (I)		Type (II)		
P-two sided	**Cohen's (d)**	**alpha**	**Power**	**beta**	**omega**	**Status**
0.551	0.1196	0.1	0.15	85%	0.475	Insignificant
0.551	0.1196	0.3	0.383	62%	0.4585	Insignificant
0.551	0.1196	0.32	0.404	60%	0.458	Insignificant
0.551	0.1196	0.35	0.434	57%	0.458	Insignificant
0.551	0.1196	0.4	0.483	52%	0.4585	Insignificant
0.551	0.1196	0.8	0.837	16%	0.4815	significant

optimum Alpha 0.335 P 0.551
The conclusion: **Insignificant difference** (P > α)

- SMA (900 ppm)

		type (I)		Type (II)		
P-two sided	**Cohen's (d)**	**alpha**	**Power**	**beta**	**omega**	**Status**
0.235	0.04155	0.2	0.486	51%	0.3570	Insignificant
0.235	0.04155	0.3	0.608	39%	0.3460	significant
0.235	0.04155	0.32	0.628	37%	0.3460	significant
0.235	0.04155	0.4	0.699	30%	0.3505	significant
0.242	0.04155	0.8	0.922	8%	0.4390	significant

optimum Alpha 0.31 P 0.235
The conclusion: **significant difference** P < α
(d) conclusion: **very very small difference** D <<< 0.2 "neglected"

- Total Carbohydrates for SMP

		type (I)		Type (II)		
P-two sided	**Cohen's (d)**	**alpha**	**Power**	**beta**	**omega**	**Status**
0.504	3.1421	0.25	0.349	65%	0.4505	Insignificant
0.504	3.1421	0.3	0.402	60%	0.449	Insignificant
0.504	3.1421	0.32	0.422	58%	0.449	Insignificant
0.504	3.1421	0.35	0.452	55%	0.449	Insignificant
0.504	3.1421	0.45	0.547	45%	0.4515	Insignificant

optimum Alpha 0.32 P 0.504
The conclusion: **Insignificant difference** (P > α)

- Total Carbohydrates for EPS-LB

		type (I)		Type (II)		
P-two sided	**Cohen's (d)**	**alpha**	**Power**	**beta**	**omega**	**Status**
0.165	5.27	0.15	0.507	49%	0.3215	Insignificant
0.165	5.27	0.25	0.645	36%	0.3025	significant
0.165	5.27	0.27	0.666	33%	0.302	significant
0.165	5.27	0.3	0.695	31%	0.3025	significant
0.165	5.27	0.4	0.772	23%	0.314	significant

optimum Alpha 0.27 P 0.165
The conclusion: **significant difference** P < α
(d) conclusion: **big difference** D >> 0.8

- Total Carbohydrates for EPS-TB

		type (I)		Type (II)		
P-two sided	**Cohen's (d)**	**alpha**	**Power**	**beta**	**omega**	**Status**
0.777	4.636	0.3	0.319	68%	0.4905	Insignificant
0.777	4.636	0.35	0.369	63%	0.4905	Insignificant
0.777	4.636	0.37	0.389	61%	0.4905	Insignificant
0.777	4.636	0.38	0.399	60%	0.4905	Insignificant
0.777	4.636	0.45	0.469	53%	0.4905	Insignificant

optimum Alpha 0.37 P 0.777
The conclusion: **Insignificant difference** (P > α)

- Protein for SMP

		type (I)		Type (II)		
P-two sided	**Cohen's (d)**	**alpha**	**Power**	**beta**	**omega**	**Status**
0.434	6.594	0.25	0.384	62%	0.4330	Insignificant
0.434	6.594	0.3	0.437	56%	0.4315	Insignificant
0.434	6.594	0.32	0.457	54%	0.4315	Insignificant
0.434	6.594	0.35	0.487	51%	0.4315	Insignificant
0.434	6.594	0.5	0.623	38%	0.4385	significant

optimum Alpha 0.32 P 0.434
The conclusion: **Insignificant difference** (P > α)

- Protein for EPS-LB

		type (I)		Type (II)		
P-two sided	**Cohen's (d)**	**alpha**	**Power**	**beta**	**omega**	**Status**
0.055	2.8585	0.05	0.485	52%	0.2825	Insignificant
0.055	2.8585	0.15	0.735	27%	0.2075	significant
0.055	2.8585	0.2	0.794	21%	0.203	significant
0.055	2.8585	0.25	0.837	16%	0.2065	significant
0.055	2.8585	0.3	0.868	13%	0.216	significant

optimum Alpha 0.2 P 0.055
The conclusion: **significant difference** P < α
(d) conclusion: **big difference** D >> 0.8

- Protein for EPS-TB

		type (I)		Type (II)		
P-two sided	**Cohen's (d)**	**alpha**	**Power**	**beta**	**omega**	**Status**
0.897	7.0329	0.15	0.153	85%	0.4985	Insignificant
0.897	7.0329	0.3	0.304	70%	0.498	Insignificant
0.897	7.0329	0.35	0.354	65%	0.498	Insignificant
0.897	7.0329	0.4	0.404	60%	0.498	Insignificant
0.897	7.0329	0.6	0.603	40%	0.4985	Insignificant

optimum Alpha 0.37 P 0.897
The conclusion: **Insignificant difference** (P > α)

8.9 Appendix (9): Phenol and p-cresol loading rates

This appendix represents more details about the loading conditions of the reactors.

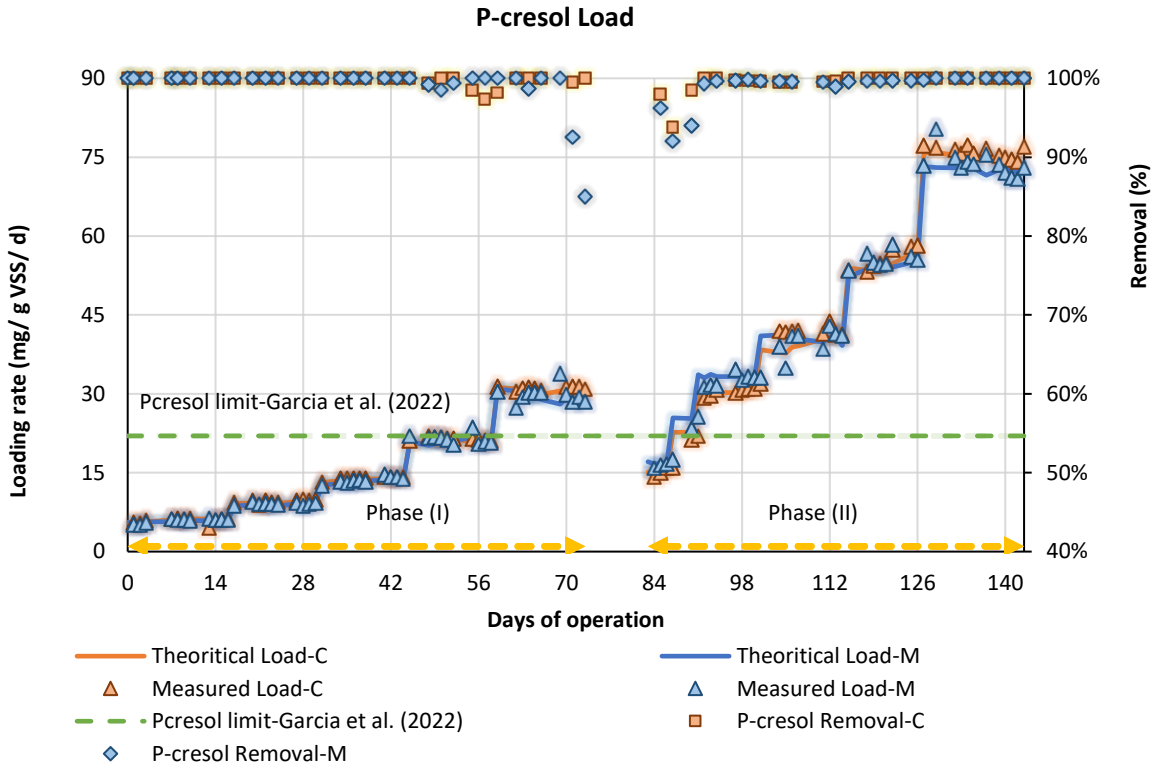

Appendix (9A): P-cresol specific loading rate for both reactors and the corresponding removal percentage

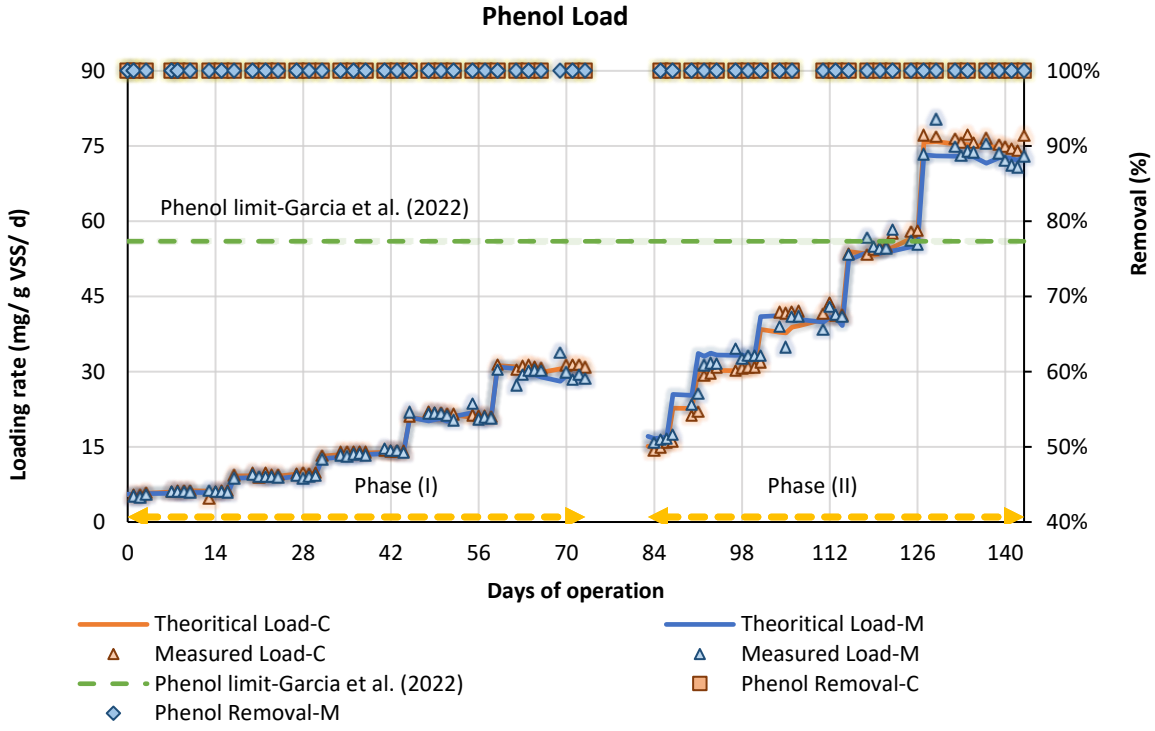

Appendix (9B): Phenol specific loading rate for both reactors and the corresponding removal percentage

8.10 Appendix (10): Modified Gompertz model fitting for the SMA analysis

Phase (I) SMA results and python fitting

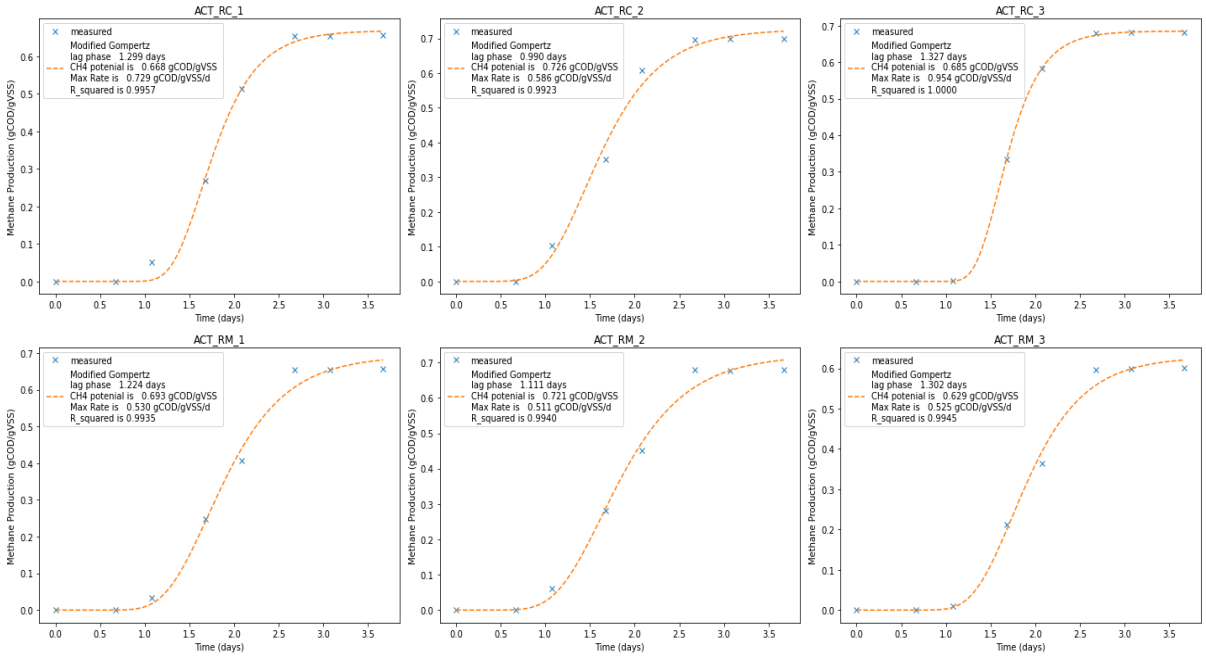

Appendix (10.A): SMA results for phase (I) based on triplicates, whereas the test was conducted by applying substrate to fresh sludge from the reactors, by which the lag phase could be determined.

Phase (II) SMA results and python fitting

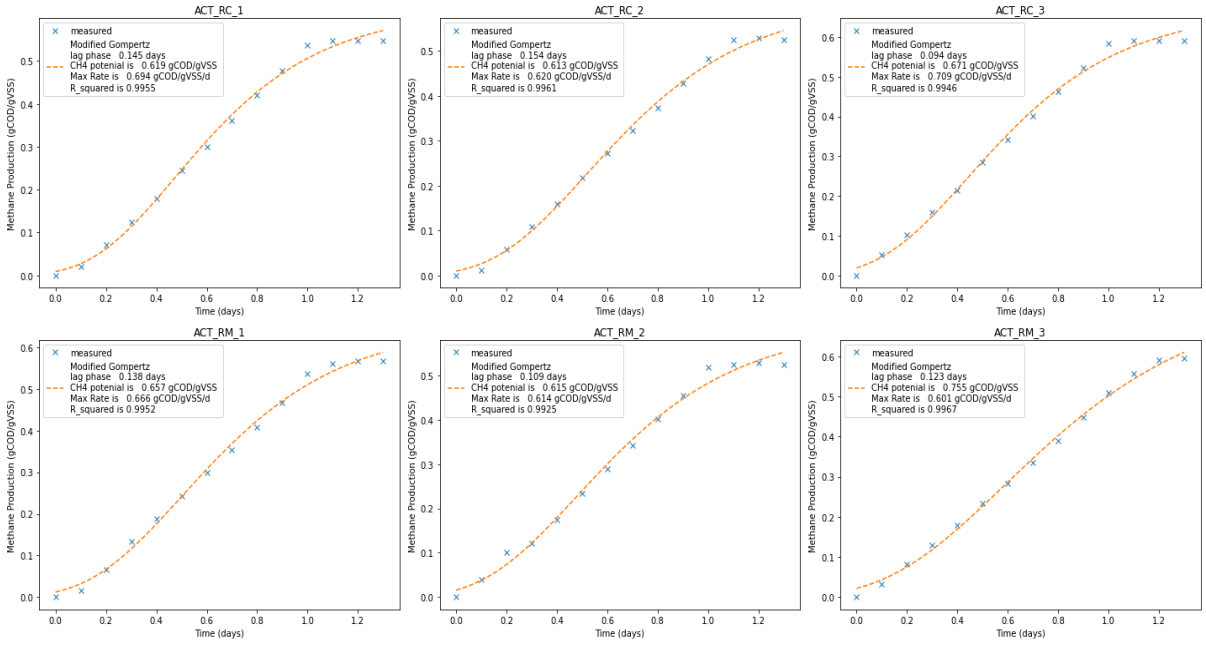

Appendix (10.B): SMA results for phase (II) based on triplicates, whereas the test was conducted by applying 2 runs of substrate to fresh sludge from the reactors, by which the second run was recorded and thus the lag phase could not be properly identified.

8.11 Appendix (11): Modified Gompertz model fitting for p-cresol degradation

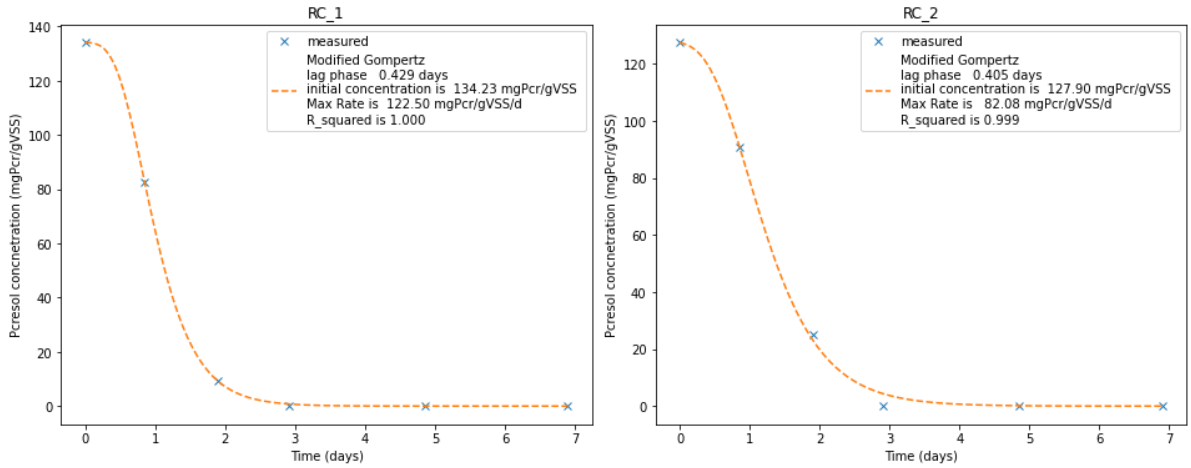

Appendix (11.A): Batch data fitted through modified Gompertz model for control reactor

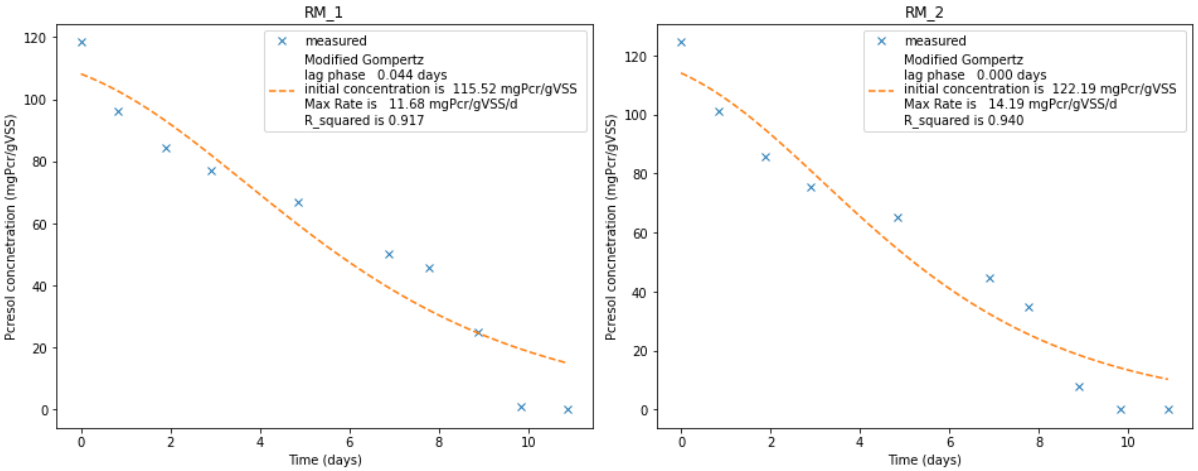

Appendix (11.B): Batch data fitted through modified Gompertz model for magnetite reactor

8.12 Appendix (12): Langmuir and Freundlich model fitting

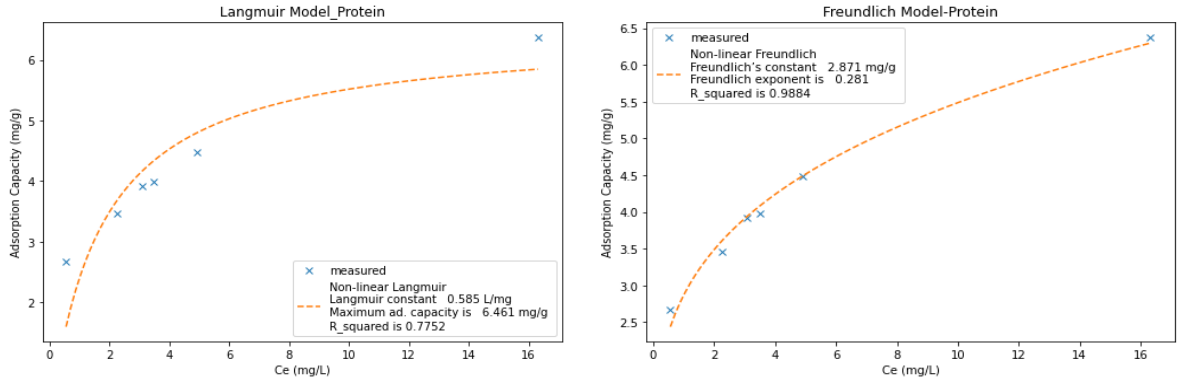

Appendix (12.A): Protein data fitted through Langmuir model (left), and Freundlich model (right).

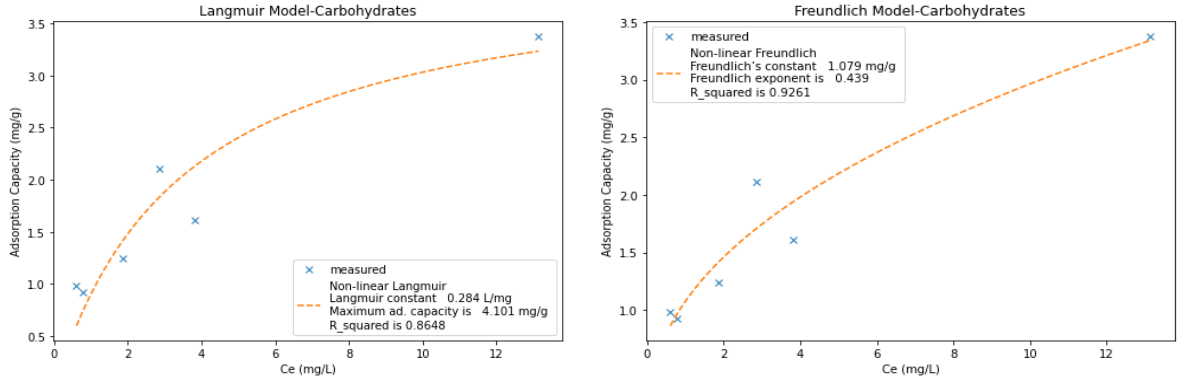

Appendix (12.B): Total Carbohydrates data fitted through Langmuir model (left), and Freundlich model (right)

8.13 Appendix (13): Pearson correlation analysis of the SMP/EPS with particle size

AnMBR-C data for both phases

Protein Content

	SMP	*EPS-LB*	*EPS-TB*
SMP	1		
EPS-LB	0.435	1	
EPS-TB	0.241	-0.064	1
Size-0.9	-0.420	-0.956	-0.091
Size-0.5	-0.423	-0.956	-0.052
Size-0.1	-0.420	-0.930	0.039

Carbohydrates Content

	SMP	*EPS-LB*	*EPS-TB*
SMP	1		
EPS-LB	0.590	1	
EPS-TB	0.426	0.641	1
Size-0.9	-0.515	-0.699	-0.381
Size-0.5	-0.513	-0.703	-0.357
Size-0.1	-0.451	-0.701	-0.315

AnMBR-M data for both phases

Protein Content

	SMP	*EPS-LB*	*EPS-TB*
SMP	1		
EPS-LB	0.682	1	
EPS-TB	0.847	0.721	1
Size-0.9	-0.255	-0.762	-0.352
Size-0.5	-0.191	-0.716	-0.296
Size-0.1	-0.216	-0.729	-0.275

Carbohydrates Content

	SMP (mg/l)	*EPS-LB*	*EPS-TB*
SMP	1		
EPS-LB	-0.020	1	
EPS-TB	0.377	0.341	1
Size-0.9	-0.350	-0.717	-0.358
Size-0.5	-0.319	-0.749	-0.358
Size-0.1	-0.262	-0.751	-0.311

8.14 Appendix (14): Membrane working flux and TMP for phase (II)

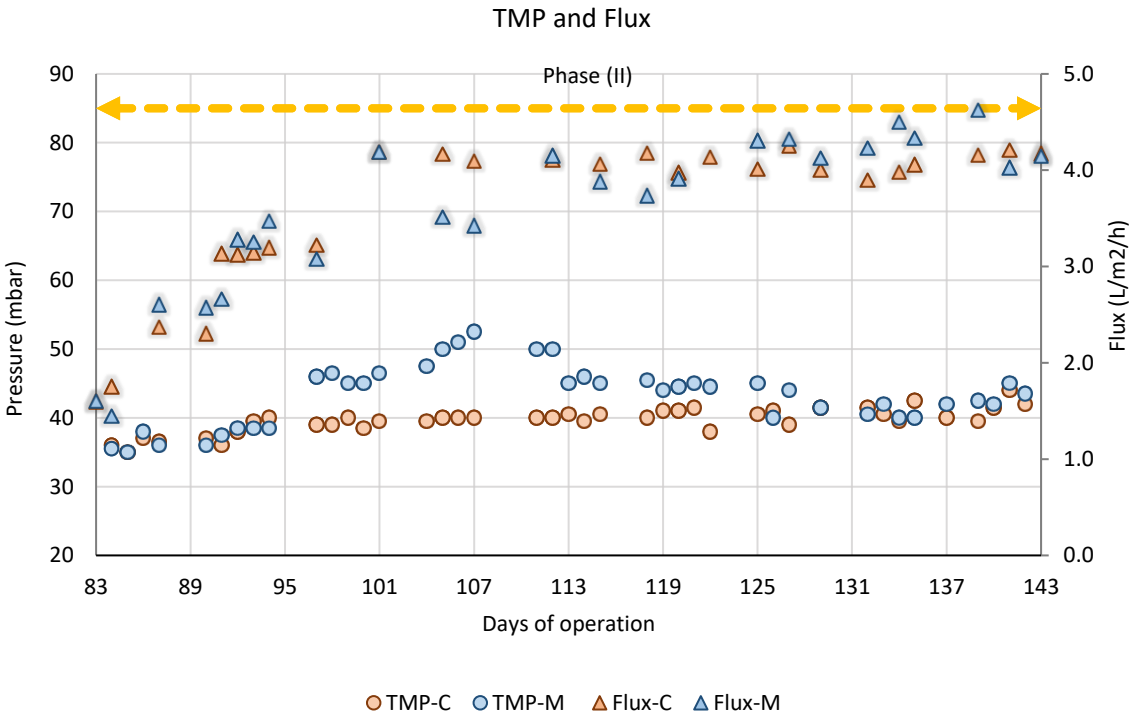

Appendix (14): The operating flux of the membrane in phase (II) for both reactors and the corresponding TMP

8.15 Appendix (15): Total iron concentration in the permeate and sludge

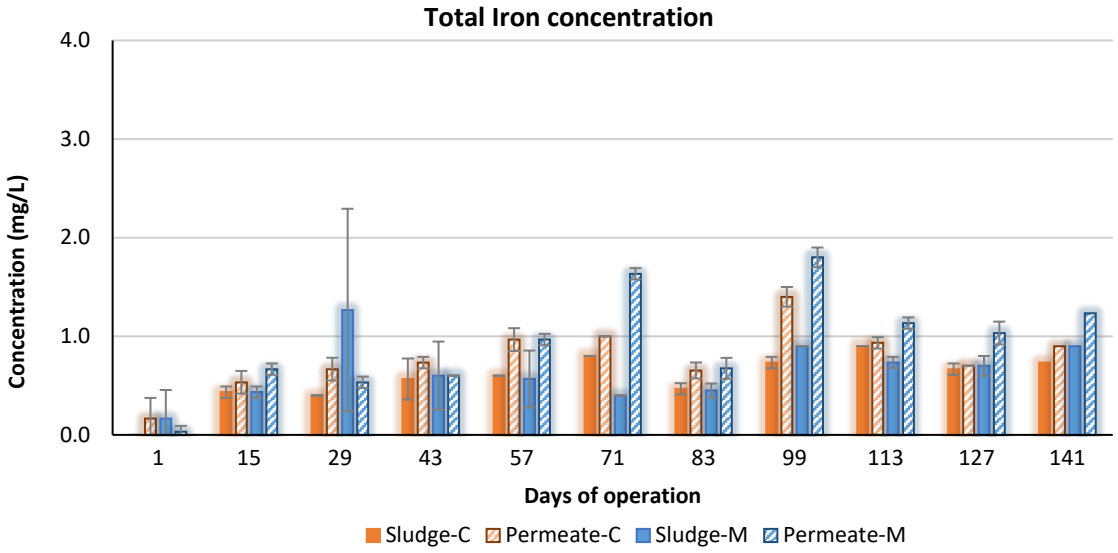

Appendix (15): Total iron concentration of both reactors and in both the solublized part of lsudge and in effluent

8.16 Appendix (16): Python code for curve fitting using modified Gompertz model

Python Code for fitting the modified Gompertz model to the observed biogas production rate:

```
import numpy as np
import matplotlib.pyplot as plt
import sympy as sp
import scipy.optimize
import pandas as pd

# Importing original data
Data = pd.read_csv('SMA_data.csv', header = [0])

#Saving each column in specified variable
# C-Reactor data
ACT_RC_1 = Data.ACT_RC_1
ACT_RC_2 = Data.ACT_RC_2
ACT_RC_3 = Data.ACT_RC_3

# M-Reactor data
ACT_RM_1 = Data.ACT_RM_1
ACT_RM_2 = Data.ACT_RM_2
ACT_RM_3 = Data.ACT_RM_3
Time = Data.Time_d
Time1= np.linspace(Time.min(), Time.max(), 100)
list1 = ['ACT_RC_1','ACT_RC_2','ACT_RC_3', 'ACT_RM_1','ACT_RM_2','ACT_RM_3']
```

```
plt.subplots(figsize=(20,10))

def Gomp_model(t, A, lamda, Rate):
    """ A: Biogas production potenial (ml/gVSS), Lamda: lag phase period (days), Rate: Maximum
    biogas production rate (ml/gVSS/d), t : input data interms of time (days)"""
  E = np.exp(1)
  Cum_Press = A * np.exp( - np.exp(Rate * E / A * (lamda - t) + 1))
  return Cum_Press

for i in range (len(list1)):
  p, cov = scipy.optimize.curve_fit(Gomp_model, Time, Data.iloc[:,i+1], p0=[0.1, 0.1, 0.1],\
                    bounds=[(0, 0, 0), (0.8, 2, 5)], ftol= 1e-20, maxfev= 1e5)

  A, lamda, Rate = p[:]
  print(f'For {list1[i]}: ')
  print(f'Biogass Production potenial is {A:13.3f}')
  print(f'Lag phase is {lamda:13.3f}')
  print(f'Maximum Rate is {Rate:13.3f}')

  #Calculating R_squared
  residuals = Data.iloc[:,i+1] - Gomp_model(Time, *p)
  ss_res = np.sum(residuals**2)
  ss_tot = np.sum((Data.iloc[:,i+1] - np.mean(Data.iloc[:,i+1]))**2)
  r_squared = 1 - (ss_res / ss_tot)

  plt.subplot(2,3,i+1)
  plt.plot(Time, Data.iloc[:,i+1], "x", label= "measured")
  plt.plot(Time1, Gomp_model(Time1, A, lamda, Rate), "--", label= f"Modified Gompertz\n"
      f"lag phase {lamda:7.3f} days \n"
      f"CH4 potenial is {A:7.3f} gCOD/gVSS \n"
      f"Max Rate is {Rate:7.3f} gCOD/gVSS/d \n"
      f"R_squared is {r_squared:3.4f} ")
  plt.xlabel("Time (days)")
  plt.ylabel("Methane Production (gCOD/gVSS)")
  plt.legend()
  plt.title(f"{list1[i]}")

plt.tight_layout()
```